→ RESEARCH LIBRARY

key words:
1- box columns
2- connections

1399

UNIVERSITY OF
SOUTHERN CALIFORNIA
DEPARTMENT OF CIVIL ENGINEERING

STEEL BEAM TO BOX COLUMN CONNECTIONS

by

James C. Anderson — main author
Department of Civil Engineering
University of Southern California

Robert R. Linderman
Department of Civil Engineering
University of Idaho

Report No. CE 91-03

A Report on Research Conducted Under Grants from
The California Field Ironworkers Trust
American Institute of Steel Construction
Los Angeles, California

December 1991

STEEL BEAM TO BOX COLUMN CONNECTIONS

by

James C. Anderson
Department of Civil Engineering
University of Southern California

Robert R. Linderman
Department of Civil Engineering
University of Idaho

Report No. CE 91-03

A Report on Research Conducted Under Grants from

The California Field Ironworkers Trust
American Institute of Steel Construction

Los Angeles, California

December 1991

ABSTRACT

This report describes an experimental investigation and associated finite element study of the behavior of steel wide flange beam to steel box column moment connections. Box columns are increasingly being used in perimeter moment frames of mid to high rise construction in California and other seismically active areas. At present these connections are detailed to include internal stiffeners or diaphragm elements inside the box column at the levels of each beam flange. This results in a costly and labor intensive connection. It has been proposed that in cases where the box column wall connecting to the beam is sufficiently thick, the internal stiffener plates may not be required. At present, little experimental data is available on the behavior of this type of connection under cyclic loading.

This study considers the behavior of ten specimens which include both stiffened and unstiffened beam to box column connections. In addition, one wide flange beam to wide flange column connection was considered and the results used as a benchmark. Two specimens had internal stiffener plates, one stiffener was half the thickness of the beam flange and the other the full thickness of the beam flange. Two specimens had external stiffeners extending the width of the beam flanges out to the width of the column face and the remaining specimens were unstiffened.

The results show that box column connections with internal stiffeners having a thickness equal to the beam flange perform in a similar manner to a typical wide flange column connection. Using internal stiffeners of reduced thickness or increasing the size of the box column face plate also resulted in satisfactory performance. If the thickness of the unstiffened column face plate is reduced too much, the resulting deformations give rise to high stress gradients across the beam flange and unsatisfactory connection performance. Exterior stiffeners show promise but caused some problems with the column face plate. Nonlinear finite element analyses show reasonable correlation with experiments and offer a promising means of evaluating connection behavior.

ACKNOWLEDGEMENTS

This research was funded in part by grants from the American Institute of Steel Construction and the California Field Iron Workers Trust. The support of Mr. James Marsh of the Western Regional Office of AISC Marketing is greatfully acknowledged. The authors also want to thank members of the project guidance committee which included the following practicing engineers and steel fabricators: Dr. Gregg Brandow, Dr. Lauren Carpenter, Mr. Ed Teal, Mr. Nate Cyns, Mr. George Osterwick and Dr. Farzad Naeim. Test specimens were donated by the following steel fabricators: Riverside Steel, Central Industrial, Junior Steel, Herrick Stockton Steel, Buckner & Wilson, Lee & Daniels, Palm Iron and Hogan Manufacturing. This support is gratefully acknowledged.

TABLE OF CONTENTS

LIST OF TABLES

LIST OF FIGURES

1.0 INTRODUCTION

1.1 Overview and Description of Problem

Historically the predominate load carrying member used in mid to high rise steel buildings, both as beams and as columns, has been the wide flange and I shaped rolled sections. These two shapes require relatively little fabrication, other than at the connection, and lend themselves to use in both concentric braced frames (CBF) and eccentric braced frames (EBF) as well as in moment resisting frames (MRF). The MRF is the most common steel building system used for earthquake resistant design.

Current design practice requires that a structure must have adequate strength and stiffness to remain serviceable after small to moderate earthquakes and adequate strength and ductility to avoid collapse during a major earthquake. The widespread use of MRFs can be attributed to their strength and excellent ductility properties. MRFs possess less inherent elastic stiffness than braced frames and control of story drift can be a problem, particularly for perimeter frames. Indeed, story drift is often the controlling factor in the design. However, through adequate sizing of the members and careful detailing of the beam column joints story drift can be limited in MRF's to values permitted in the code. Typically, MRF's have been designed as two dimensional structures to resist an assumed lateral loading applied along the major or minor horizontal axis of the building. In this type of frame, the beams are usually connected to the column flanges by full penetration bevel welds of the beam flanges to the column flange with a shear tab welded to the column and bolted to the beam web.

More recently the concept of the framed tube or three dimensional perimeter framing has become popular. Some of the impetus for the use of three dimensional frames has been the orthogonal force requirements mandating that a structure be capable of withstanding 100 percent of the design seismic load along an axis of the building with a load acting along an orthogonal axis equal to 30% of the design seismic load. In the framed tube system the lateral loads applied to the structure are resisted by moment resisting framing at the perimeter of the building only. Interior beam column joints are designed as simple shear connections. The columns are typically spaced quite closely at the perimeter and connected with deep spandrel girders. The use of three dimensional framing requires that corner columns be able to resist moments from beams framing into them from two perpendicular directions. When framing into wide flange columns this requires that one of the beams frame into the column web in the direction of the weak axis. In many cases the moments applied to the column by each of the beams are similar in magnitude. This requires the column to be considerably overdesigned in the strong axis direction in order to have the required strength in the weak axis direction. Such overdesign can greatly increase the size of such columns, leading to an increase in the dead load and in the total cost of the structure.

To avoid the design problems which arise from the inherent dissymmetry of wide flange shapes, many engineers have adopted the use of box columns fabricated from steel plate. Such box columns solve the dissymmetry problems and are also very efficient structural shapes for carrying axial load. They provide a larger radius of gyration for a given column dimension than a wide flange section and have much better torsional capabilities than an equivalent open section. However, very little research has been done on welded moment connections of beams to box columns. Other than an analysis of the strength of the column wall by yield line theory proposed by Blodgett [1], no acceptable criteria exists for the design of unstiffened connections. The yield line analysis has the weakness that it focuses entirely on the strength of the column wall and neglects any interaction effects of the column wall with the beam or the possibility of local yielding in the beam flanges. It is clear that the face of the column will be much more flexible than the flange of the beam framing into it. This could result in the connections having the properties of a semirigid joint rather than a fully rigid joint. One could also expect more rotation of the joint for a given moment than with a properly detailed connection to the flange of a W section. Given a suitably rigid beam and a relatively thin column face it could also lead to plastic hinges forming in the face of the column before they form in the beam, which could cause a weak column to strong beam condition in the frame.

Due to the lack of design criteria, the structural engineer has been forced to detail an internal stiffener plate at each beam flange. A view along the length of a box column during fabrication is shown in Fig. 1.1 and a close up of a stiffener plate during fabrication is shown in Fig. 1.2. To be conservative, these stiffener plates are customarily detailed to be the same thickness as the beam flange with full penetration welds to the column wall. Because it is only possible to make a conventional full penetration weld to three of the column faces before closing the box, the weld between the stiffener plate and the fourth side of the box is usually made using the electroslag process. The fourth wall of the column prepared for welding of the stiffener plate by the electroslag process is shown in Fig. 1.3. and a typical weld on one of these columns is shown in Fig. 1.4.

The connections described require a considerable amount of fabrication time in the shop and are consequently quite costly. Because the connections represent a substantial percentage of the total framing cost, it is often possible to optimize the cost of the structural frame by decreasing the complexity of the connections and increasing the size and weight of the members. Stiffener plates may be necessary in the upper floors of a building where the columns are smaller and the column walls are thinner due to the lower axial loads. However, in the lower stories of a structure where increased axial loads dictate thicker column walls, it may be possible to omit the internal stiffener plates and thereby reduce fabrication costs.

As a result of the paucity of experimental research into the properties and behavior of welded beam to box column connections, engineers are reluctant to omit the internal stiffener plates. While it is possible to estimate the strength of the connection using the method suggested by Blodgett, it remains to evaluate the accuracy of this technique by large scale testing. Also, there is currently no means to determine the serviceability of the connection as measured by the rotation of the beam to box column connection as a function of the moment applied to the joint. Several papers, which will be discussed later, have discussed methods of obtaining solutions to this problem for other types of non-rigid connections, and these methods may be applicable to the beam to box column connection. In addition, although the Blodgett calculations allow an estimate of the connection strength by yield line theory, there is no empirical evidence that the welds will be strong or ductile enough to permit development of the full plastic moment in the beam. Preliminary studies using linear elastic finite elements [2,3] have shown that there are very high strain concentrations in the beam flange tips at the connection between the beam and the box column. These strain concentrations appear to be very similar to those reported by Driscoll and Beedle [4] as causing fracture failure in beam to column web connections.

1.2 Objective and Scope

Motivated by the need for experimental and analytical research in steel beam to box column moment connections, an integrated experimental and analytical study of large scale beam to box column connections was initiated. The following objectives were developed for the initial investigation:

(i) Collect experimental data on the rotation capacity and ultimate strength of welded beam to box column connections.

(ii) Develop an understanding of actual failure modes and yielding mechanisms.

(iii) Compare experimental data with the results of finite element models to determine the applicability of their use in analyzing this type of connection.

(iv) Compare experimental data with the design criteria of Blodgett and assess its validity.

(v) Determine the effectiveness and need of internal stiffener plates.

(vi) Test external stiffener plates and determine their effectiveness as a replacement for internal plates.

In addition to the experimental studies, a parallel investigation using the nonlinear finite element program NIKE3D [5] was conducted with the intent of establishing a close correlation between the results of the finite element models and the experimental program. This would reduce the need for expensive experimental work and permit parametric studies to be made using only the finite element models, thus reducing both cost and time constraints.

1.3 Approach

In order to accomplish the above objectives, a series of experimental investigations, coupled with finite element analyses, consisting of ten beam to column subassemblies was undertaken. It was necessary to use specimens that were smaller than those normally found in large structures due to the limitations of the test frame and the substantial additional cost that fabrication of very large specimens entails. The specimens tested were typical of the size of beams and columns found in the upper stories of tall steel structures and in the lower floors of smaller steel structures. If the results of the finite element studies correlated closely with the results obtained from the experimental work, the analysis of very large connections typical of those found in the lower stories of tall buildings could be undertaken on the computer with a high degree of confidence in the results.

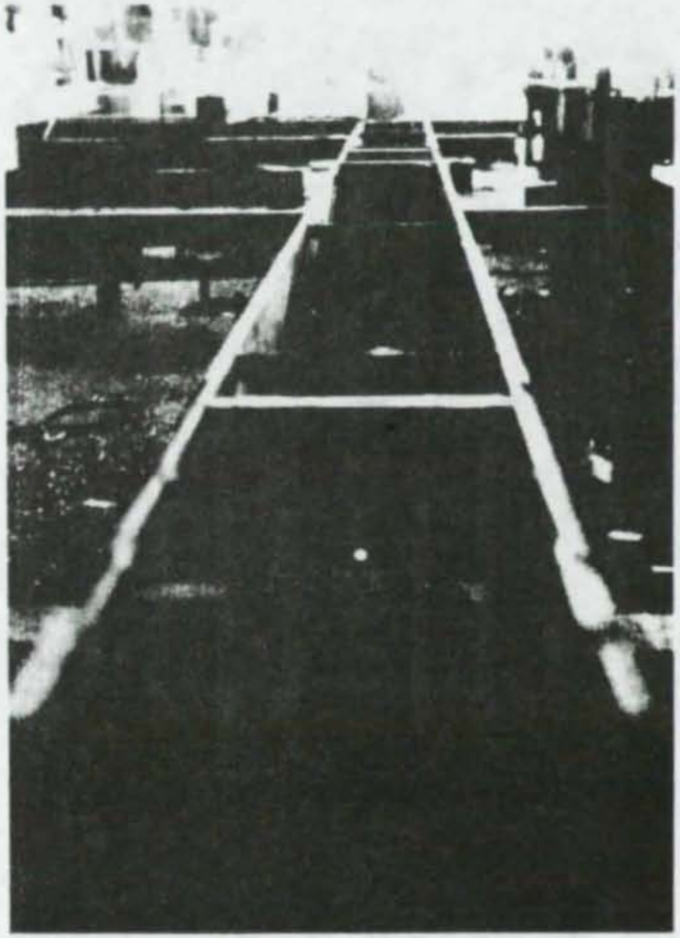

Figure 1.1
Typical Box Column During Fabrication

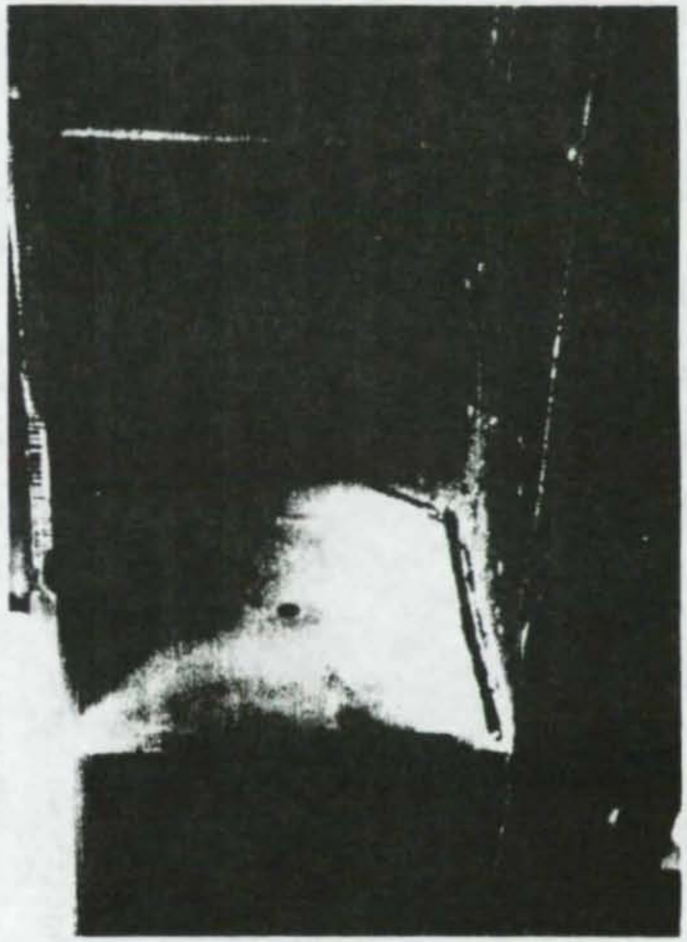

Figure 1.2
Stiffner Plate in Box Column
During Fabrication

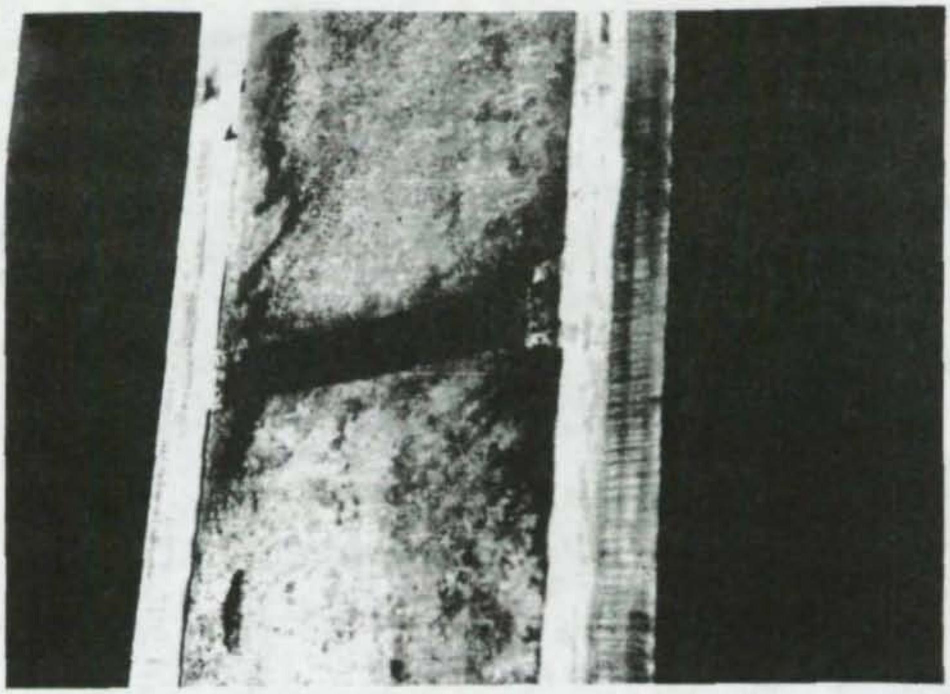

Figure 1.3
Back Wall of Column at Stiffner Prepared
for Welding by Electro-Slag Process

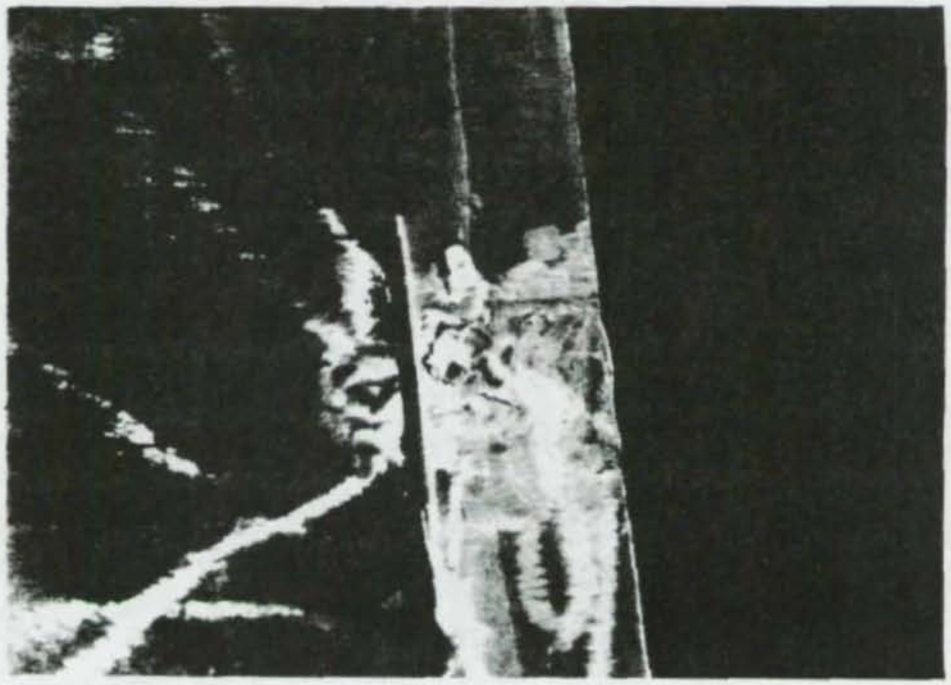

Figure 1.4
Typical Full Penetration
Weld on a Box Column

2.0 REVIEW OF PREVIOUS RESEARCH

2.1 General

As previously stated, a major impetus for the use of box columns in mid to high rise construction has been the adoption of the framed tube concept [6]. This requires that the corner columns have two moment connections framing at angles less than 180 degrees. Prior to the development of the framed tube, beams framing into the weak axis of a column were usually connected with a simple, non-moment resisting connection. The framed tube necessitated either weak axis moment connections to rolled sections or the use of box columns.

The beam to box column connection would at first glance appear to have many similarities to connections that have already been studied more extensively. The most widely used and most thoroughly studied connection is that of a beam framing into the flange of a column. Commonly referred to as a strong axis connection, the bending moment in the column flange is similar to that of the box column faceplate as shown in Fig. 2.1. In this idealization, given by Blodgett [1], the faceplate of the box column is considered as a beam simply supported between the two sidewalls of the column. Any influence of the beam web is neglected. The column flange in the strong axis connection can be considered as a beam supported at it's center. Both cases have the same maximum bending moment due to the force of the beam flange.

The weak axis connection, where the beam flange frames into the column web, would also appear to have some similarities to the box column problem. Both the box column faceplate and the column web can be analyzed as beams spanning between either the column flanges in the weak axis connection or the box column sidewalls.

One can also see similarities between the beam to box column connection and the connection involving tubular members. This problem has been extensively studied, due to the use of tubular members in offshore construction. While most of the research has been directed at round members, square and rectangular members have been studied in England, Canada and the Netherlands. Most of the research has been directed toward solving problems of the use of tubular members as chord and web members in trusses, but there has been some work done on moment connections in Vierendeel trusses.

2.2 Recent Research on Strong Axis Connections

Strong axis connections are the most commonly used beam to column moment connections and an extensive number of experimental studies have been conducted on this type of connection. In the U.S. much of the research has been done at Lehigh University in the east and at the University of California, Berkeley in the west. The Lehigh tests tend to emphasize monotonic loading of full scale subassemblies in which the column is subject to axial load which is on the order of one half the yield strength [7]. Tests at Berkeley generally employ increasing cyclic loading of the test specimen with the effect of axial loading on the column being neglected. However, more recently a series of tests on full scale subassemblies were run at Berkeley with axial load applied to the column [8]. The differences in philosophy concerning monotonic and cyclic loading reflect the fact that Berkeley is in an active seismic region and is very much concerned with dynamic loading of structures. Reports describing experiments involving cyclic loading of beams were published in the 1960's by Bertero and Popov [9] and Popov and Pinkney [10]. The latter article reported on a series of tests conducted on 24 connection specimens, including both strong and weak axis, and bolted and welded connections. One of the specimens considered in this study, provided for moment transfer by the use of flange plates.

A further series of tests employing cyclic loading of beam to column connections was reported by Krawinkler and Popov [11] in 1982. This paper described a series of full scale experiments involving fully welded specimens, bolted specimens and specimens with welded flanges and bolted shear tabs. The connections with welded beam flanges and bolted web connections were reported to exhibit bolt slippage early in the inelastic cycles, leading to localized bending in the beam flanges and eventually to weld fractures which were common for that type of connection. In this paper it was again reported that "In welded connections, deterioration is usually a consequence of crack initiation and propagation at points of stress concentrations at welds. Unless failure is imminent, this deterioration takes place at a slow rate and will not affect the hysteresis loops to a significant degree."

In 1986 Popov, Amin, Louie and Stephen [8][12] reported on a series of cyclic tests on large scale beam-column assemblies. These tests were undertaken to address specific questions regarding the need for stiffeners and doubler plates at the beam column joints during the construction of a 47 story office building in San Francisco. Due to the very large size of the prototype assemblies that were studied in this series of tests the test specimens were fabricated half size. The paper does not give an explanation of any scaling factors that should be or were applied in scaling down the size of the specimens. Unlike previous tests at Berkeley, the columns in this series of experiments were subject to an axial load. The axial load applied generated a nominal stress in the column of 21 ksi. It was concluded from this study that even with 1-1/4 inch thick column flanges, stiffener plates are essential. It was also stated that the design of stiffeners on the basis of nominal yielding in the beam flanges is not conservative and that full penetration welding of the stiffeners to the column flanges is preferable to fillet welding. However, the report goes on to state that "for geometries of the tested column cross sections the flanges were relatively thin. As the thickness of the column flanges increase, requirements for the stiffener sizes . . . would likely decrease." This appears to leave unanswered the question as to whether stiffener plates could be omitted or reduced in size for columns with very thick flanges. Finally the paper closes with the caveat that "extending the studies to columns with thicker flanges and narrower panel zones as well as to tubular columns may lead to different conclusions."

Two years after the report of the experiments of Popov and Pinkney, Fielding and Huang [13] reported on a test of a single full scale subassembly at Lehigh University. In this test the column was axially loaded to 819 kips, corresponding to a stress in the column of one half yield, and the beam was loaded monotonically. The testing actually consisted of two monotonic tests, with the specimen being loaded during each test until a crack appeared. It was then unloaded, the cracked area rewelded and the load was reapplied to the specimen. This was repeated twice. The primary conclusions of this study were the following:(a) axial loading accelerated the onset of yielding in the subassembly;(b) weld detail and quality were shown to be important factors in joint capacities;(c) stiffeners designed to the 1969 AISC code performed satisfactorily; (d) a revision of connection stiffening requirements must be based on required rigidity rather than on yield criteria.

These required rigidities will require evaluation of the effect of connection deformation on the frame behavior.

2.3 Weak Axis Connections

Weak Axis connections are usually designed as shown in Fig. 2.2. While at present there is no design criteria in the AISC Specification for this type of connection, they have recently been the subject of several experimental and analytical studies. Stockwell [14] presented a yield line analysis of column webs with welded beam connections. This yield line analysis differed from that presented by Blodgett for box columns in that a yield mechanism was proposed around the entire beam rather than just one beam flange. The assumed yield pattern proposed by Stockwell is shown in Fig. 2.3. Plastic hinges are shown as dotted lines and the rotation of the beam is shown off to the side. Equating the external work done in bending the beam to the internal work required to form the hinges along the yield lines results in the following equation:

$$M = F_y * \left(\frac{(a+b)dt}{12} + \frac{(ab+d^2)t^2}{2a} + \frac{6dt^3}{a} \right) \tag{2.1}$$

where a = width between column flanges minus width of beam flange divided by two

b = width of beam flange

d = depth of beam

t = thickness of column web

In 1980, Rentschler, Chen and Driscoll [15] published results of tests on beam to column web moment connections. During their experiments they tested eight different specimens with four different geometries. Two of the geometries have some applicability to box columns. One considers a beam flange which is considerably narrower than the depth of the column and the other considers a beam flange which is just narrower than the width between the column flanges. In these tests, steel plates representing the beam flanges were loaded in tension and compression, rather than using actual beams. It was concluded that both specimen types failed to reach the load calculated by the yield line method. For the initial configuration, one of two specimens reached a maximum load which was 77% of that predicted by the theoretical yield line mechanism and the other reached 89%. In the second configuration which also involved two specimens, the beam flange was attached to the full width of the column web, but not to the column flanges on either side. In these two tests the theoretical load based on the formation of a plastic hinge was not reached. The first specimen attained only 64% of the calculated load and the second 87%. These results seem to imply that the yield line analysis method for sizing box columns may not be conservative. Stress distributions across the flange plate were also reported as being nonuniform, resulting in high concentrations of stress at the edge of the flange plates. This resulted in local yielding and eventual failure of the specimens by fracture at the areas of high stress concentrations.

More recently, Tsai and Popov [16] have also tested beam to column web connections. Their studies indicated that a small amount of welding of the shear tab can eliminate slippage under severe cyclic loading. They also introduced the use of reinforcing ribs at the beam to column web interface to increase cyclic performance.

2.4 Connections Involving Tubular Members

Connections involving tubular members are geometrically very similar to the beam to box column connection, especially where the column or chord member is a rectangular hollow section. A large amount of research has been conducted on round tubular connections due to their prevalence in offshore construction. Connections involving rectangular hollow sections have also been the subject of a considerable amount of research in England [17], Canada [18][19][20][21][22] and the Netherlands [23]. Most of the work with both round and rectangular hollow sections has been concerned with connections in trusses, where the forces are primarily axial and bending moments are only considered as secondary forces. Because most of the research has been conducted on trusses the terms used in the literature corresponds to trusses rather than frames with beams most often referred to as branches or webs and the column being referred to as the chord.

There has been some research on moment connections, particularly in vierendeel trusses. In 1977, Korol, El-Zanaty and Brady [18] reported on the results of tests on unequal width connections of square hollow sections in Vierendeel trusses. These tests were performed on specimens where the beam was also a square hollow section but many of the results can be applied to beams made of rolled sections. The paper reports on some work done at Drexel by Cute [24]. Among the connection types tested were some with branch flange reinforcing plates and chord flange stiffeners. Among the conclusions considered applicable to box columns were the observations that unreinforced joints did not perform adequately. Even equal width connections did not attain the branch member's plastic moment capacity, which was in contrast to earlier results reported by Jubb and Redwood [17]. Tests on subassemblies with branch flange stiffeners did not perform as well as other joint reinforcement types due to very high stresses in the flange plate corners which leads to premature weld failure. The chord flange stiffener plate performed very well. This would be equivalent with putting a doubler plate on the box column face at the beam connection.

2.5 Blodgett's Yield Line Analysis

At present the only criteria for the design of beam to box column joints is that developed by Blodgett [1] based on yield line analysis. The analysis was based in turn on a similar analysis of a line force applied to a cover plated wide flange column developed by Higgins of AISC. The following derivation is based on Blodgett's work.

The analysis makes the following assumptions:

(i) The length of the box column wall resisting the line force is limited to a distance equal to six times the wall thickness above and below the application of the line force.

(ii) The edges of the column wall perpendicular to the column wall are simply supported. The upper and lower boundaries of the column wall affected by the connection, six times the thickness of the wall as given in (i) above, are fixed.

(iii) The line force applied to the column wall is uniformly distributed.

(iv) At ultimate load, P_u, it is assumed that the rectangular plate defined in (i) and (ii) above has failed as a mechanism with plastic hinges forming along the dotted lines shown in Fig. 2.4.

The analysis proceeds by setting the internal work done by the resisting face plate of the column, which is the summation of the plastic moments (M_p) multiplied by the angle change, ϕ, along the edges the moments act, equal to the external work done by the ultimate load, which is the ultimate load (P_u) multiplied by the virtual displacement, delta. The equation is then solved for the ultimate load (P_u), which is the maximum allowable force in the flange plate. At failure, a mechanism involving seven plastic hinges has formed as shown in Fig. 2.4. The internal work is found by calculating the length of each hinge and the angle changes along each hinge at ultimate load. Equating internal and external work leads to the equation

$$P_u\delta = \frac{\delta * \sigma_y * t}{6} * (2a + b + 36*t^2/a) \qquad (2.2)$$

where a = (column width - width of beam flange)/2

b = width of the beam flange

t = thickness of the column wall

Applying a load factor of 2, and using the yield strength σ_y gives the allowable force, P which may be applied to the plate

$$P = \frac{t * \sigma_y}{12} * (2a + b + 36*t^2/a) \qquad (2.3)$$

2.6 Other Research on Box Columns

Croad, Mead and Shepherd [25] performed a test on a star plate cruciform connection in 1975 in New Zealand. The test specimen consisted of a 14 inch square box column fabricated from 3/4 inch plate with wide flange beams framing into it from all four sides. For testing purposes only two beams were framed into the specimen and it was tested as a cruciform section. Loading followed a predetermined program of nine cycles extending into the plastic range and developing ductilities of up to 5.0. The loading program was taken from previous work done on a concrete joint by Hanson and Conner [26]. After the nine cycles the connection was loaded to failure. Results reported indicate that the beams in the connection started yielding 20% below the calculated nominal yield for the beam. High stress levels were found in the central panel zone accompanied by substantial yielding of this area. Deflections computed by a finite element model were also compared with the experimental results in the paper. The finite element model in this study predicted deflections which were smaller than experimental results by an average of 11% with greater error at larger deflections.

At the instigation of the Western Regional Office of the American Institute of Steel Construction, Richard [3] in late 1984 undertook a finite element study of the beam-box column connection problem. The study performed an elastic analysis using the finite element program NASTRAN to model the column connection. The prototype subassembly which was modeled consisted of a column 20 inches square with varying flange widths of 10, 15 and 20 inches. Column plate thicknesses of one inch and three inches were studied and the beam flange was modelled as a 3/4 inch plate. The study made several simplifying assumptions which affected the geometry and properties of the model. Richard reported that his analysis showed very high strain in the beam flange tips. The 20 inch wide beam flange (equal in width to the column face) showed maximum strains 35 times yield strain and the 10 inch flange showed maximum strains of 16 times yield strain, both at working load levels with a one inch thick column face. By increasing the thickness of the column face plate, the stresses and strains were reduced by a factor of ten for the three inch plate compared to the one inch plate. When the thickness of the continuity plates was varied, the plate that was half the thickness of the beam flange performed satisfactorily at working loads but had unacceptable levels of stress and strain at near-ultimate levels.

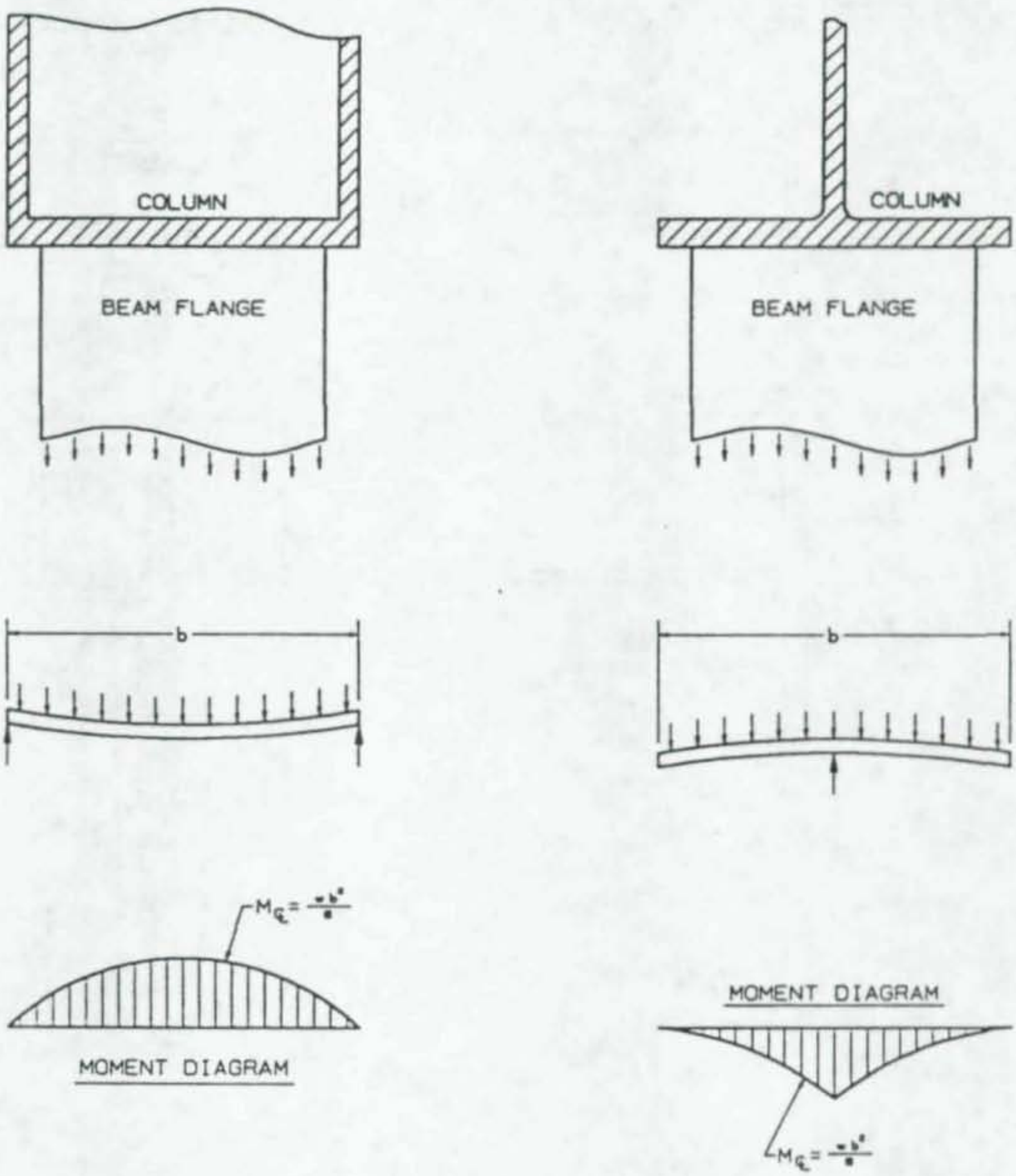

Figure 2.1 Simplified Model of Flange Moments

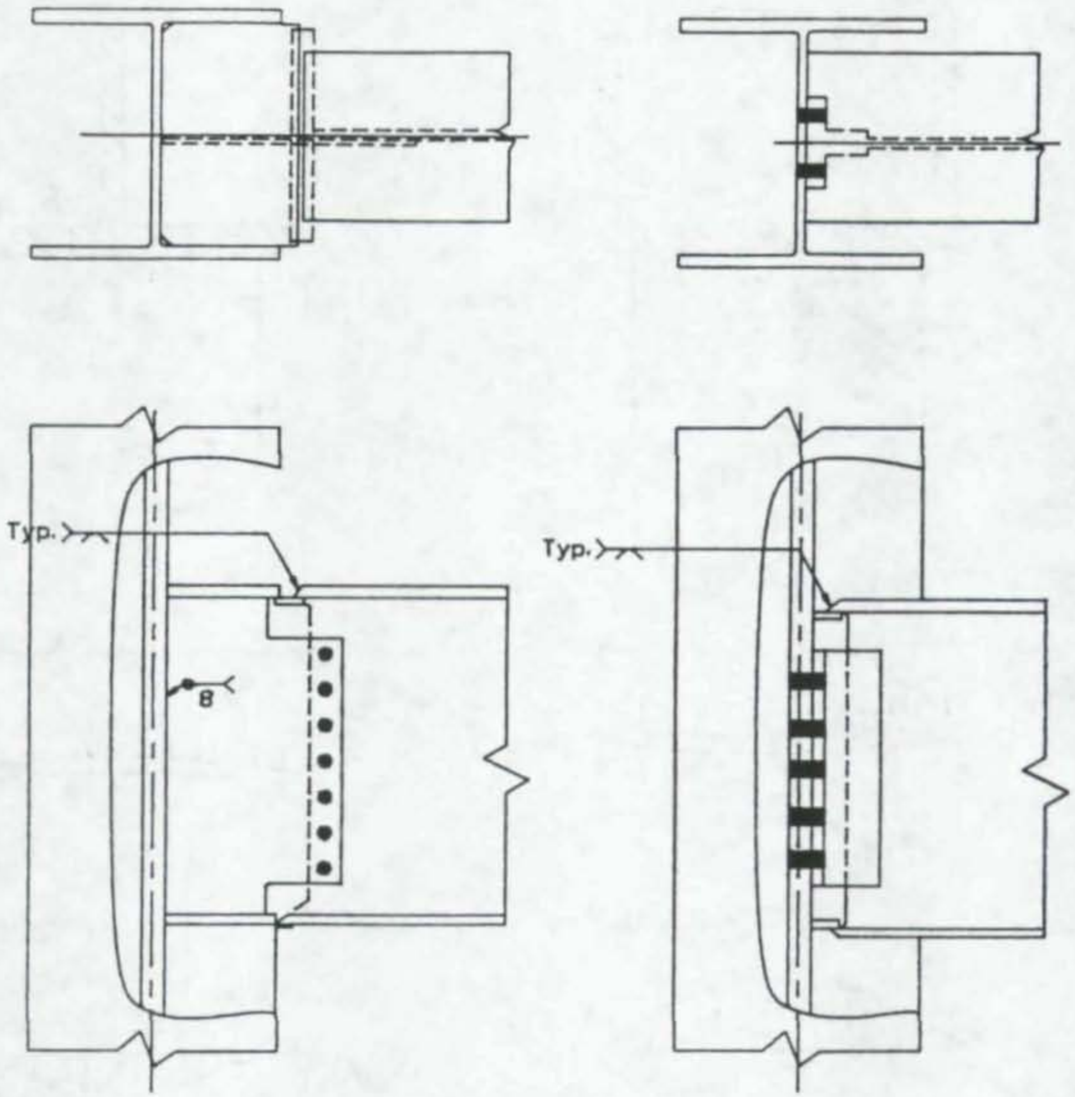

Figure 2.2 Typical Weak Axis Moment Connections

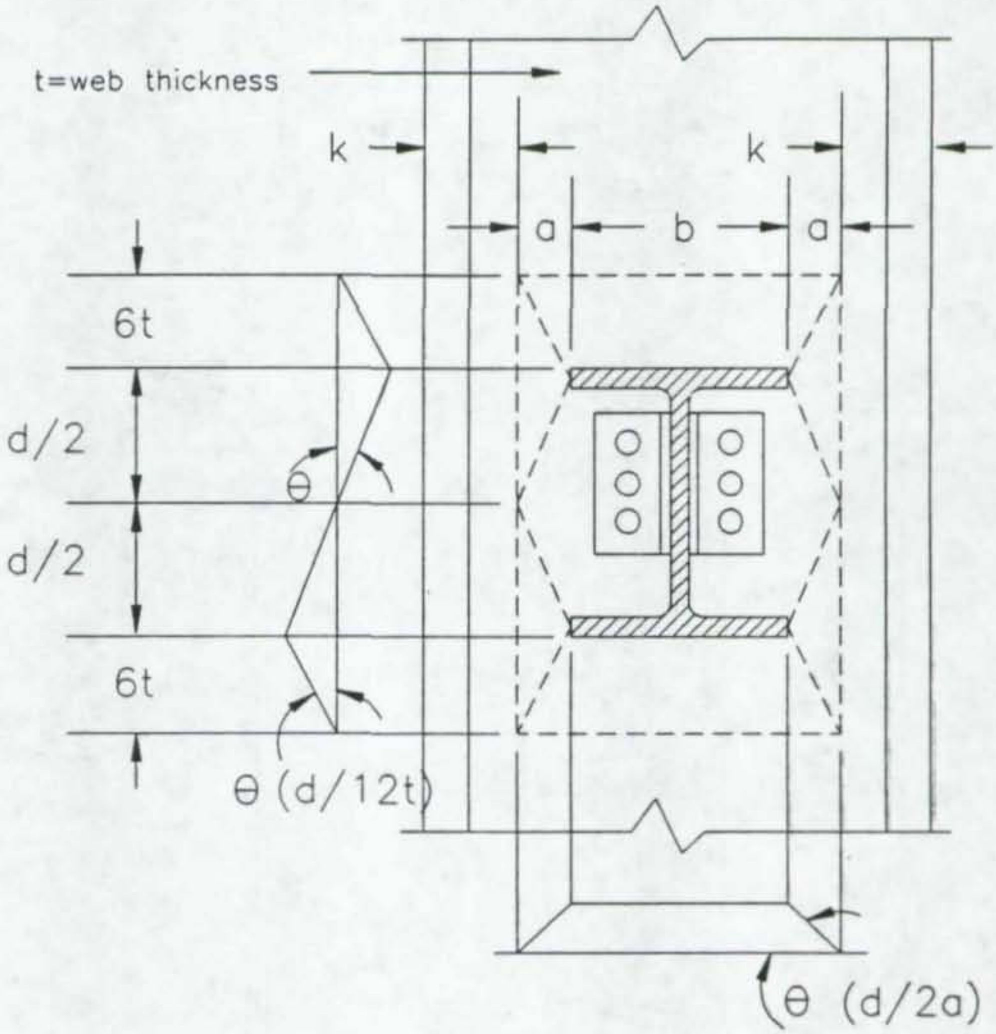

Figure 2.3 Yield Line Analysis, Weak Axis Connection

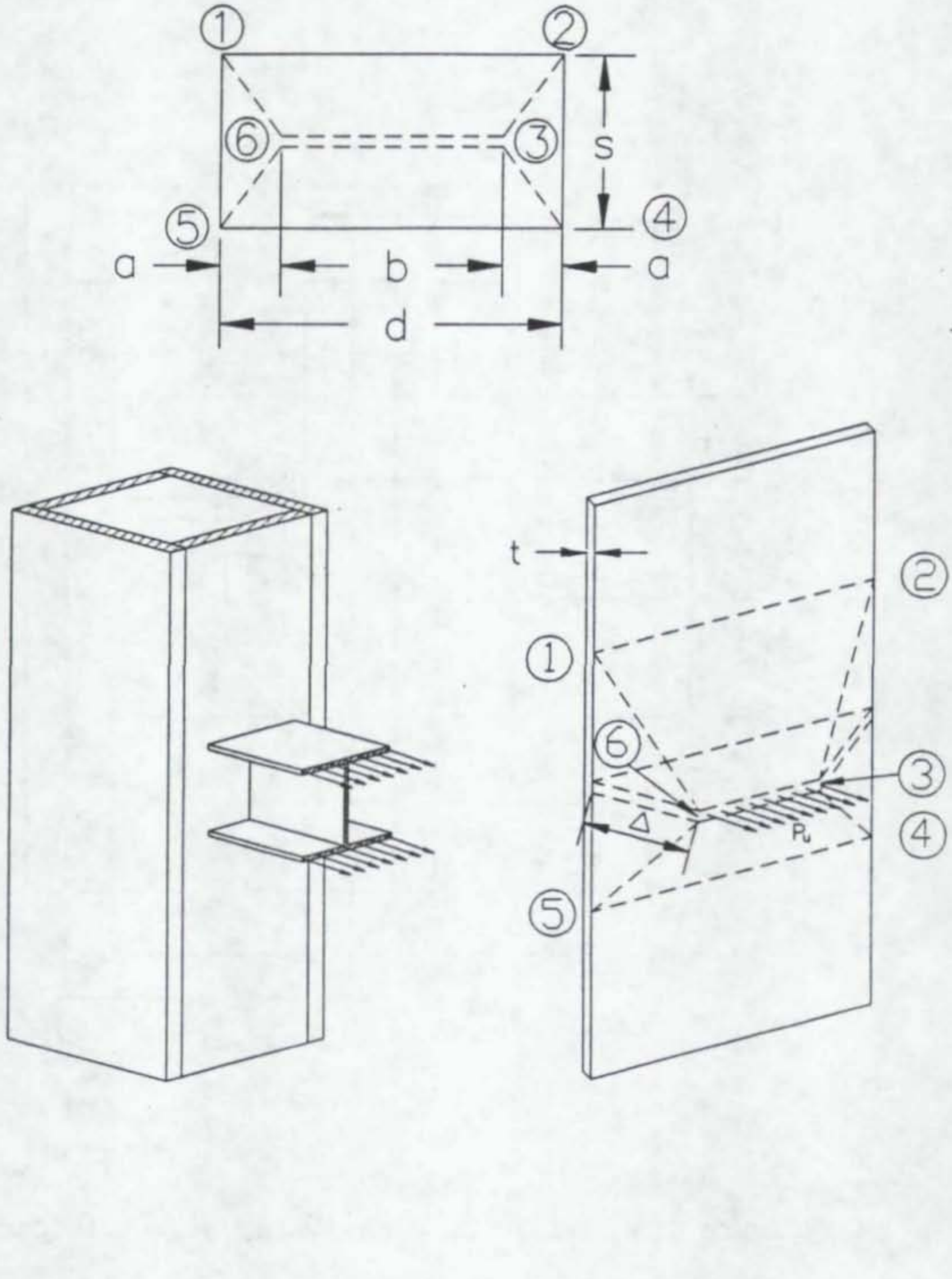

Figure 2.4 Yield Line Analysis of Box Columns

3.0 EXPERIMENTAL SYSTEM

3.1 General

A subassembly consisted of a wide flange beam framing into a box column. In order to accommodate the current limitations of the test frame, to simplify the initial investigation and to reduce the number of parameters, the current investigation considered the interaction of only one beam with the box column leaving the orthogonal beam problem for a future investigation. Box columns, as typically used in California construction, vary in size from twelve to thirty six inches square. Because of the limitations of the test equipment it was determined that the experiment would be done on an eleven inch square column.

For investigating the effect of the ratio of the beam flange width to the column width it was decided that two ratios would be investigated; one where the flange was half the width of the box column and one where the width was 3/4 the width of the column. This led to the selection of W16x26 and W16x40 beams. Because the behavior of the column wall has an important effect on the overall behavior of the connection, an axial load was applied to the column to simulate the dead and live load in an actual column.

3.2 Experimental Setup

The test frame in which the tests were conducted is shown in Figs. 3.1 and 3.2. The test frame was originally built by the Smith Emery Company of Los Angeles to perform biaxial compression testing of concrete. On completion of the testing at Smith Emery, the frame and hydraulic cylinders were donated to the University of Southern California and redesigned to suit the requirements of the current program of tests. The frame as originally configured was capable of exerting a force of 600 tons in the horizontal direction and 400 tons in the vertical direction. For the connection tests, it was desired to keep the vertical loading capability in order to simulate the axial column load while at the same time applying a parallel load, approximately 5 feet from the column face, in order to apply a moment to the beam column connection.

Vertical loads are applied to the top of the subassembly by two 200 ton Simplex hydraulic cylinders acting on a two inch loading platen. The forces are reacted out through the frame by four, 4 inch diameter rods spanning between two 12 inch thick blocks of steel. The moment inducing load at the end of the beam is applied by a 75 ton Atlas hydraulic cylinder. An eye on the end of the cylinder plunger is connected by a 3 inch diameter pin to a clevis which is bolted to the beam end plate with 4 - 1 3/4 inch diameter bolts. The Atlas cylinder is connected through another clevis to the test frame. The cylinder plunger was instrumented with strain gauges and then calibrated in the laboratories testing machine, thus allowing the cylinder plunger to act as the load cell.

The beam was braced against lateral buckling and out of plane motion of the beam by two braces, constructed of 1 inch x 2 inch structural steel tubing, mounted on the test frame near the end of the beam. A pair of teflon pads on the edges of the beam flanges reduced friction between the beam and the braces allowing the beam to move freely in the vertical direction. Pressure to drive the cylinders is developed by an Enerpac 2025 pump with a capacity of 250 in^3/min. at 200 psi and 42 in^3 /min. at 10,000 psi. The hydraulic pressure to the cylinders was regulated using Enerpac safety relief valves.

3.3 Instrumentation

The test specimens were instrumented with a combination of strain gauges and Linear Variable Differential Transformers (LVDTs). The strain gauges were used to measure the strain in the beam flanges at the beam-column connection as well as the strain in the box column just above the beam. The location of the strain gauges on the beam and the box column are shown in Fig. 3.3. The strain gauges used were single element high elongation type gauges (Micro Measurements No. EP-08-250BG-120). They were attached to the specimen using Hottlinger Baldwin Messtechnik's X-60 epoxy, a two part, quick drying epoxy capable of undergoing high strains.

Although the gauges used were high strain, post yield gauges, it appears that they are best suited for cases where the loading is monotonic. During cyclic loading the underlying carrier in the gauge yields and suffers fatigue damage, which causes the output of the gauge to drift. Thus much of the data acquired from the gauges at cyclic high strains was not usable.

To measure horizontal displacement at the face of the column several Schaevitz Engineering Type 1000-HRDC LVDTs were used. The placement of the LVDTs on the specimen is shown in Fig. 3.4.

The vertical displacement of the beam relative to the test frame (which was assumed rigid) was measured by a Columbia Research Model H-3000-S3R LVDT. This LVDT was positioned to measure vertical displacements of the beam 36 inches from the face of the column. The centerline of the cylinder applying the load to the end of the beam tip was 58 inches from the face of the column. For specimens 9 and 10 an additional vertical LVDT was placed to read the absolute displacement between the beam and the test frame at the end of the beam. This was done as a check on the vertical LVDT at 36 inches from the column face and to read true beam tip displacement versus force applied at the beam tip.

Power was supplied to the strain gauges and LVDTs and the signals from the strain gauges were amplified by a Vishay 2100 Strain Gauge Conditioner and Amplifier system with 16 channels of output. The system consisted of two Vishay 2150 racks with a 2110 power supply in each rack and five 2-channel Vishay 2120 strain gauge conditioners in one rack and three in the other.

From the signal conditioning equipment the output from each of the channels was fed into a sixteen channel analog to digital converter (A to D Board). The digital signals were then read by a Vipac card, supplied by ANCO Engineers, and written onto the hard disk of an IBM XT personal computer. The Vipac card acted much like a multiplexer, reading each channel sequentially on to the hard disk, after being triggered either from the keyboard or by an internal clock. The data was written onto the hard disk in blocks of data, each block containing a data point for each of the sixteen channels.

The data written onto the PC hard disk by the Vipac card was in terms of voltages, which varied as either the strains or the displacements were changed. After the test was run the data was converted to engineering units by using a calibration program, Statprc, which was supplied with the data acquisition card. A calibration file was compiled using the calibration values for voltage to engineering units supplied by the manufacturers of the LVDTs and using data taken during calibration of the strain gauges by shunting through a known resistance [27].

3.4 Description Of Test Specimens

The wide flange beams and plates used in the fabrication of all test specimens were made of ASTM A36 steel. All welding was specified as AWS E70 stick welding. The shear tabs were connected to the beam webs using four A325-X bolts which were tightened by the turn of the nut method except where twist off bolts were used as indicated in the following descriptions. Bolt holes were drilled or punched 1/16 inch oversize. All welding was visually inspected and all full penetration welds between the beam flanges and the column wall were ultrasonically tested. Web copes (ratholes) were approximately one inch in width. After the second specimen, in which failure appeared to originate at the web cope, the specifications supplied to the steel fabricators called for the web copes to be ground smooth. However many of the specimens arrived from the fabricators with very rough web copes. The column plates were joined using full penetration welds at the corners. This is standard practice in the design of box columns in California. The beam flanges were welded to the column walls using single bevel full penetration welds with 1/4 inch root opening and with a fillet weld cover. The shear tabs were welded to the column wall using 3/16 inch fillet welds each side of the shear tab plate.

Due to the limited funding for the program the specimens were donated by local structural steel fabricators. This meant that each specimen was built by a different fabricator which resulted in some variation in the quality of the work and the method of fabrication as well as in the source of the steel used. However, the greatest variation in the specimens was in the quality of the welding.

Except where noted in the descriptions of the individual specimens the back up bars at the full penetration welds between the beam flange and the column were removed. Although it is not a customary practice in the field to remove the backup bars this was done in order to facilitate viewing of the welds during the test. Removing the backup bars and the associated tack welds, which are initially used to attach the backup bar to the column, also eliminated the possibility of a crack initiating in the area around the backup bar and propagating into the full pen weld. This resulted in a better indication of how and where the initial crack originated and propagated. Removal of the backup bars is accomplished by using copper plates as the backup bars. These are readily removed after the weld is complete.

In many cases a specimen was reused by cutting the beam off one side of the box column and welding a new beam on the opposite side of the column. It is felt that reusing the opposite face of a box column would have very little effect on the subsequent behavior of the new specimen as the back face of the column was not highly stressed. This was indicated by observation of the whitewash on the back side of the columns.

A summary of the characteristics of each specimen is given in Table 3.1. The third column labeled "Front & Back" refers to the thickness of the front and rear column plate and the fourth column of the table labeled "Sides" refers to the thickness of the sidewalls of the column, which were three quarters of an inch in all cases for uniformity. The sixth and seventh columns of Table 3.1 refer to the section modulus and plastic modulus properties of the beam and the final two columns of the table give the same properties for the box column. Typical fabrication details for all of the specimens are shown in Fig. 3.5. Detailed descriptions of each specimen are given in the following paragraphs.

3.4.1 Specimen 1

Specimen 1 was made by connecting a W16x40 beam to an 11 inch square (outside dimensions) box column fabricated from 3/4-inch plates. No internal or external stiffener plates were used. Details of the column are shown in Fig. 3.6. The heavy beam and light column walls were chosen to ensure that there would be significant interaction of the connection with the column wall. This being the first specimen, there were several details present which were corrected on subsequent specimens. The back up bars were left in place and the web copes were not ground smooth. The beam was bent slightly about its vertical axis, out of the plane of the web, and the column itself was slightly out of plumb. On subsequent specimens the specification provided to the fabricator was revised to clearly state that the subassembly should be checked to insure that it was "square, plumb and level" both before and after welding and also that the web copes were ground smooth.

3.4.2 Specimen 2

Specimen 2 was made by connecting a W16x26 beam to an 11 inch box column with front and back walls made of 1-1/4 inch plate and side walls made from 3/4 inch plate. No stiffeners were provided. Overall fabrication details are shown in Figure 3.7. For Specimen 2, a lighter beam was used in conjunction with a much heavier column wall in order to simulate a beam framing into a column closer to the base of a structure, where the higher axial loads dictate much thicker walls than near the top of the structure. By using thicker walls on the front and back of the column the plastic modulus of the column was increased by 36% while the reduction in beam size decreased it's plastic modulus by 40%.

3.4.3 Specimen 3

Specimen 3 was made by welding a W16x40 beam to an 11 inch column with walls fabricated from 3/4 inch plate. The beam and column dimension were the same as Specimen 1. In addition two 1/4 inch stiffener or continuity plates were welded inside the box column in the same plane as the beam flanges. The idea was to take a very flexible connection and add internal stiffener plates to determine how much the plates improved the performance of the connection. The heavy beam and 3/4 inch walls used in Specimen 1 caused the connection to be quite flexible and the test data attained from the first specimen would provide a baseline against which to compare the stiffened connection.

The continuity plates were fabricated from 1/4 inch plate which was half the thickness of the 1/2 inch beam flanges although normal design practice is to make the continuity plates the same thickness as the beam flanges. This was done in order to determine if the half thickness continuity plates would perform as well as full thickness stiffeners which would be tested later. It is also normal design practice to weld the stiffeners to the interior side of the box column walls using full pen groove welds on three walls of the column while welding the fourth side of the plate to the column using an electroslag weld.

Because the test specimen had a beam on only one side of the column, rather than on two adjoining sides as would be found in the field, it was decided to weld the stiffener to the side of the column carrying the beam and the two adjacent sides using full pen groove welds and to leave the side of the stiffener plate away from the beam unwelded. Studies of a finite element model of this connection showed that this would not greatly effect the behavior of the connection. Overall fabrication details are shown in Fig. 3.8.

Normally, specimens were delivered from the fabricators fully assembled, however in the case of Specimen 3, the top and bottom bearing plates were left off the column to allow access to the internal stiffener plates for the attachment of strain gauges. It could be seen that small angles were used as backup bars for the full penetration welds along the corners of the columns. After the strain gages were placed, the column cap and base plates were welded onto the column walls in the lab prior to installation in the test frame.

3.4.4 Specimen 4

Specimen 4 was fabricated by removing the W16x24 beam from Specimen 2 and welding a W16x40 beam on the opposite side of the column. Details of Specimen 4 are shown in Fig. 3.9. The work was done by a commercial fabricator on their premises. It was felt that the testing of Specimen 2 had not affected the back wall of the column and would not effect the results of the tests of Specimen 4. The new welds were ultrasonically tested and no defects were found. While the column in Specimen 4 had the same properties as Specimen 2, using the larger size beam increased the section modulus of the beam by 68% and the plastic modulus of the beam by 65%. The ratio of the width of the beam flange to the width of the column increased from 1:2 to 1.5:2.

3.4.5 Specimen 5

Specimen 5 was made by welding a W16x26 column to an 11 inch box column with one inch front and back walls and 3/4 inch side walls. Fabrication details are shown in Fig. 3.10

No stiffeners were provided. Specimen 5 was similar to Specimen 4 in all respects except for the reduction in the thickness of the column wall. By variation of one parameter only it was hoped to obtain a better understanding of the role the thickness of the column wall plays in the stiffness and strength of the connection.

3.4.6 Specimen 6

Specimen 6 was made by removing the W16x26 beam from Specimen 5 and welding a W16x26 beam to the back side of the column. The column was rebuilt at a commercial fabricators works. The backup bars were not removed for this test. After the new beam was welded in place the welds were tested ultrasonically and proved to be satisfactory. Overall fabrication details are shown in Fig. 3.10.

3.4.7 Specimen 7

Specimen 7 was made by welding a W16x26 beam to an 11 inch column with 3/4 inch walls. The W16x26 beam had a plate welded to the outside edge of each flange to extend the width of the flange to equal the width of the box column. A detail of the specimen is shown in Fig. 3.11. The "external stiffeners" were welded to the edge of the beam flanges using full penetration welds. Extending the beam flange width to the full width of the column was intended to provide a direct stress path from the flange into the side walls or webs of the column. This should reduce the deformation of the front wall of the column, as it would no longer have to transfer the tensile or compressive force in the flange to the side walls of the column through bending. By reducing the deformation of the front wall of the column the connection should become more rigid as well as having more ductility. The external stiffeners would also be more economical to fabricate than the internal ones.

3.4.8 Specimen 8

Specimen 8, as shown in Fig. 3.6, was made by removing the beam from Specimen 7 and welding a new W16x40 beam to the back side of the column. This specimen had the same beam size and wall thickness of Specimen 1. Specimen 1 was only loaded monotonically and Specimen 8 was tested by increased cyclic loading. It was also intended that Specimen 8 would provide a check on the results from testing Specimen 1. After welding the beam to the column, the welds were tested ultrasonically and were found to be satisfactory. The welding was done by a fabricator at their plant.

3.4.9 Specimen 9

Specimen 9 was made by welding a W16x40 beam to an 11 inch box column with 3/4 inch walls. The column had 1/2 inch internal stiffener (continuity) plates in the plane of both beam flanges. The continuity plates were attached to the front and two side walls of the column by full penetration welds and not welded to the back wall of the column. This specimen differs from Specimen 3 only in respect to the thickness of the continuity plates. Specimen 3 had 1/4 inch continuity plates which were half the thickness of the beam flange. This specimen is representative of current design practice in the industry, with the exception that the continuity plate is not welded to the fourth wall of the column. Fabrication details for the specimen are shown in Fig. 3.12.

3.4.10 Specimen 10

Specimen 10 was fabricated by welding a W16x40 beam to an 11 inch box column with 3/4 inch walls, No internal stiffeners or continuity plates were provided but the beam flange was widened to the full width of the column by welding 1/2 inch cover plates to the top and bottom beam flanges. The concept being tested in this specimen is similar to that tested in Specimen 7. However, instead of welding the plates by full penetration groove welds directly to the beam flange tips the plates extend the full width of the box column, and are welded over the top and bottom flange using fillet welds to connect to the beam flanges. The cover plates were welded to column wall using full penetration single bevel welds. These welds were ultrasonically tested after welding and found to be satisfactory. However, it was not possible to ultrasonically test that part of the cover plate to column weld located over the beam flange due to the beam cover plate interface which interfered with the ultrasonic waves. Fabrication details are shown in Fig. 3.13.

3.4.11 Specimen 13

Specimen 13 was fabricated as a typical strong axis connection with a W16x40 wide flange beam framing into the flange of a W12x132 column and was tested to serve as a baseline connection for comparison with the results from the box column tests. The connection included 1/2 inch web stiffener plates but no web doubler plates. Fabrication details are shown in Fig. 3.14.

3.5 Test Procedure

After receipt of the test specimen from the fabricator the areas where the strain gauges were to be applied were ground to remove rust and mill scale and to provide a smooth surface. The specimens were moved into position in the test frame by means of an gantry crane and the base of the specimen was welded to the base of the test frame with 3/8 inch fillet welds. The top of the specimen was held rigid against horizontal motion by two angles which were bolted to the test frame using A325 high strength bolts. In early tests the angles were also bolted to the specimens but after Specimen 3 the angles were welded to the specimens.

The beam was loaded using a 75 ton hydraulic cylinder. The end plate of the beam was bolted to a clevis which was connected to an eye on the end of the cylinder plunger by a 3 inch diameter pin. In the first specimens the end plate was welded to the beam in the shop, however, due to difficulties in getting the holes to align between the beam end plate and the base plate of the clevis, in later specimens the plate was shipped loose and welded to the beam end in the lab after it had been bolted to the clevis base plate.

After the beam was welded and bolted in place the strain gauges were epoxied in place using high strain epoxy and the LVDTs were attached with a two part epoxy. The location of the strain gauges is shown in Fig. 3.3 and the position of the LVDTs is shown in Fig. 3.4. It should be noted that in Specimens 1 through 7 the load was applied 58 inches from the face of the column but displacements were measured 36 inches from the face of the column. The signal from the strain gauges was amplified through Vishay signal conditioning equipment and data from the strain gauges and LVDTs was collected by a data acquisition program running on an IBM PC/XT. The data acquisition program allowed the collection of 16 channels of data either by self triggering or when triggered from the keyboard. During this series of tests each set of data points were taken after triggering from the keyboard at approximately 4 second intervals, however, the time between data points is not uniform.

At the start of each test the strain gauges were calibrated with a known resistance and the strain gauges and LVDTs were zeroed. The column was then axially loaded to a uniform stress of approximately 12 ksi. The required load was calculated by multiplying the cross sectional area of the column by 12 ksi. The applied load was read by multiplying the pressure of the hydraulic fluid by the piston area of the two hydraulic cylinders. A separate data file was created for stresses and displacements measured during loading of the column.

After loading the column to the 12 ksi stress level, the strain gauges, except for those measuring strains in the column wall, were re-zeroed and the initial load was applied to the beam tip. The loads on the initial cycle were approximately those which would cause a stress in the beam due to moments at the column face of 0.66 F_y. The applied tip loads were increased in subsequent cycles by approximately 4 kips per cycle until failure of the beam.

The load applied to the beam was controlled by varying the pressure supplied to the hydraulic cylinder using two variable pressure relief valves. The applied tip loads and beam displacements were monitored during the test by an x-y recorder attached to channels 11 and 12 which were the vertical LVDT measuring beam displacements and the load cell on the Atlas cylinder, respectively. During the test the loading was often stopped to observe the specimen and take photographs of any visible cracks or other developments. A log was maintained during the test to record observations such as flaking of the whitewash, formation and development of cracks, etc.

The test procedures used followed closely those described by Tsai and Popov [16][28] and Engelhardt [29] in their experiments conducted at the University of California, Berkeley.

TABLE 3.1

SPECIMEN MECHANICAL PROPERTIES

Specimen Number	*Beam Size*	*Front & Back*	Sides	*Stiffeners*	S_x	Z_x	S_{col}	Z_{col}
1	$W16 \times 40$	3/4	3/4	–	64.7	72.9	78.9	118.4
2	$W16 \times 26$	1-1/4	3/4	–	38.4	44.2	107.4	161.2
3	$W16 \times 40$	3/4	3/4	1/4″ *Internal*	64.7	72.9	78.9	118.4
4	$W16 \times 40$	1 1/4	3/4	–	64.7	72.9	107.4	161.2
5	$W16 \times 26$	1	3/4	–	38.4	44.2	93.6	140.4
6	$W16 \times 26$	1	3/4	–	38.4	44.2	93.6	140.4
7	$W16 \times 26$	3/4	3/4	1/2″ *External*	38.4	44.2	78.9	118.4
8	$W16 \times 40$	3/4	3/4	–	64.7	72.9	78.9	118.4
9	$W16 \times 40$	3/4	3/4	1/2″ *Internal*	64.7	72.9	78.9	118.4
10	$W16 \times 40$	3/4	3/4	1/2″ *External*	64.7	72.9	78.9	118.4
13	$W16 \times 40$	$W12 \times 136$	–	–	64.7	72.9	186	214

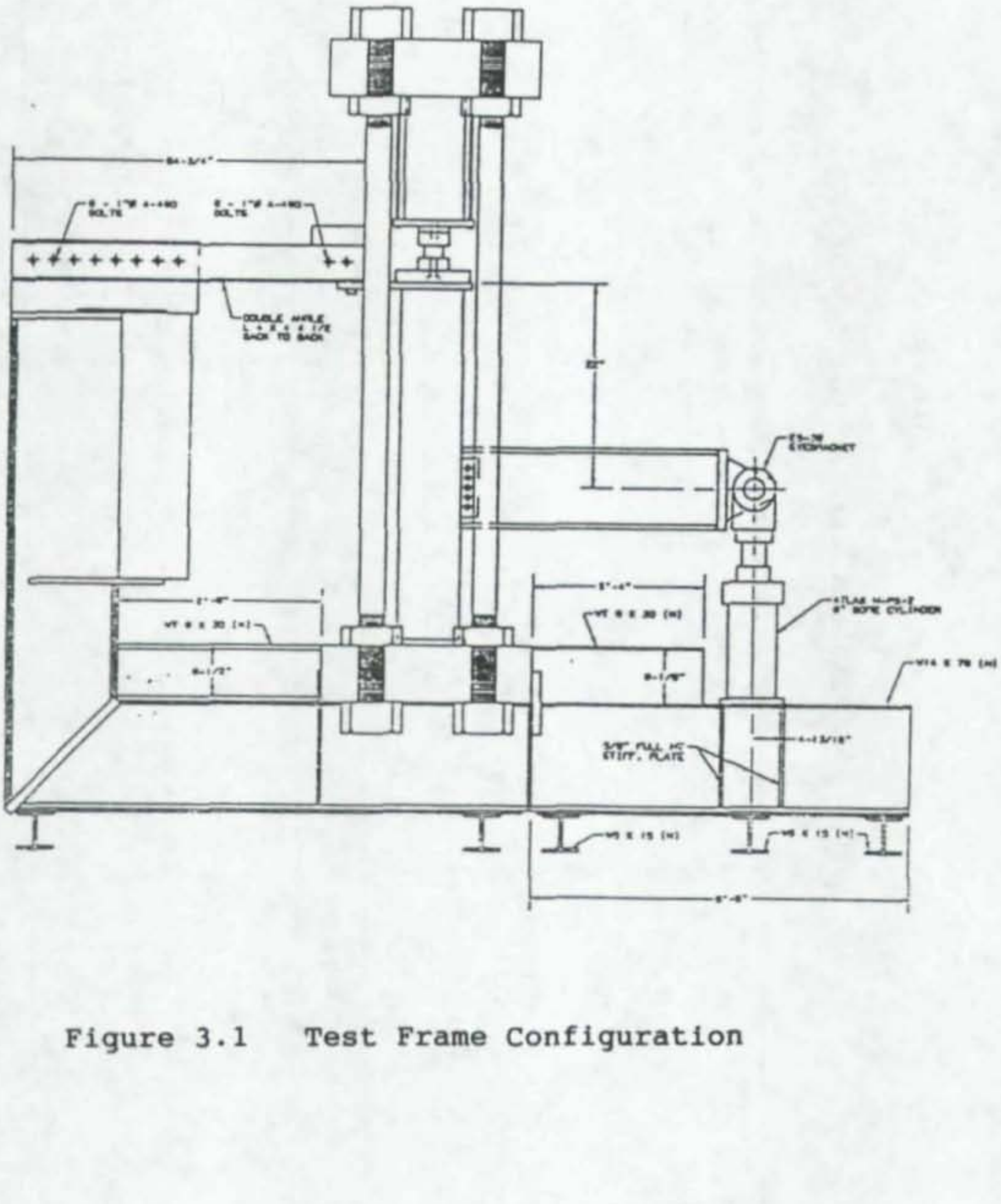

Figure 3.1 Test Frame Configuration

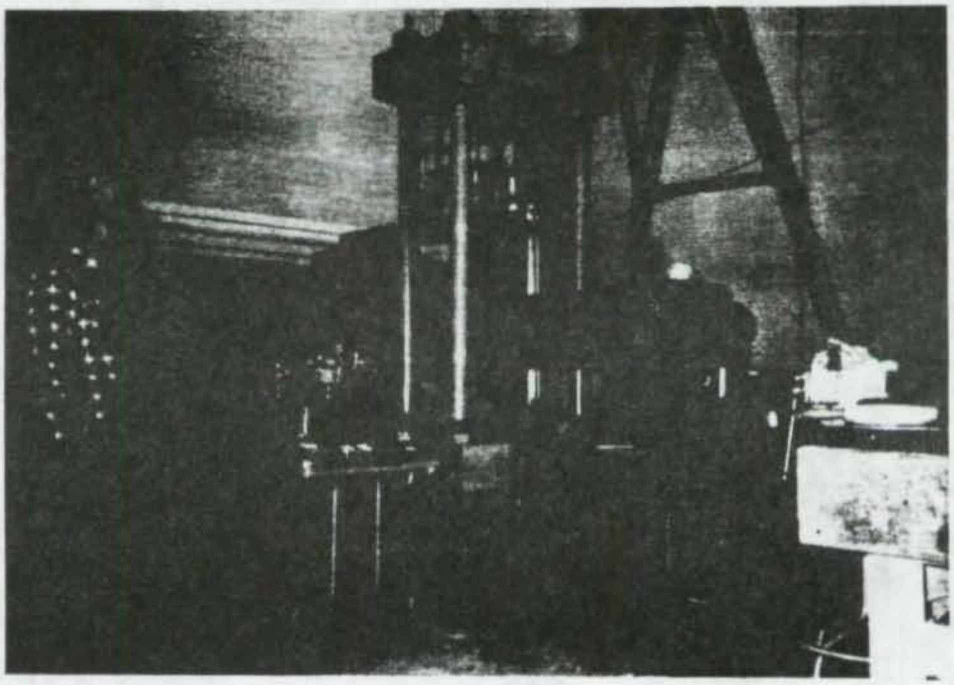

Figure 3.2 Test Frame for Connection Tests

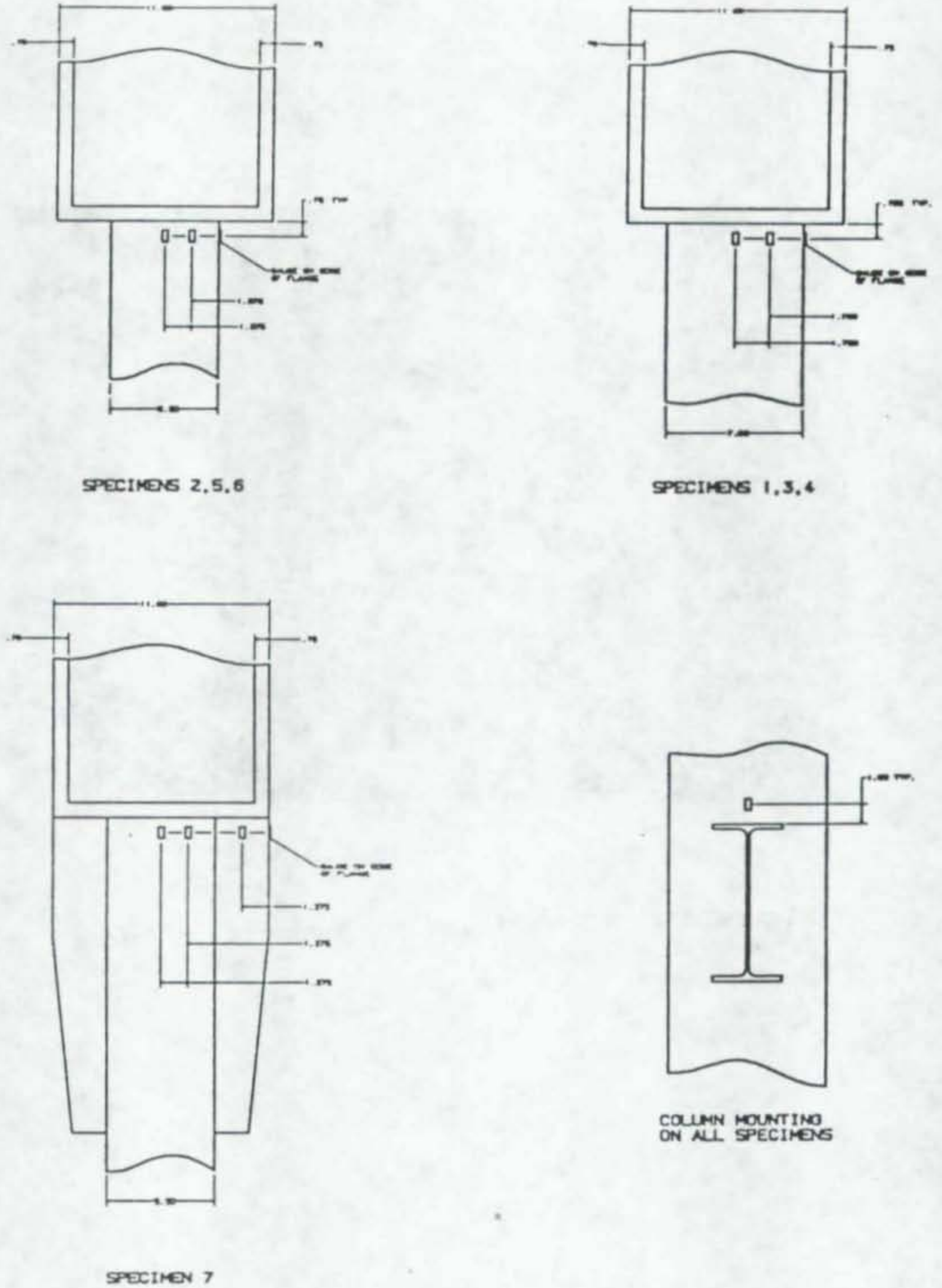

Figure 3.3 Strain Gage Locations

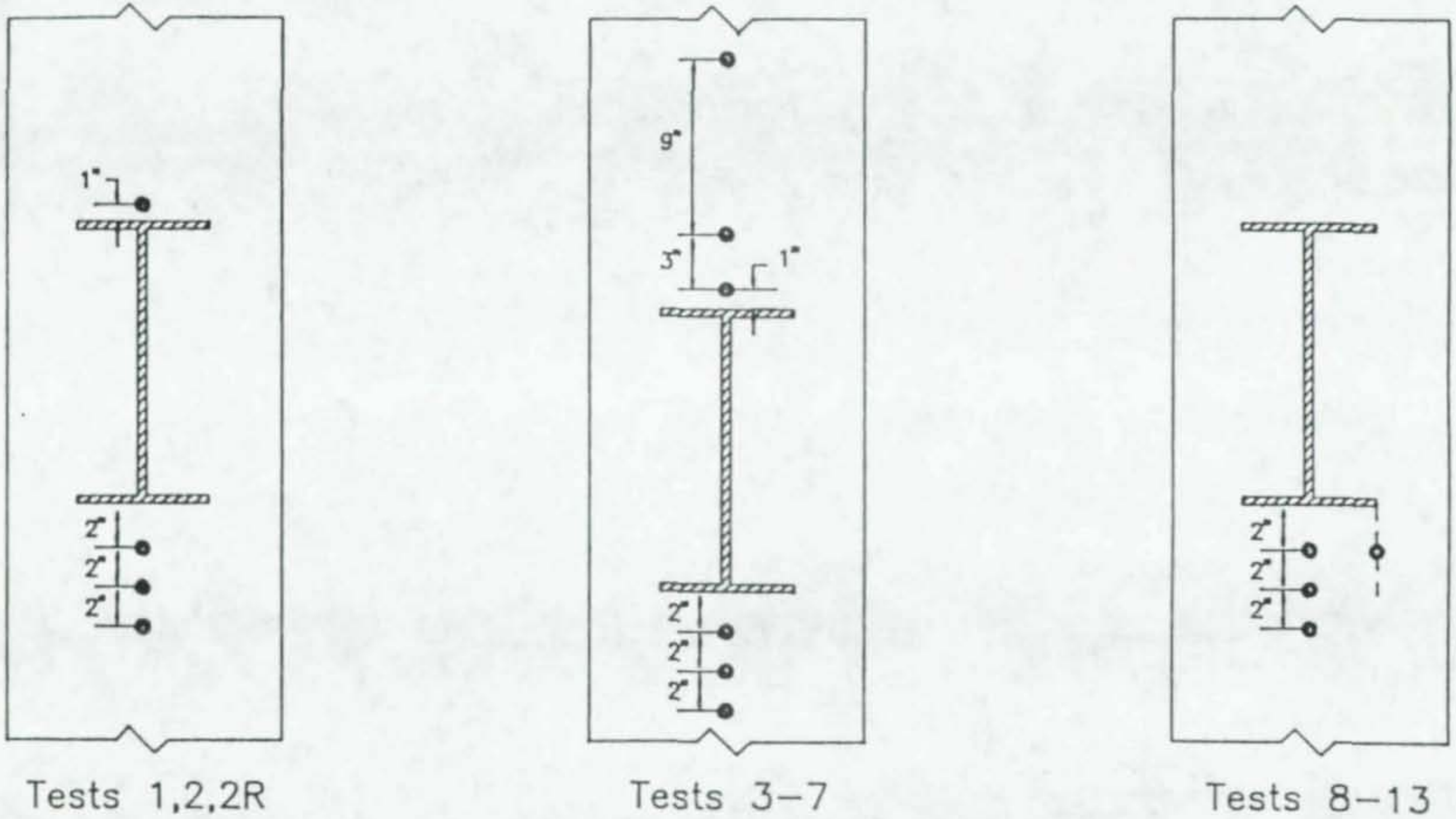

Location of LVDTs on Column Face

Figure 3.4 LVDT Locations

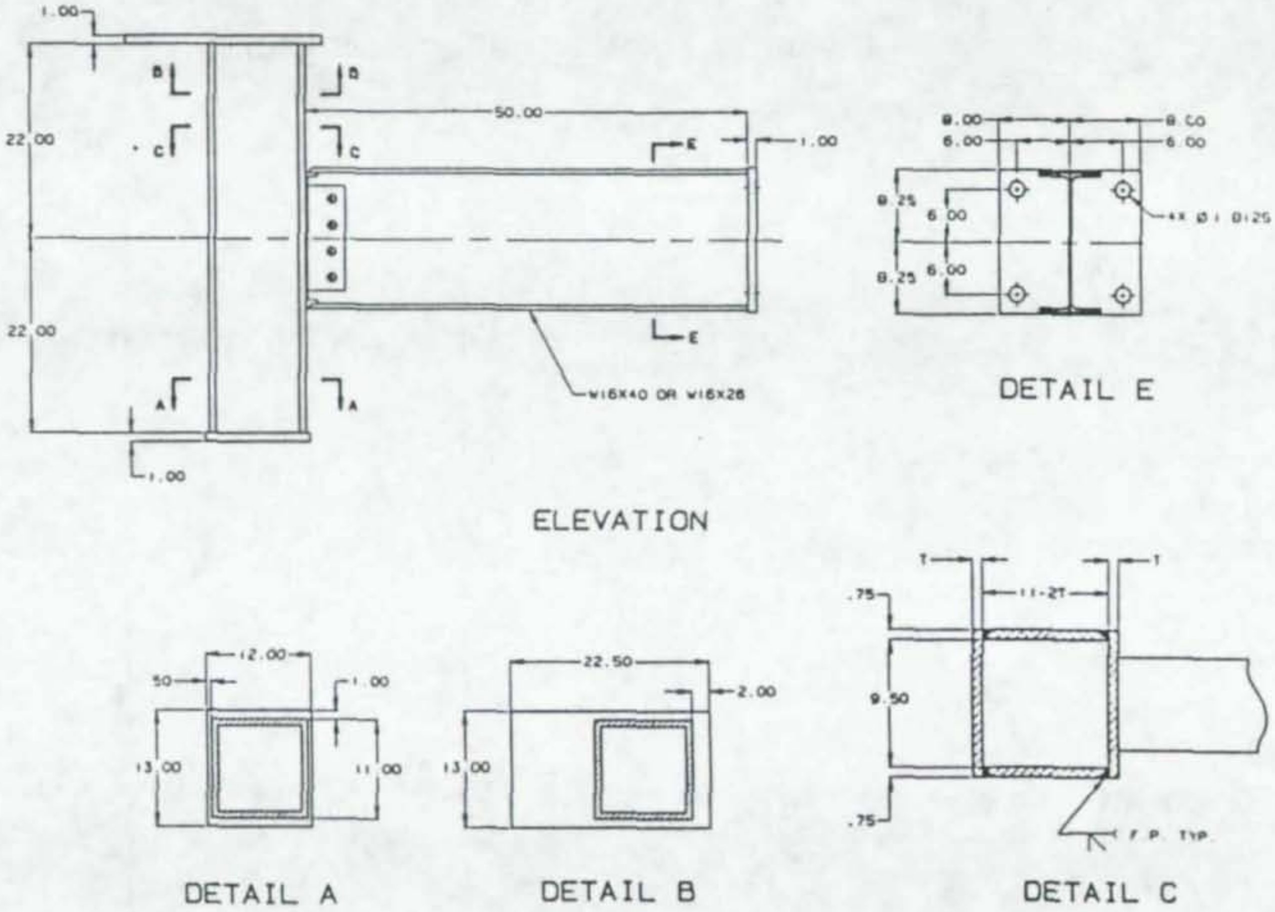

Figure 3.5 Typical Detail For All Specimens

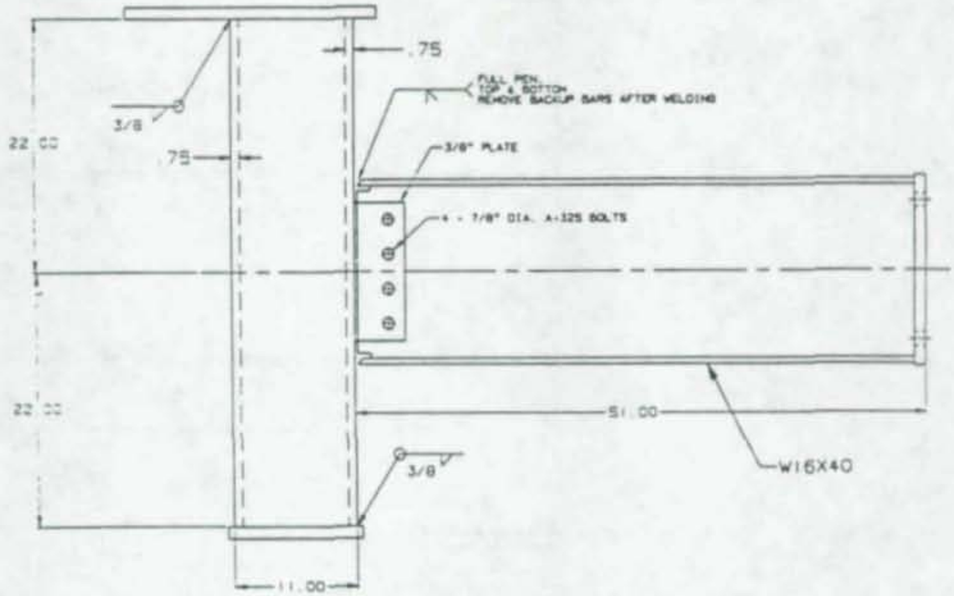

Figure 3.6 Test Specimen #1 and #8 Details

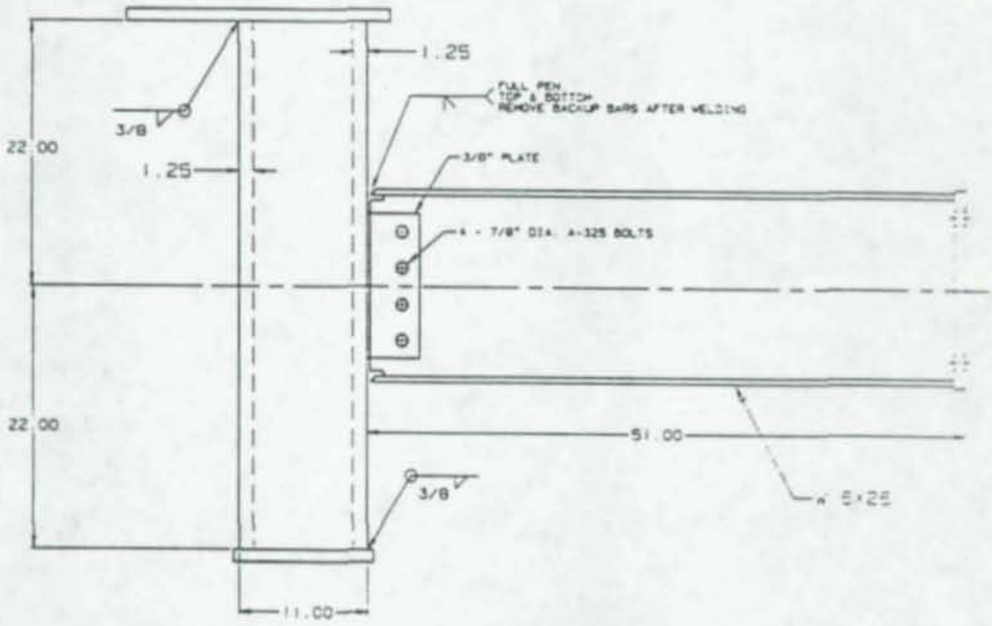

Figure 3.7 Test Specimen #2 Details

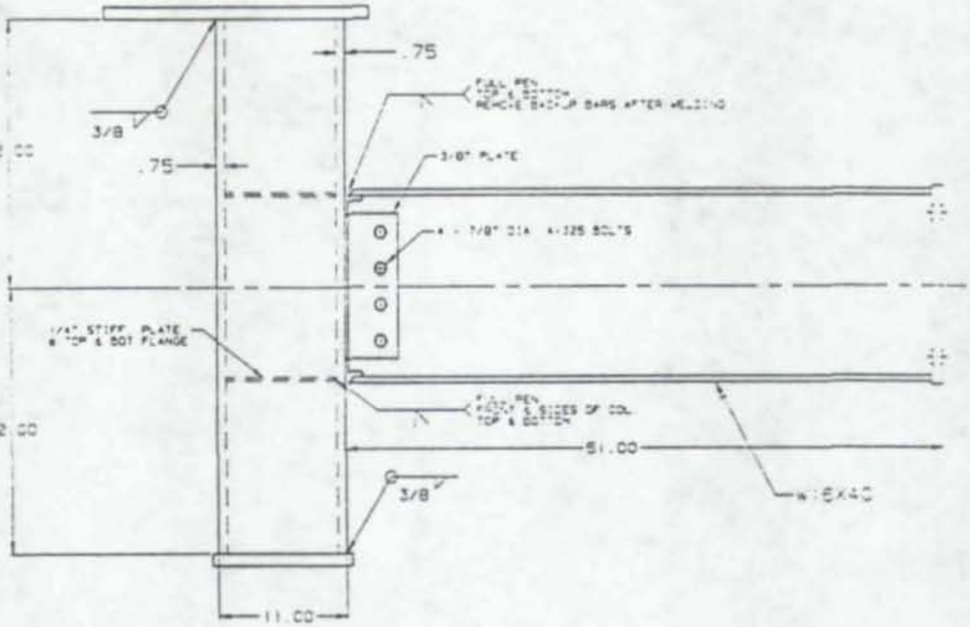

Figure 3.8 Test Specimen #3 Details

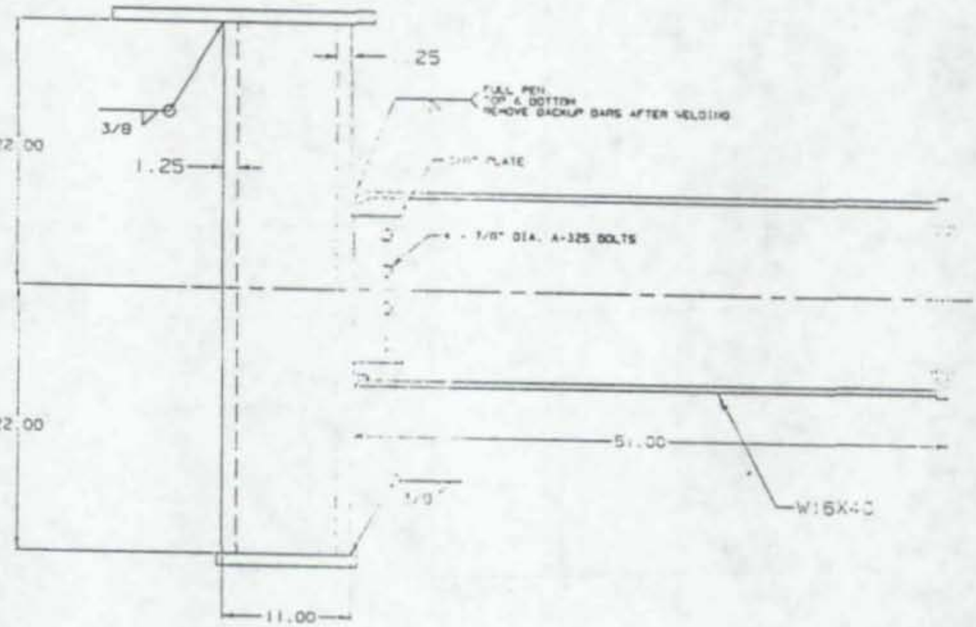

Figure 3.9 Test Specimen #4 Details

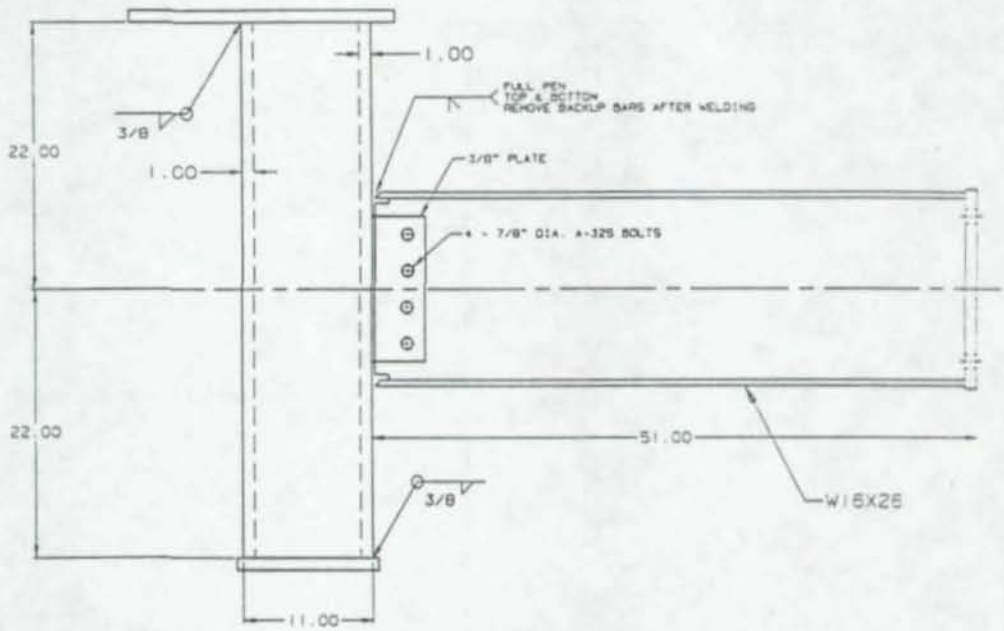

Figure 3.10 Test Specimen #5 and #6 Details

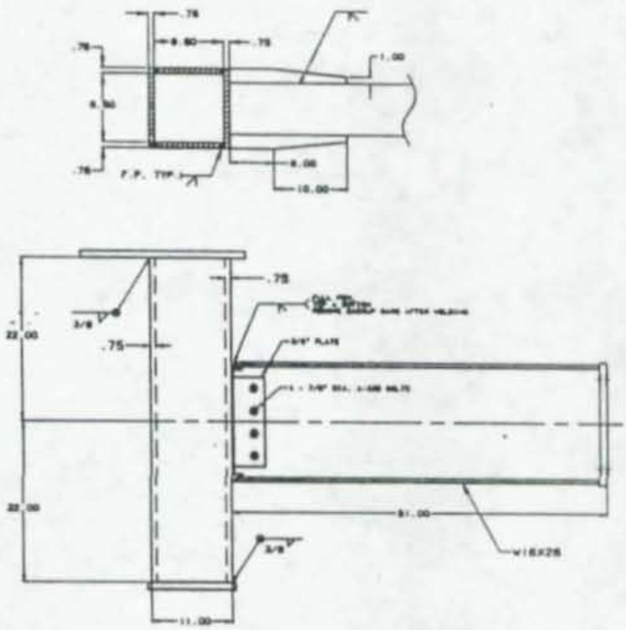

Figure 3.11 Test Specimen #7 Details

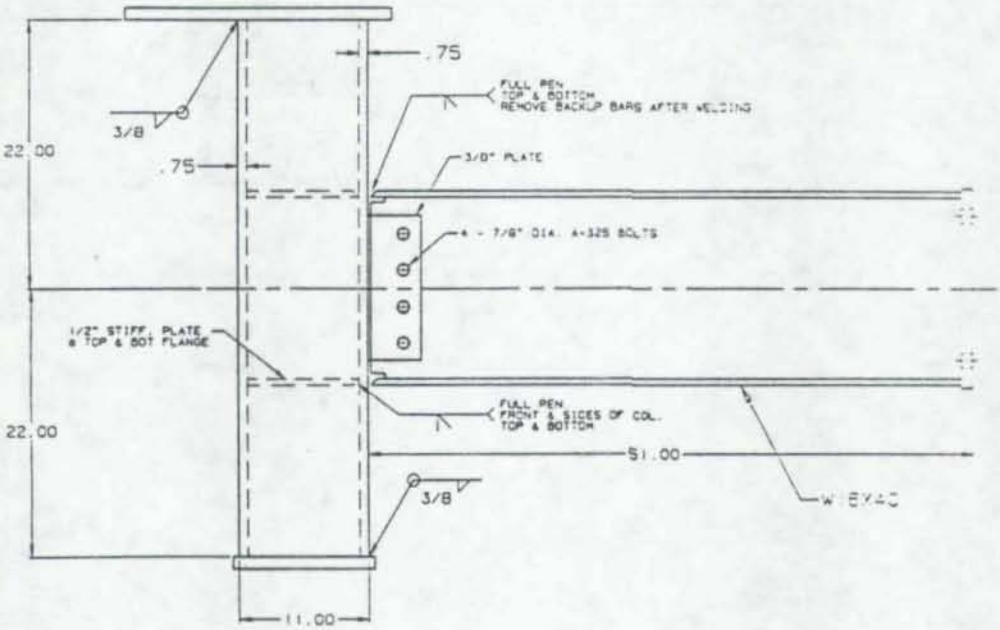

Figure 3.12 Test Specimen #9 Details

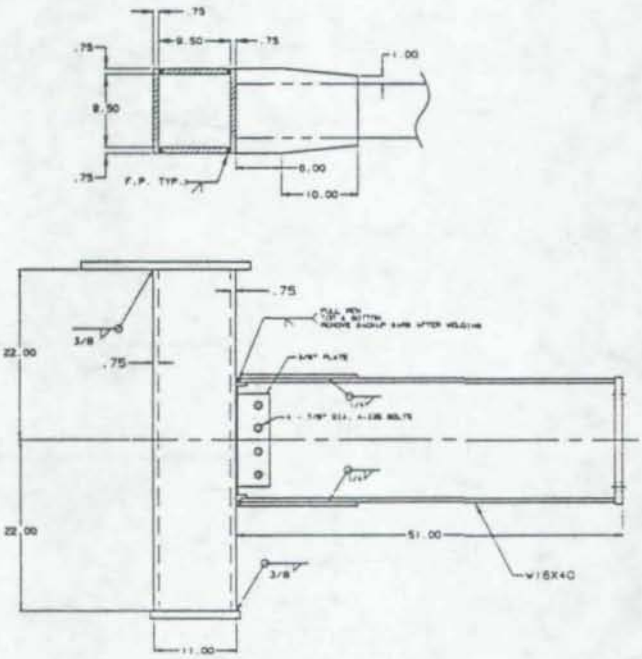

Figure 3.13 Test Specimen #10 Details

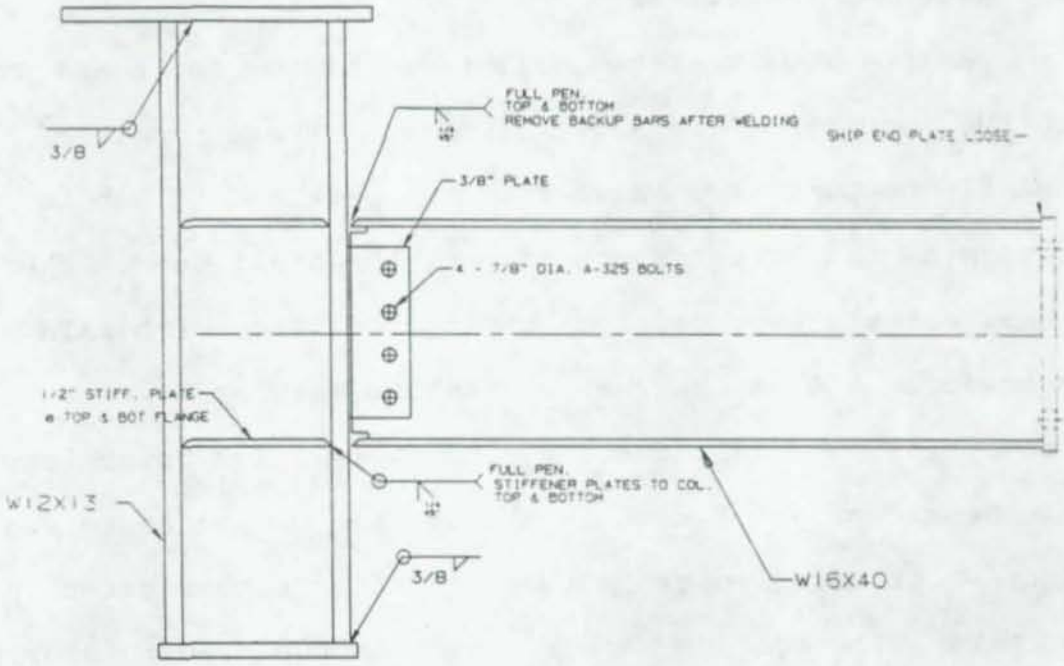

Figure 3.14 Test Specimen #13 Details

4.0 EXPERIMENTAL RESULTS

4.1 Material Properties

As previously stated, all steel plates and beams used in the specimens were ASTM A36 steel. Where possible tensile coupons were taken from the beam and column to determine the actual properties of the steel used. These tensile tests were carried out in accordance with ASTM procedures [30] on an Instron testing machine by a commercial materials testing laboratory. The gauge length of the extensometer used in the tensile coupon tests was one inch which corresponds to the half size coupons given in ASTM E8. The testing machine used was equipped to provide a continuous graph of force versus displacement during the testing of the coupon and the curves produced were typical of those for 36 ksi mild steel.

Results of the tensile testing of the coupons are tabulated in Table 4.1 and summarized in Figs. 4.1 to 4.3. The yield stresses obtained from the coupon tests are summarized in Fig. 4.1. All coupons exhibited a tensile yield stress greater than the 36 ksi nominal yield stress specified for the steel used. The mean average yield stress for the beam coupons was 49.3 ksi, which is 37% greater than nominal yield strength. The maximum value of 60.5 ksi for Specimen 5 was 68% over nominal yield and the minimum value of 41.0 ksi for Specimen 9 was 14% greater than nominal. The mean average yield stress for the steel plates used in the fabrication of the columns was 44.4 ksi or 23% over nominal yield strength. The maximum was 51.7 ksi in Specimen 3 and the minimum was 37.9 ksi, or 5% over nominal, in Specimen 9. The ultimate stresses obtained from the coupon tests are summarized in Fig. 4.2. The mean average ultimate stress for the coupons cut from the beams was 69.6 ksi with a low value of 64.5 ksi in Specimen 3 and a high value of 79.2 ksi in Specimen 2. The mean average ultimate stress in the plate steel used for the columns was 68.8 ksi with a high value of 75.7 ksi and a low value of 63.2 ksi. Coupon data for elongation is presented in Fig. 4.3. Elongation at fracture for the coupons from the beam material was 34.5% with a low value of 23% in Specimen 2. Elongation at fracture for the column steel averaged 36% with a low value of 30%.

4.2 Test Results

The performance of each specimen has been tabulated in Tables 4.2 and 4.3. Shown in Table 4.2 are the total number of cycles experienced by each specimen during the test and the maximum cantilever beam load applied to the specimen. The maximum beam load was then converted to a moment at the column face by multiplying by 52 inches, the distance from the column face to the end plate of the beam. The yield moment of the beam was calculated using the published section modulus and the nominal yield stress of the steel, F_y = 36 ksi. The full plastic moment of the beam was also calculated using the published plastic modulus for the beam and the nominal yield stress. The maximum moment in the connection during the test was then divided by the calculated yield moment and the calculated full plastic moment to give the ratios M_{max}/M_u and M_{max}/M_p. The moment capacity of the connection based on the Blodgett equation, Eq. 2.2, was also calculated and compared with the maximum test moment. Finally the rotation at yield and the ultimate rotation were tabulated. Table 4.3 follows the same format as Table 4.2 but uses the actual material properties as listed in Table 4.1 in the calculation of M_y and M_p. The variation in actual moment capacity and nominal moment capacity is shown in Fig. 4.4.

For each of the tests the actual load-displacement curves and the loading time history are presented. Superimposed on the graph of the load history are two dashed lines indicating the nominal beam tip force required to cause nominal plastic moment in the beam. A description of each of the tests conducted and a summary of the behavior of each specimen follows:

4.2.1 Specimen 1 [W16x40 Beam, 3/4" Faceplate]

Because it was the first test using the modified test frame, hydraulics and data acquisition equipment, the test of Specimen 1 was used as a shakedown of the lab equipment and test procedure as well as a subject of experimental investigation. For this reason it was decided that the test should be run monotonically. A monotonic test would also give a baseline against which to compare future cyclic load tests using a specimen built to the same specification as Specimen 1.

The column was given an initial axial load corresponding to a compressive stress in the column steel of 12 ksi. The beam was loaded slowly in an upward direction, with frequent halts in the loading to observe the beam and test equipment. The test ran smoothly and produced good data as evidenced by the load displacement curve shown in Fig. 4.5. Failure of the specimen was by cracking in the heat affected zone of the beam flange starting at the toe of the beam to column weld as shown in Fig. 4.6.

4.2.2 Specimen 2 [W16x26 Beam, 1-1/4" Faceplate]

Cyclic testing of the beam-column subassemblies was initiated with Specimen 2. An initial axial load of 600 kips was applied to the column which gave a calculated compressive stress in the column steel of 14.9 ksi. The cantilever load versus beam deflection is shown in Fig. 4.7. The beam responded elastically up to a level of about 26 kips which is somewhat less than that required to reach the nominal beam yield stress of 36 ksi (28.8 kips). The maximum load obtained was approximately 40 kips which is 68% above the force calculated to produce a stress of 36 ksi in the beam and 46% above that required to produce a full plastic hinge in the beam based on nominal yield strength.

The hysteresis loops exhibited stable characteristics throughout the entire test. The maximum rotation experienced by the connection was approximately 2.1% (0.021 radians). From the loading history, shown in Fig. 4.8, it can be noted that the beam experienced 6 1/2 cycles of which three were above the nominal plastic moment capacity. Failure occurred by a crack initiating in the web cope at the bottom flange and propagating along the flange as shown in the photograph in Fig. 4.9.

Based on the coupon tests, the beam will yield at a strain of 0.00161 in./in. and the column at 0.00168 in./in. Data from a strain gauge located at the centerline of the top beam flange is shown in Fig. 4.10. Here it can be seen that the hysteresis loop is very stable and that the maximum strain of 0.0100 is well above the yield value. Data from a gauge at the edge of the top flange is shown in Fig. 4.11. In this case the maximum strain is 0.0185 which is also well above yield and probably in the strain hardening region of the stress-strain curve which normally starts at a strain of about 0.015. The strain at the flange tip is also substantially above the value at the centerline. Data from a gauge located at the centerline of the side wall of the column is shown in Fig. 4.12 where the strains are much smaller and well within the elastic range. Data for a gauge located at the center of the front face plate of the column is shown in Fig. 4.13. Here the strains reach a maximum value of .0023 in./in. which again is well above yield.

4.2.3 Specimen 3 [W16x40 Beam, 3/4" Faceplate, 1/4" Internal Stiffeners]

Specimen 3 had internal stiffener plates as shown in Fig. 4.14. The photo shows the inside of the box column prior to the welding of the column cap plate in place. Of particular interest are the use of the angles as backup bars in each corner of the column and the welding of the stiffener plate to the column walls. An initial axial load of 360 kips was applied to the column corresponding to an axial stress in the column of 11.7 ksi. The hysteretic loops of load versus beam displacement for Specimen 3 are shown in Fig. 4.15.

The cyclic loading history for this test is shown in Fig. 4.16. The beam was initially loaded to 26 kips corresponding to the nominal allowable stress capacity of the beam. During the second cycle the load was increased by 33% to 34 kips. The third cycle increased the load to 40 kips at which time whitewash was observed flaking off the back wall in two horizontal lines eight inches and 12 inches above the base plate indicating some bending in the column. During the sixth cycle diagonal lines were observed in the whitewash between the two stiffener plates indicating panel zone effects in the box column. During cycle eight a degradation of the strength of the joint was noticed in the force displacement curve. That is the force - displacement curve was inside the previous loops showing greater displacement for the same force. This was noticed on the next cycle as well and it was determined that the top of the column was deflecting. The axial load was increased to 500 kips to attempt to prevent this deflection. This increased the stiffness of the hysteresis loop on the next cycle.

Following the eleventh cycle it was determined that the brace that stabilized the top of the specimen was not being effective due to a loosening of the bolts that hold the brace to the test frame and these bolts were then torqued tight. The location of the top of the specimen in relation to the loading platen was also marked in order to detect any deflection of the top of the column. However, no differential movement between the specimen and the loading platen was discernable after tightening the bolts on the brace.

By the twelfth cycle, cracks had appeared at the edges of the top and bottom beam flanges at the interface of the beam flange with the full penetration weld joining the flange to the column. Over the next several cycles these cracks opened but did not appear to propagate and there was no significant loss of strength in the hysteresis curve. In previous tests of unstiffened connections, cracks appearing in the weld at the beam column joint propagated much more quickly leading to failure of the connection. It can be surmised that the presence of internal stiffener plates reduces the stress gradient along the interface, thereby inhibiting the propagation of the crack and increasing the ductility in the joint. The maximum cantilever load carried by the joint was 73 kips at cycle fifteen. Failure occurred on the downward stroke of cycle fifteen at 64 kips. The failure was very sudden and was accompanied by a loud bang. The top (tension) flange separated completely from the full penetration weld holding it to the column face as shown in Fig. 4.17. There was considerable flaking of the whitewash near the bottom of the column, but not much near the top, suggesting that the column had cantilevered about its base, which was welded to the base of the test stand.

Fig. 4.18 shows the pattern of flaking of the whitewash on the column. This photograph was taken after completion of the testing. After testing the specimen was removed from the test frame and taken to a steel fabricator where the beam was removed and the column sawn lengthwise, in the plane of the beam web, to allow the internal stiffeners to be observed. Fig. 4.19 shows the column half sections with the column stiffeners. It will be noted that the column stiffeners buckled and exhibit a large displacement out of plane. Both continuity plates appeared to have buckled, however only the plate which was under the compression flange at the time of failure showed the large out of plane displacements. The tensile forces in the tension flange at the time of failure appeared to be great enough to pull the continuity plate straight again. The welds connecting the stiffener plate to the walls of the column appeared to be in good shape.

The buckling of the continuity plate appears to be a result of its high ratio of width to thickness ratio. Given a plate thickness of 0.25 inch and a width of 11 - 2(0.75) inches results in a b/t ratio of 38.0. Using plastic design requirements, the minimum width to thickness ratio for compressed flange plates in box sections (AISC Section 2.7) is given as 190 $\sqrt{F_y}$. Using F_y = 36 in the equation would give a minimum width to thickness ratio of 31.67. For the stiffener plate in the eleven inch box column with three quarter inch column walls the width would be b = 9.5 inches and the minimum required thickness of the plate would be t = 0.30 inches. This suggests that any design criteria allowing stiffener thickness less than the thickness of the beam flange include a check for b/t of the continuity plates. The buckling of the continuity plates undoubtedly resulted in a less rigid connection than if they had been designed so as to preclude buckling. Thicker continuity plates would most likely have forced the plastic hinges out into the beams rather than in the continuity plates in the columns. Having the inelastic behavior occur outside of the column rather than inside the column has some bearing on whether the connection could be adequately inspected and safely repaired after a major earthquake.

4.2.4 Specimen 4 [W16x40 Beam, 1-1/4" Faceplate]

The specimen was given an initial axial load of 500 kips which corresponds to an axial stress in the column of

12.4 ksi. The hysteretic loops of load versus beam displacement for Specimen 4 are shown in Fig. 4.20. The beam responded elastically up to approximately 54 kips which is just beyond the nominal elastic limit of the beam. The maximum load carried was 72 kips. The loading history is shown in Fig. 4.21. The beam was initially loaded to 10 kips which was 25% of the nominal yield strength of the beam. During the second cycle the load was doubled to 20 kips, increased to 30 kips during the third cycle and to 40 kips, which represented the nominal yield strength of the beam, during the fourth cycle. On the eighth cycle at 56 kips, flaking of the whitewash on the bottom flange of the beam, indicating plastic yielding, was noted (Fig. 4.22). This yielding was also confirmed by the force displacement curve. By the eleventh cycle at 62 kips the flaking of the whitewash due to yielding of the beam flange had progressed considerably as shown in Fig. 4.23. There was also some flaking of the whitewash in the front column wall. By the fourteenth cycle at 68 kips there were large cracks in the beam flange material in the bottom west flange and the top east flange (Figs. 4.24 and 4.25). Note that in Fig. 4.24 the crack has propagated two inches in from the tip of the flange but the beam was still able to sustain increasing loads.

Failure came on the downward stroke (top flange in tension) of cycle 15 with a force of approximately 40 kips. It should be noted that on the previous two cycles the maximum force that the connection and beam could sustain was 72 kips. The maximum rotation of the connection was approximately 3%. The ultimate load of 74 kips, giving a moment at the column face of 3848 in-kips, was 47% greater than that calculated to cause full plastic moment in the beam and 65% greater than that calculated to cause initial yield in the beam. The hysteretic loops were very stable until the last cycle and showed good symmetry. As shown in Fig. 4.21, the specimen underwent seven full cycles after reaching the nominal plastic capacity of the beam. During each of these cycles the connection and beam were able to carry an increasing load.

4.2.5 Specimen 5 [W16x26 Beam, 1 "Faceplate]

The hysteretic loops of force versus displacement are shown in Fig. 4.26. The bottom east flange had a slight bend in it prior to the start of the test, probably due to mishandling in fabrication or during transport. The loading sequence is shown in Fig. 4.27. An initial axial load of 400 kips was applied to the column at the beginning of the test and maintained throughout the test. The specimen behaved elastically through seven cycles up to a load of 34 kips, which was 41% larger than nominal yield stress but 16% less than first yield calculated using the yield stress obtained from the tensile coupon, F_y =60 ksi. During the eighth cycle at 36 kips there was some whitewash flaking of the sidewalls of the column indicating some panel zone interaction. During cycle ten, at a load of 40 kips, significant flaking of the whitewash on the top flange was noticed extending a distance of four inches from the column face. At cycle twelve, cracks had developed at both the east and west flange tips of the top flange. This occurred with an applied beam force of 44 kips which was just 10% over the yield strength of the beam based on the actual yield strength of the beam steel and 69% more than the nominal yield of the beam. On the upward stroke of cycle 14 with a force of 44 kips, a small crack started to show in the west tip of the bottom flange. On the downward stroke of cycle 14, it failed at a load of just over 40 kips. The maximum rotation of the connection was 2.9%. The ultimate load carried by the beam was 45 kips, producing a moment at the column face of 2340 in-kips. This moment was 69% over the moment required to produce nominal yield in the beam and 47% greater than the full plastic moment capacity of the beam. Failure was due to a complete separation of the flange from the full pen weld to the column face (Figs. 4.28 and 4.29). Note in Fig. 4.28 that the crack was located some distance away from the beam to column full penetration weld.

4.2.6 Specimen 6 [W16x26 Beam, 1" Faceplate]

The column in Specimen 6 was loaded during the test with an axial load of 800 kips, corresponding to an axial stress in the column of 22.5 ksi. The hysteretic loops of force versus displacement are given in Fig. 4.30 and the loading history in Fig. 4.31. This specimen was the same as Specimen 5 and one should expect similar results subject to the variability of the different beam material and the differences in workmanship. The specimen remained elastic until the seventh cycle when it showed some signs of yielding at 36 kips which compares with 34 kips for the previous specimen. During the eighth cycle some cracks appeared at the bottom of the backup bars. The welds used to attach the backup bars to the column appear to be a weak point in the connections where they are used. On the ninth cycle at a force of 43 kips some flaking of the whitewash was apparent indicating the initiation of inelastic behavior in the beam. During the fourteenth cycle at a force of 49 kips, there was a very noticeable buckling of the top flange as shown in Fig. 4.32. A crack formed at the tip of the bottom east flange and a crack also formed in the center of the top flange in the web cope area. Failure came on the downward stroke of cycle 15 and was characterized by an opening of the crack in the center of the beam (Fig. 4.33). Maximum load applied to the beam was 50 kips, which corresponds to a maximum moment of 2600 in-kips. This was 188% more than the moment required to develop the nominal yield strength of the beam and 134% more than the moment to develop the actual yield strength of the beam as calculated from the properties obtained from the tensile coupon tests. Maximum rotation of the beam and connection was 2.3%.

4.2.7 Specimen 7 [W16x26 Beam, 3/4 " Faceplate, Ext. Stiffener]

Specimen 7 was fabricated with a 3/4 inch column wall, and a W16x26 beam with beam flange extensions on each of the beam flanges. The force versus displacement curve is shown in Fig. 4.34. An axial load of 400 kips was applied to the top of the column inducing an average stress of 13 ksi. The cyclic loading history is shown in Fig. 4.35. The specimen showed elastic behavior for the first eight cycles up to a force of about 50 kips. During the ninth cycle at a force of 56 kips the whitewash on the specimen began to show signs of a plastic hinge forming in the beam just behind the flange extension plates as shown in Fig. 4.36. During the tenth cycle at a force of 60 kips diagonal flaking of the whitewash on the beam web began to appear indicating yielding due to shear in the beam web. On the downward stroke of the eleventh cycle a crack appeared in the west tip of the top flange. The crack at this point measured approximately 1/8 inch in length. Also, a longitudinal crack occurred in the column face plate at the east top beam flange as shown in Fig. 4.37. The force applied at the beam end at this time was 58 kips. During the upward stroke on cycle twelve the upper flange, which was under compression showed significant buckling at a force of 63 kips. The photograph in Fig. 4.38 shows the magnitude of the buckling of the beam flanges. On the downward stroke of the same cycle, at a force of 56 kips the crack widened to 1-1/4 inches. The connection failed on the downward stroke of the thirteenth cycle due to a propagation of the crack across the top beam flange as shown in Figs. 4.39 and 4.40.

The maximum rotation of the connection was approximately 2%. The ultimate load on the beam and connection was 63 kips, which produced a moment at the connection of 3276 in-kips. This moment exceeded the plastic moment of the beam by 106% and the moment calculated to cause nominal yield in the beam by 137%. The hysteresis loops were stable except for the last cycle. As shown in Fig. 4.35, the specimen underwent nine full cycles after reaching its full plastic moment. The use of flange extension plate allowed two plastic hinges to form at the end of the beam, the first just behind the extension plates and the second at the column face. The greatest plasticity of the beam occurred at the column where significant buckling of the beam flange took place. In calculating the applied forces as a percentage of nominal yield strength of the beam it is important to note whether the section modulus used is that of the beam or that of the beam with the extension plates attached. The addition of the extension plates increases the section modulus significantly. For the purposes of this paper the section modulus of the beam was used unless otherwise noted.

4.2.8 Specimen 8 [W16x40 Beam, 3/4" Faceplate]

Specimen 8 has the same configuration as Specimen 1. Specimen 8 was loaded cyclically while Specimen 1, as reported earlier, was loaded only monotonically. The force vs displacement curve for this test is shown in Fig. 4.41 and the load history is shown in Fig. 4.42. The first cycle took the load at the end of the cantilever up to 20 kips in both the upward and downward stroke. By the fifth cycle, which loaded the beam to 36 kips in both the up and down directions, there was very noticeable flaking of the whitewash on both the top and bottom flanges close to the column, indicating plastic strains in the beam flanges. The majority of the flaking was at the tips of the beam flanges. This flaking progressed on the sixth cycle which had a total force on the cantilever of 40 kips. On the seventh cycle cracks formed at the flange tips of the welds of both the top and bottom flanges as shown in Fig. 4.43. The eighth cycle which increased the force applied to the beam end to 44 kips, saw some degradation of the hysteresis loops. The tenth and eleventh cycles were done at reduced loadings of 22 and 30 kips respectively to see if the lower loading would have any effect on the response of the connection. The twelfth cycle was run at 41 kips which led to failure in the flange as shown in Fig. 4.44. The load of 41 kips at failure is equivalent to a maximum moment of 2340 inch-kips which is less than the yield moment calculated from actual material properties, M_y of 3021 inch-kips (see Table 4.3) and just slightly above the nominal yield moment calculated of 2329 inch-kips (Table 4.2). The moment at failure was also well below the calculated full plastic moment M_p using both nominal values for the steel yield strength (2624 in-kips) and actual material properties from the coupon tensile tests (3404 inch-kips). The specimen also experienced large rotations as can be seen from the moment rotation curves.

4.2.9 Specimen 9 [W16x40 Beam, 3/4" Faceplate, Int. Stiffener]

Specimen 9 represents current design practice in California. The force versus displacement hysteresis curves are presented in Fig. 4.45 and the loading sequence in Fig. 4.46. An initial axial load of 400 kips was applied to the column of the specimen, corresponding to an axial stress in the column of 13 ksi. The subassembly remained elastic up to cycle 6 and a force of 44 kips at which time flaking of the whitewash was noticed on the upper west and lower east beam flanges. First yield was noticed during the eighth cycle at a force of 55 kips.

The testing proceeded uneventfully until cycle 15 when it was observed that the shear tab had slipped on the web bolts. This occurred at a force of approximately 72 kips. During cycle 18 and again during cycle 19 several loud pops were heard but no cracking was evident and none appeared later. It is thought that the pops accompanied the formation of cracks in the internal welds between the column wall and the continuity plates. These took place at a cantilever end load of about 80 kips which would give a moment at the column of 4160 in-kips. The test was finally stopped due to extreme buckling of the beam flanges as evidenced in the photographs in Figs. 4.47 and 4.48. At the end of the testing there were no apparent cracks in the beam flanges and the connection continued to carry load.

The maximum load carried by the beam was 80 kips, causing a moment at the column face of 4160 in-kips. This moment was 59% greater than the nominal full plastic moment of the beam and 79% greater than the moment at nominal yield of the beam. Based on the actual material properties, the maximum moment was 24% greater than actual plastic moment capacity of the beam and 56% greater than the yield moment for the beam. Fig. 4.46 shows that the specimen had ten full cycles after reaching the nominal plastic moment of the beam. The photograph in Fig. 4.49 shows the condition of the whitewash on the bottom flange at the end of the test. The photograph shows the extent of the plastic strains in the beam flange during the test and give a good indication of the length of the plastic hinge in the flange.

4.2.10 Specimen 10 [W16x40 Beam, 3/4" Faceplate Ext. Stiffener]

Specimen 10 was a test to determine if the internal continuity plate could be replaced by an exterior cover plate on the beam flange extending the full width of the column. The force vs. displacement curves for the subassembly are shown in Fig. 4.50 and the load history of the test is shown in Fig. 4.51. An initial axial load of 400 kips was applied to the column producing an axial stress in the column of 13 ksi. The first several cycles were uneventful. Some flaking of the whitewash did appear on the back and sides of the column during cycles 6 and 7 at a cantilever load of 45 to 50 kips. During cycle 8, at a beam load of 56 kips, there was some flaking of the whitewash on the bottom beam flange just past the end of the cover plate. The increased section modulus due to welding the cover plates onto the beam flanges force the first yielding to occur some distance from the beam-column connection, at the point where the cover plate ends and the beam reduces to its nominal section modulus. On the twelfth cycle at a beam force of 80 kips the weld holding the angles bracing the top of the specimen to the test frame broke abruptly, thus leaving the specimen unsupported at the top. The test was stopped while the services of a welder were obtained and the angle braces were rewelded to the test frame. As a result of the stoppage of the test a new force-displacement curve was started. The test resumed on cycle 13 with a reduced beam force of 40 kips. During cycle 16, at a force of 74 kips, a crack initiated in the top east flange cover plate (see Fig. 4.52). During cycle 18 a crack initiated on the top west flange at a force of approximately 85 kips. The crack in the east flange had grown to about 2-3/4 inches long at this point. The connection failed during cycle 19 at a force of 85 kips as a result of delamination of the column face plates as shown in Fig. 4.53. The delamination occurred in the column at the level of the top flange of the beam and appeared to have occurred on both sides of the column simultaneously.

The ultimate load carried by the beam was 85 kips which would produce a moment of 4420 in-kips at the column face. This moment is 90% greater than the moment required for nominal yield in the beam and 68% greater than the full plastic moment of the beam, based on nominal yield. Based on the actual material properties as determined by the coupon tests, these figures are 35% and 29%, respectively. The maximum rotation in the connection was approximately 1.75%. During the test it was apparent from the flaking of whitewash that yielding occurred in both the area at the beam-column junction and at a point just beyond the end of the cover plate.

4.2.11 Specimen 13 [W16x40 Beam, W12x13 Column Strong Axis]

Specimen 13, a typical connection to the strong axis of a wide flange column, was tested to provide a basis of comparison for the box column connections. The force-displacement curve is shown in Fig. 4.54 and the load history of the test is shown in Fig. 4.55. Flaking of whitewash in the panel zone of the column was first observed during cycle 5 under a load of 52 kips. First yield was noticed by flaking of the whitewash on the beam flange at cycle 8 under an applied load of 66 kips. The maximum beam load sustained by the connection before failure was 91 kips. Failure was from a crack initiating in the web cope of the bottom flange and propagating into the beam flange as shown in Fig. 4.56. Prior to failure there was noticeable buckling of the bottom flange of the beam. Plastic hinge formation in the beam is shown in Fig. 4.57.

4.3 Discussion of Results

This section summarizes, discusses and compares the performance of the 11 test specimens. Comparison of Specimens 1 and 8, which had the same dimensions, show reasonable correlation. Using actual material properties, the ratio of maximum test moment to yield moment was 0.82 and 0.77 for specimens 1 and 8 respectively while the ratio of maximum test moment to calculated full plastic moment was 0.73 and 0.69. The rotation at yield and the ultimate rotation were substantially larger for specimen 1 than for specimen 8 but this may have had more to do with experimental technique on the first test than with variation in the actual performance. During the first test there was some difficulty in holding the top of the specimen horizontally rigid which was corrected in later tests.

Specimens 2, 5 and 6 were all quite similar, each having the same beam size, W16x26. The only difference was that Specimens 5 and 6 had a one inch column faceplate while specimen 2 had a 1-1/4 inch column faceplate. Based on the nominal material properties, specimen 2 is shown as having attained a maximum moment 1.51 times the nominal yield moment and 1.31 times the calculated full plastic moment while for specimen 6 the figures were 1.88 and 1.63 respectively. For specimen 5, which has the same dimensions as specimen 6, the ratios were 1.69 and 1.47. A comparison of the experimental performance of specimens 2, 5 and 6 using the actual material properties of Table 4.3 shows respective values for the ratio of maximum moment to calculated yield moment of 1.16, 1.01 and 1.37. For the ratio of maximum experimental moment to calculated plastic moment based on actual material properties the numbers for the three specimens were 1.01, 0.88 and 1.19. The ultimate rotations achieved were 1.6, 2.3 and 2.3 percent.

A comparison of specimen 3 and specimen 9, which were similar in all respects except that the internal stiffener plate in specimen 3 was half the thickness of the beam flange while the stiffener in nine was the full thickness of the beam flange, show that the maximum cantilever beam load carried by nine was only 10% greater than that carried by three. Using the values in Table 4.3 for actual material properties the ratio of the maximum moment to yield moment and plastic moment is about 12% greater in specimen 9 than it is for specimen 3, indicating that the full thickness internal stiffener plates do not increase the ultimate capacity of the connection significantly over internal stiffeners half the thickness of the beam flange. The difference in performance is seen in a comparison of the rotations of the two specimens. While the rotation at yield is very similar, 0.8% for three compared with 0.7% for nine, the maximum rotation experienced by three, 3.3%, was 22% greater than that experienced by nine, 2.7%. This could be attributed to the buckling of the stiffener plates in specimen 3, as shown in Fig. 4.19. This buckling was due to a width to thickness ratio in excess of that allowed by Section 2.7 of the AISC Specification.

Specimens 7 and 10, had external stiffener plates, which were either extension plates on the edges of the beam flanges (Specimen 7) or a cover plate on the beam flange (Specimen 10). The behavior of these specimens can be compared to specimens 3 and 9. All four of these specimens had 3/4 inch column faceplates and all except seven had W16x40 beams. The maximum cantilever beam load carried by 3, 7, 9 and 10 was 73 kips, 63 kips, 80 kips and 85 kips, respectively. Using Table 4.3 for actual material properties of the ratios of maximum test moment to calculated yield moment was 1.40, 1.48, 1.57 and 1.45 and the maximum test moment to calculated full plastic moment was 1.24, 1.29, 1.39 and 1.29. Rotations at yield were 0.8, 0.7, and 0.7 percent. No yield point could be determined for specimen 10. For the four specimens the ultimate rotations were 3.3, 2.1, 2.7 and 1.75 percent. From these results it appears that the external stiffener plates performed as well as the internal stiffener plates.

Specimen 1, 4 and 8 all shared the same dimensions with the exception that 4 had a 1-1/4 inch column faceplate and 1 and 8 had 3/4 inch faceplates. Comparing the thick wall of four to the thin wall of one and eight shows a considerable increase in the performance of the thick wall column. The maximum cantilever beam load carried by specimen 4 was 74 kips compared with 45 kips for specimen 8 and 48 kips for specimen 1. Using Table 4.3 the ratio of experimental moment to plastic moment capacity was 0.95 for specimen 4 and 0.69 for specimen 8, a difference of 38%. The maximum rotation was greater for specimen 4 than for specimen 8, by 2.8% compared to 2.1%. This was a 33% increase compared with the 64% increase in cantilever beam load carried by the two specimens. The additional rotation in 4 was most likely caused by the additional moment in the beam due to the higher cantilever load.

Specimen 13 was a typical wide flange beam (W16x40) to wide flange column (W12x136) connection. The maximum beam cantilever load carried was 91 kips, which exceeded any other test but was only 7% greater than specimen 10 with its full thickness cover plate and 14% greater than the box column with full thickness stiffener plates. Using Table 4.3 the maximum test moment to the calculated yield moment based on actual material properties was 2.03 and the test moment to plastic moment was 1.80 or 29% greater than the fully stiffened box column. Rotations at yield for specimen 13 compare with all the other specimens and the ultimate rotation of 2.5% was greater than several of the specimens. The greater rotations are probably an indication of greater ductility in this connection rather than greater flexibility.

4.4 General Observations

Many of the observations made during the present series of tests confirm those observations reported by others during previous tests on steel connections. During these tests it was observed that cracks often initiated in the tack welds used to hold the backup bars in place where they were present. The same observations were made by Popov and Pinkney [10]. Another observation made in that paper which was confirmed in the present series of tests was that sharp cornered and rough web copes were "a recurring source for the initiation of web cracks." In the current series of tests the web cope was the source of the initial crack in several of the specimens, in spite of the requirement in the purchase specification that the web copes were to be ground smooth. Popov and Pinkney further reported that fracture usually occurred at or near the groove welds which attach the beam flange to the column flange, which was also observed in this series of tests. Another observation which has also been reported by others is the slow rate at which cracks in the beam flanges propagate, normally taking several cycles after initiation before reaching a point of sudden failure. It was interesting to note that even after a crack had grown to be an inch or two long the beam was able to handle increasing loads, indicating that the stresses had redistributed themselves away from the cracked area. This same observation was made by Krawinkler and Popov [11].

TABLE 4.1
SPECIMEN MATERIAL PROERTIES

Specimen Number	Coupon Location	Yield Stress (ksi)	Ultimate Stress (ksi)	Elongation At Fracture %
1	Beam	47.1	68.9	34
	Column	43.5	71.4	30
2	Beam	46.7	79.2	23
	Column	48.6	75.5	36
3	Beam	42.0	64.5	43
	Column	51.7	69.4	37
4	Beam	55.1	65.1	40
	Column	48.6	75.7	36
5	Beam	60.5	75.3	38
	Column	46.5	61.6	45
6	Beam	49.5	69.2	30
	Column	46.5	61.6	45
7	Beam(web)	57.5	75.8	33
	Column	41.5	74.5	30
8	Beam	46.7	64.9	36
	Column	41.5	74.5	30
9	Beam	41.0	67.5	34
	Beam(web)	49.1	69.6	34
	Column	37.9	63.2	38
10	Beam	47.0	65.9	34
	Beam(web)	51.7	69.3	33
	Column	41.3	65.9	36

Note: All Beam Coupons taken from the Flange unless noted.

TABLE 4.2
EXPERIMENTAL RESULTS - APPLIED MOMENTS
COMPARISON WITH DESIGN CRITERIA
NOMINAL MATERIAL PROPERTIES

Specimen	Number of Cycles	P (kips)	M_{max} in − kip	M_y Nominal in − kip	M_{max} /M_y	M_p Nominal in − kip	M_{max} /M_p	$M_{Blodgett}$ in − kip	M_{max} /$M_{Blodgett}$	Rot_y	Rot_{ULT}
1	1^+	48	2496	2329	1.07	2624	0.95	736	3.39	1.4	4.5
1R	1^+	50	2600	2329	1.12	2624	0.99	736	3.53	–	
2	6	40	2080	1382	1.51	1591	1.31	1810	1.15	0.65	1.6
2R	10	45	2340	1382	1.69	1591	1.47	1810	1.29	0.9	2.5
3	15	73	3796	2329	1.63	2624	1.45	736	5.16	0.8	3.3
4	14	74	3848	2329	1.65	2624	1.47	2272	1.69	0.75	2.8
5	14	45	2340	1382	1.69	1591	1.47	1109	2.11	0.75	2.3
6	15	50	2600	1382	1.88	1591	1.63	1109	2.34	0.7	2.3
7	13	63	3276	1382	2.37	1591	2.06	N/A	N/A	0.7	2.1
8	12	45	2340	2329	1.00	2624	0.89	1348	1.74	0.7	2.1
9	18	80	4160	2329	1.79	2624	1.59	736	5.65	0.7	2.7
10	19	85	4420	2329	1.90	2624	1.68	736	6.01	–	1.75
13	12	91	4732	2329	2.03	2624	1.80	N/A	N/A	0.75	2.5

+ - Monotonic Loading

* - Stiffener Plates

TABLE 4.3
EXPERIMENTAL RESULTS - APPLIED MOMENTS
COMPARISON WITH DESIGN CRITERIA
ACTUAL MATERIAL PROPERTIES

Specimen	Number of Cycles	P (kips)	M_{max} $in - kip$	M_y $in - kip$	M_{max} $/M_y$	M_p $in - kip$	M_{max} $/M_p$	$M_{Blodgett}$ $in - kip$	M_{max} $/M_{Blodgett}$
1	1^+	48	2496	3047	0.82	3433	0.73	963	2.59
1R	1^+	50	2600	3047	0.85	3433	0.76	963	2.70
2	6	40	2080	1793	1.16	2064	1.01	2348	0.88
2R	10	45	2340	1793	1.31	2064	1.13	2348	0.99
3*	15	73	3796	2717	1.40	3062	1.24	859	4.42
4	14	74	3848	3565	1.08	4016	0.95	3477	1.10
5	14	45	2340	2323	1.01	2674	0.88	1864	1.26
6	15	50	2600	1901	1.37	2188	1.19	1525	1.71
7*	13	63	3276	2208	1.48	2542	1.29	N/A	N/A
8	12	45	2340	3021	0.77	3404	0.69	1749	1.34
9	18	80	4160	2652	1.57	2989	1.39	838	4.96
10	19	85	4420	3041	1.45	3426	1.29	960	4.60
13	12	91	4732	2329	2.03	2624	1.80	N/A	N/A

+ - Monotonic Loading

* - Stiffener Plates

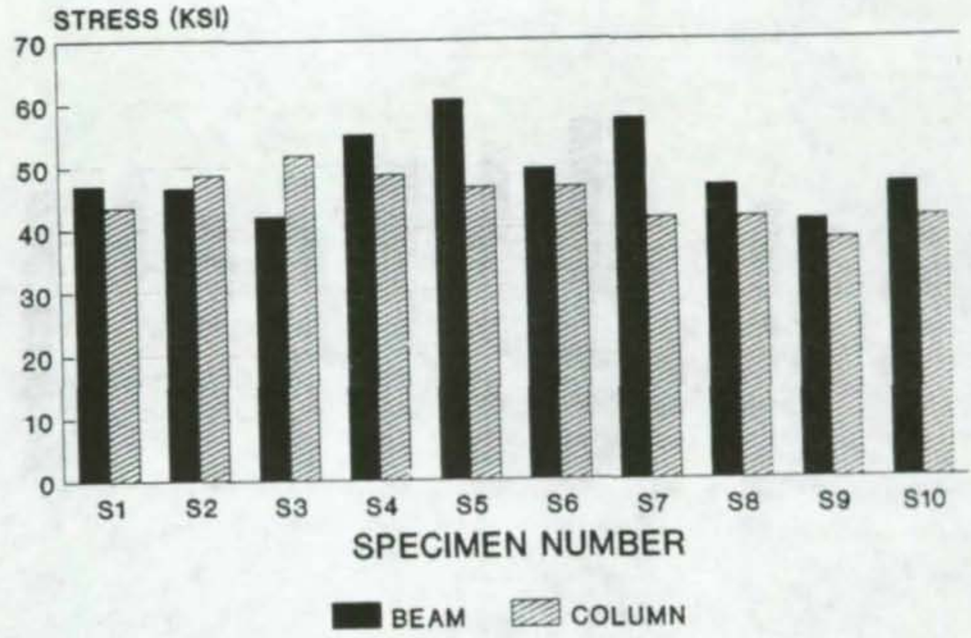

Figure 4.1 Test Specimen Yield Stress

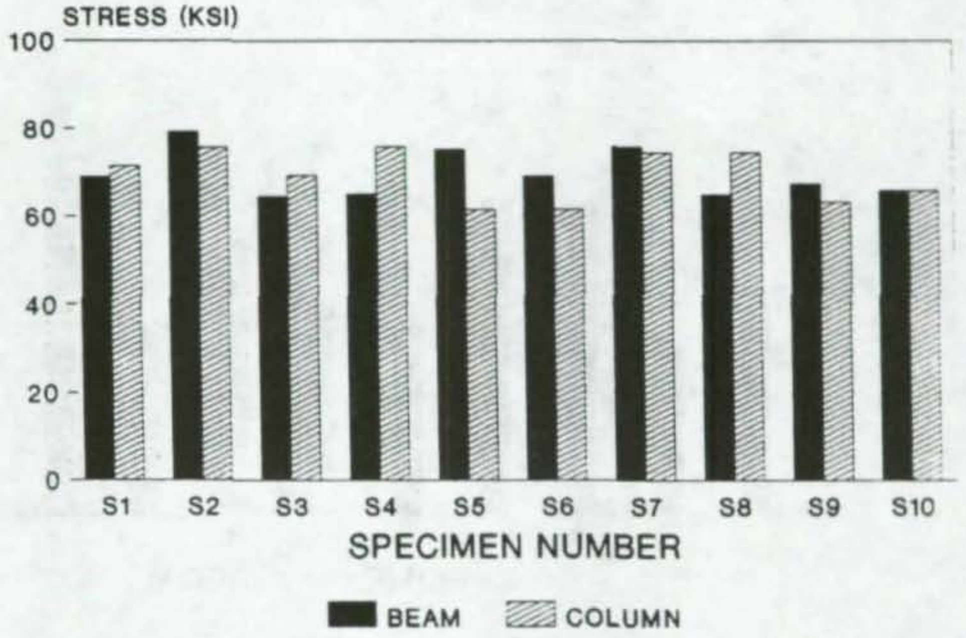

Figure 4.2 Test Specimen Ultimate Stress

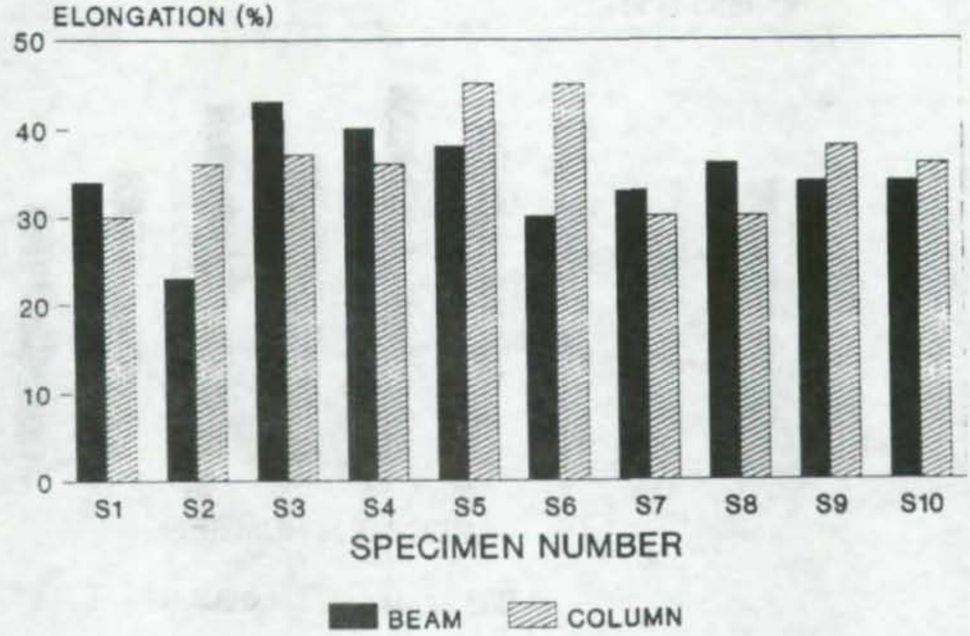

Figure 4.3 Test Specimen Elongation at Fracture

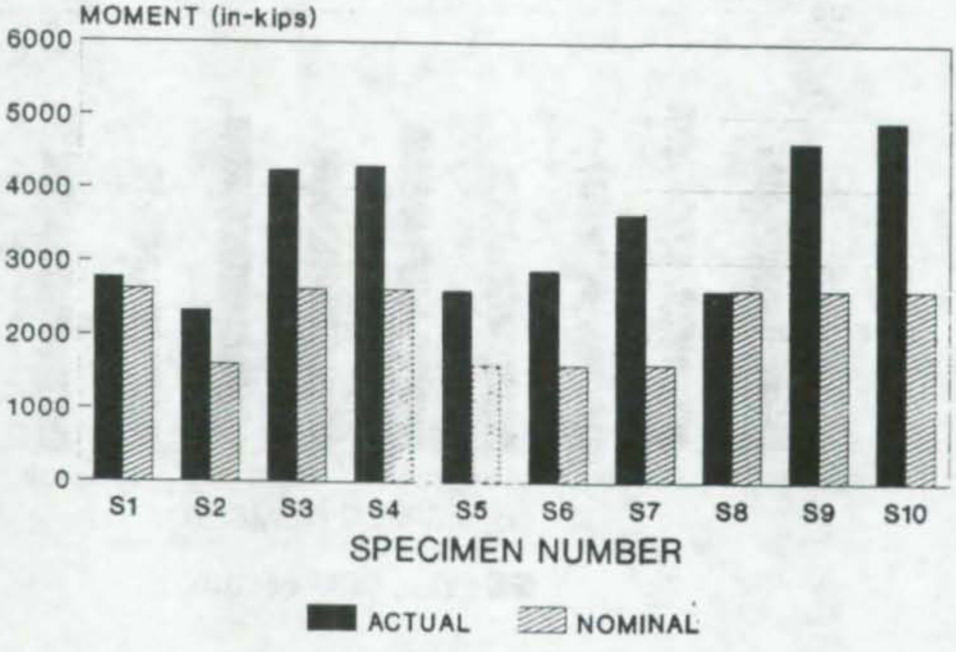

Figure 4.4 Actual vs. Nominal Moment Capacity

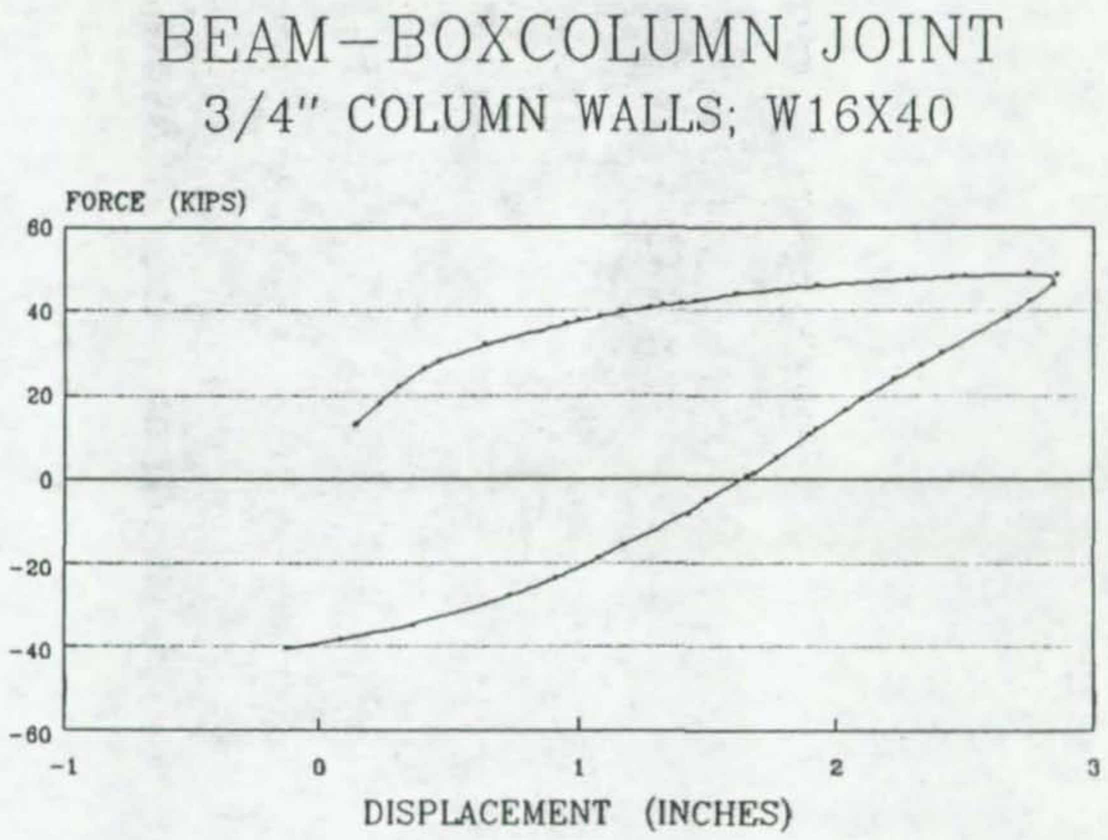

Figure 4.5 Beam Shear vs. Displacement, Specimen 1

Figure 4.6 Crack in Beam Flange, Specimen 1

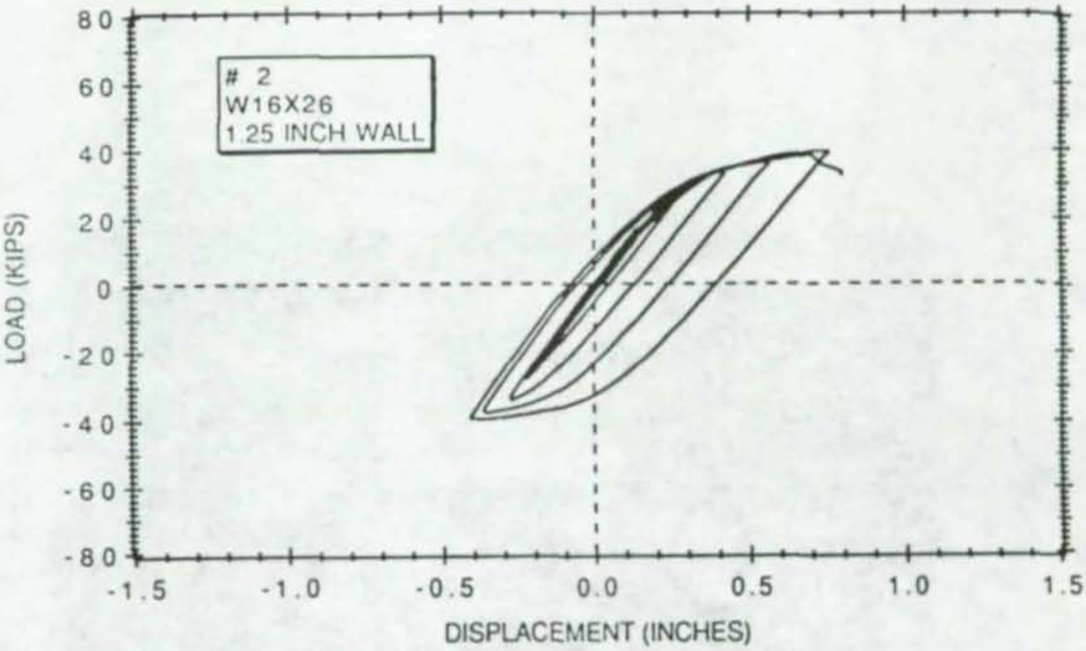

Figure 4.7 Beam Shear vs. Displacement, Specimen 2

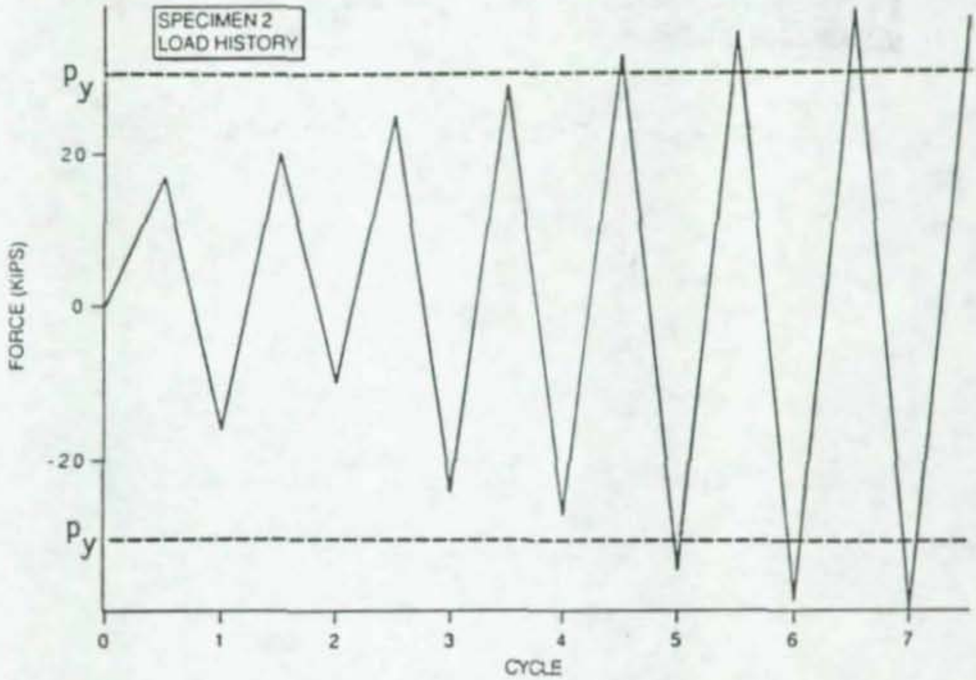

Figure 4.8 Loading Sequence, Specimen 2

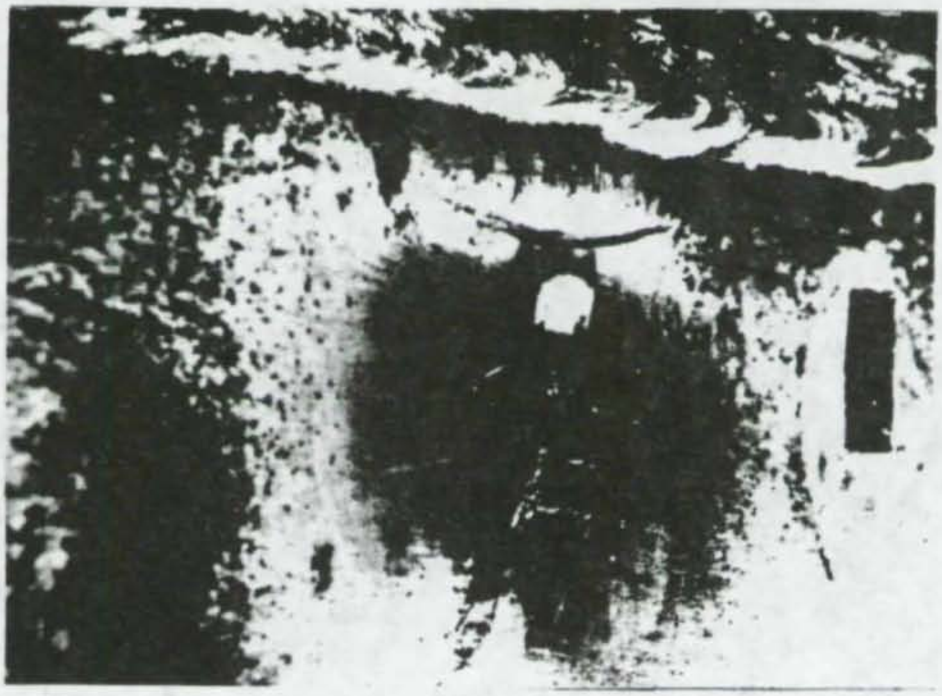

Figure 4.9 Crack in Bottom Beam Flange, Specimen 2

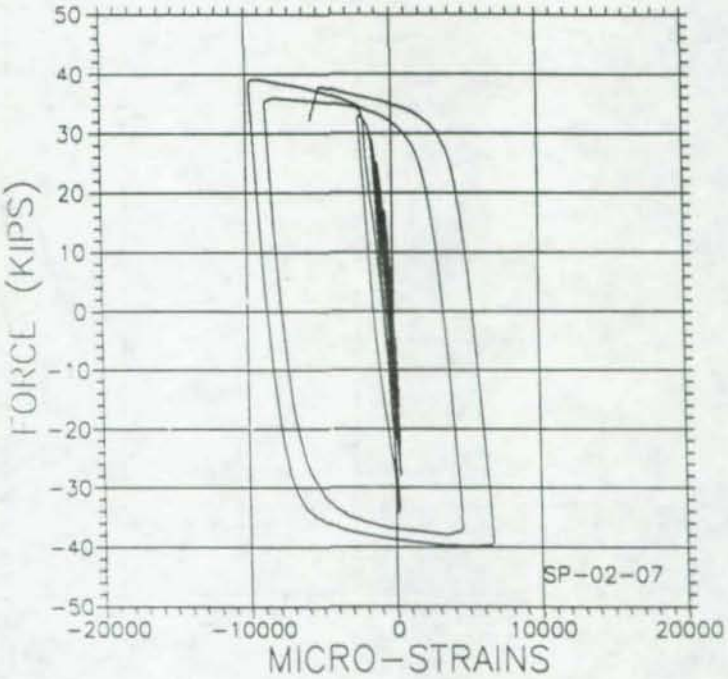

Figure 4.10 Beam Flange Strain at Centerline, Specimen 2

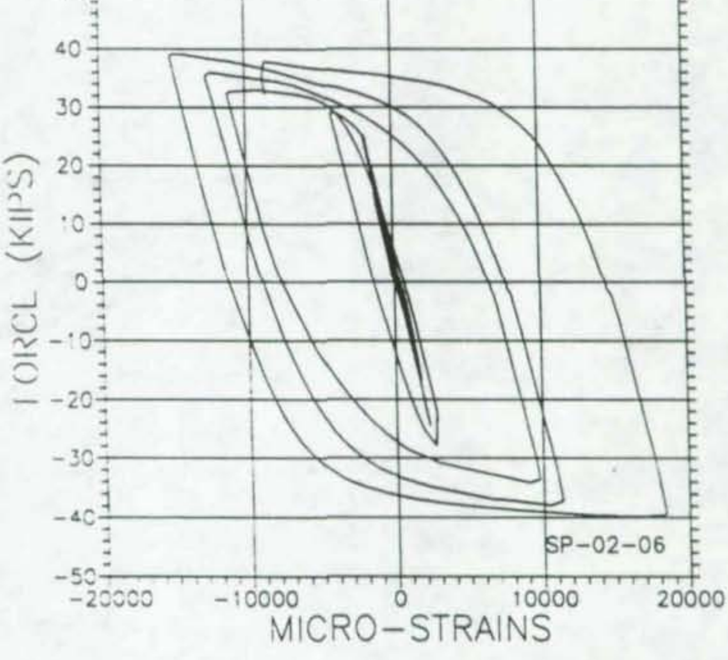

Figure 4.11 Beam Flange Strain at Tip, Specimen 2

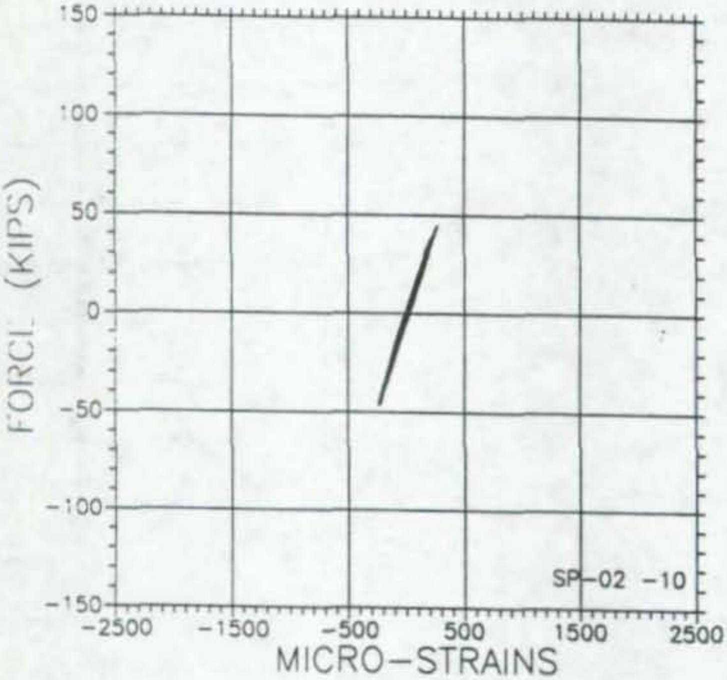

Figure 4.12 **Column Web Plate Strain, Specimen 2**

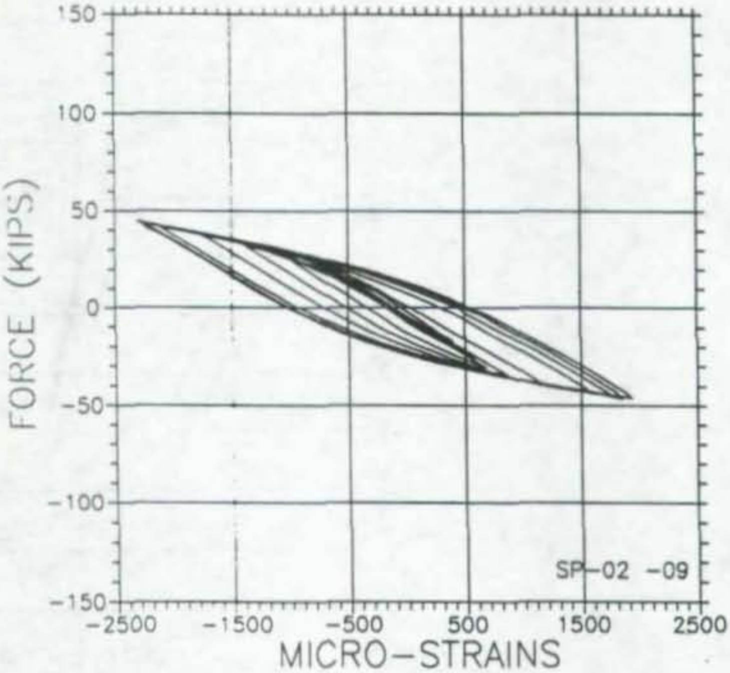

Figure 4.13 **Column Face Plate Strain, Specimen 2**

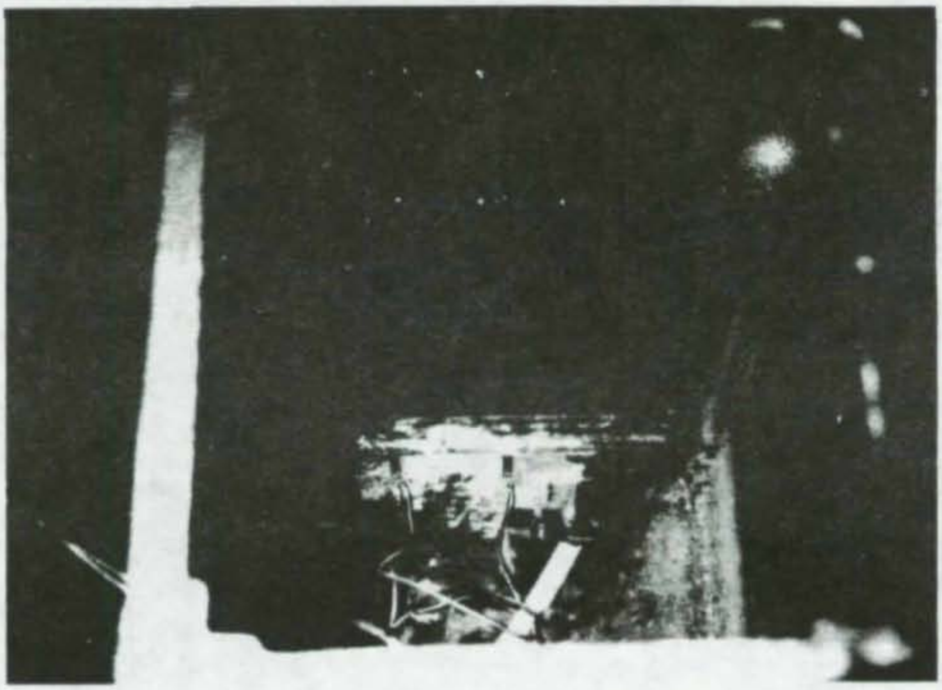

Figure 4.14 View of Internal Stiffner Plate,
Specimen 3

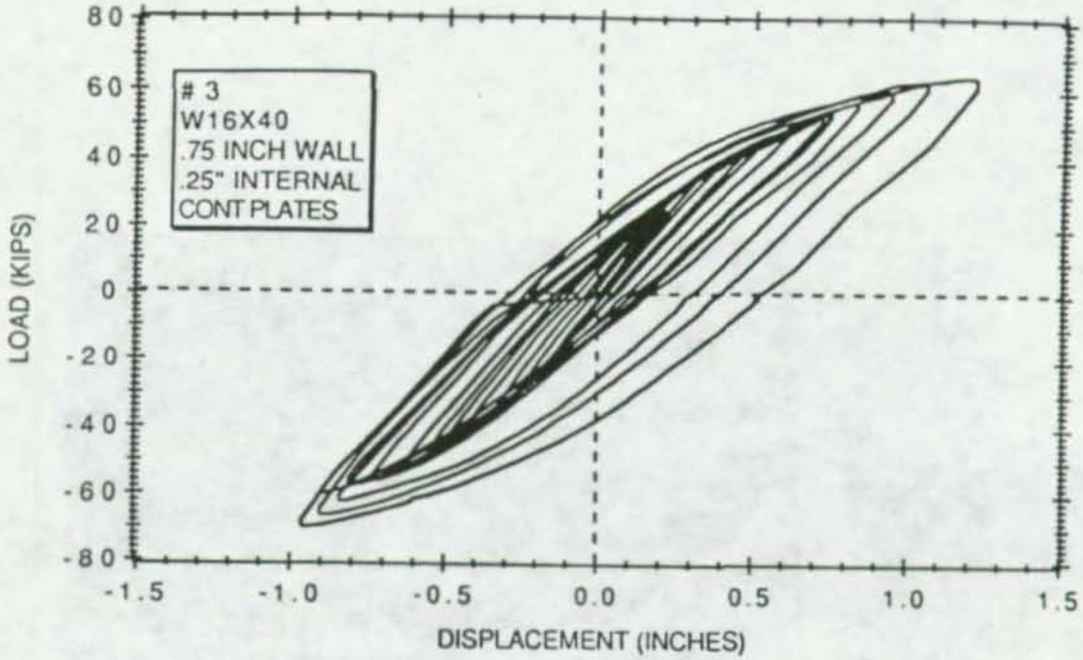

Figure 4.15 Beam Shear vs. Displacement, Specimen 3

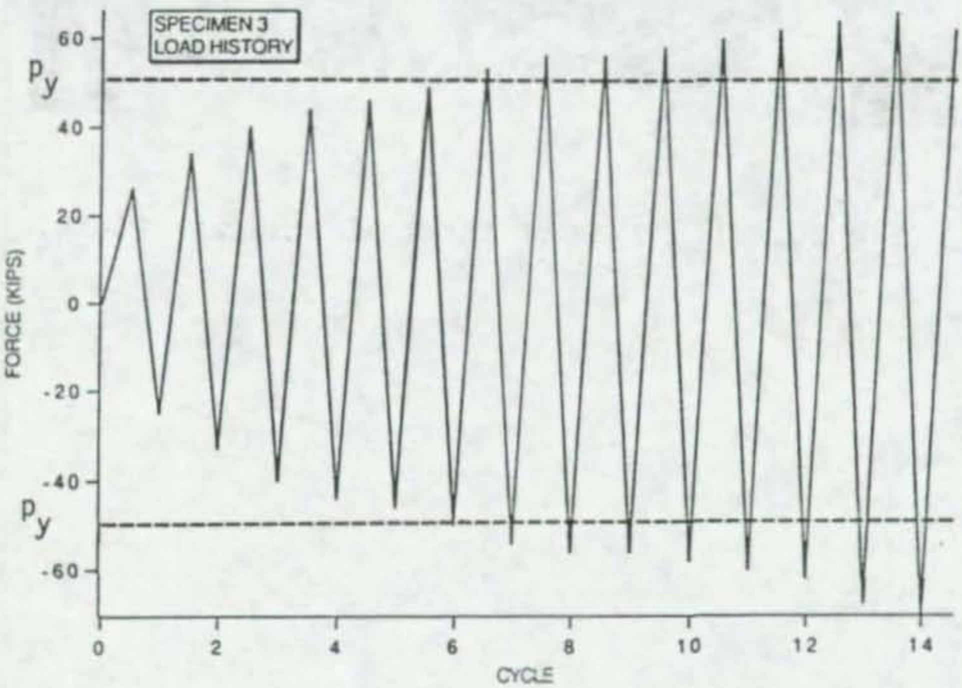

Figure 4.16 Loading Sequence, Specimen 3

Figure 4.17 Top Flange Crack at Failure, Specimen 3

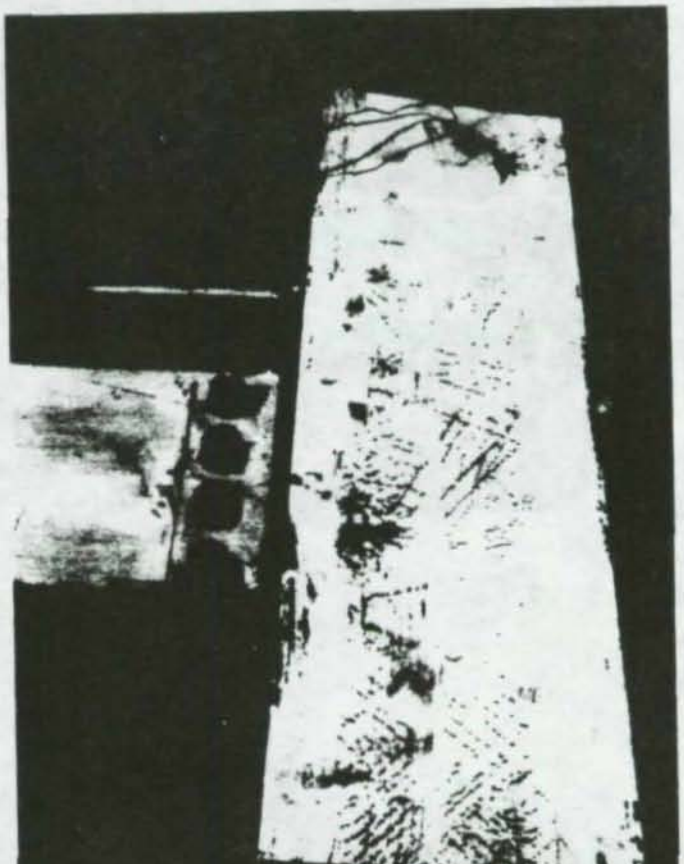

Figure 4.18 Flaking of Whitewash on Column, Specimen 3

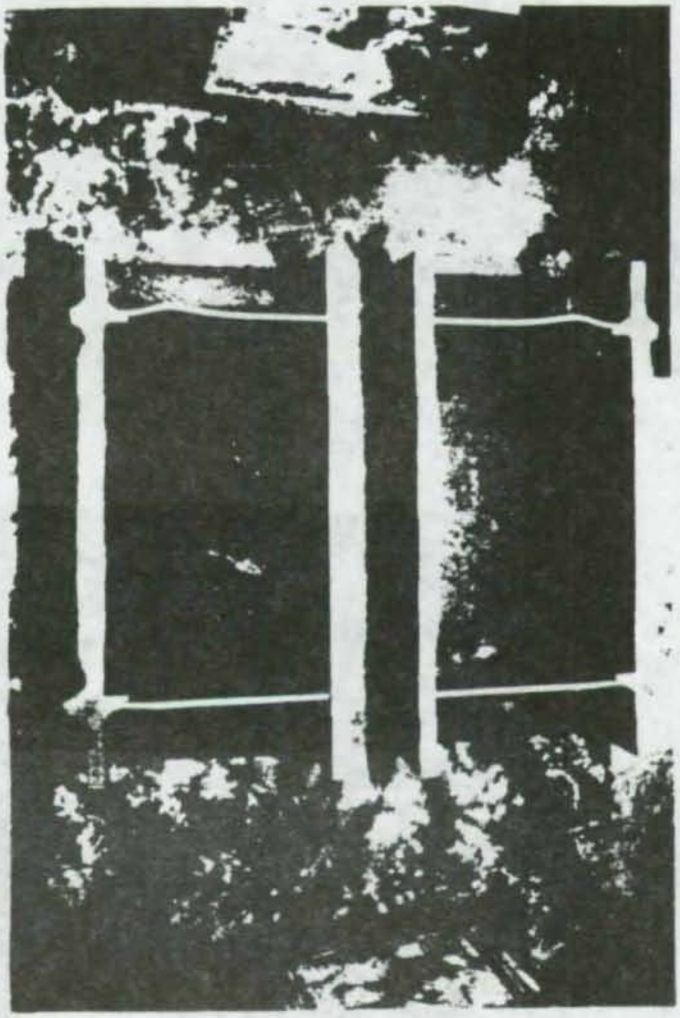

Figure 4.19 Section Showing Stiffner Plates, Specimen 3

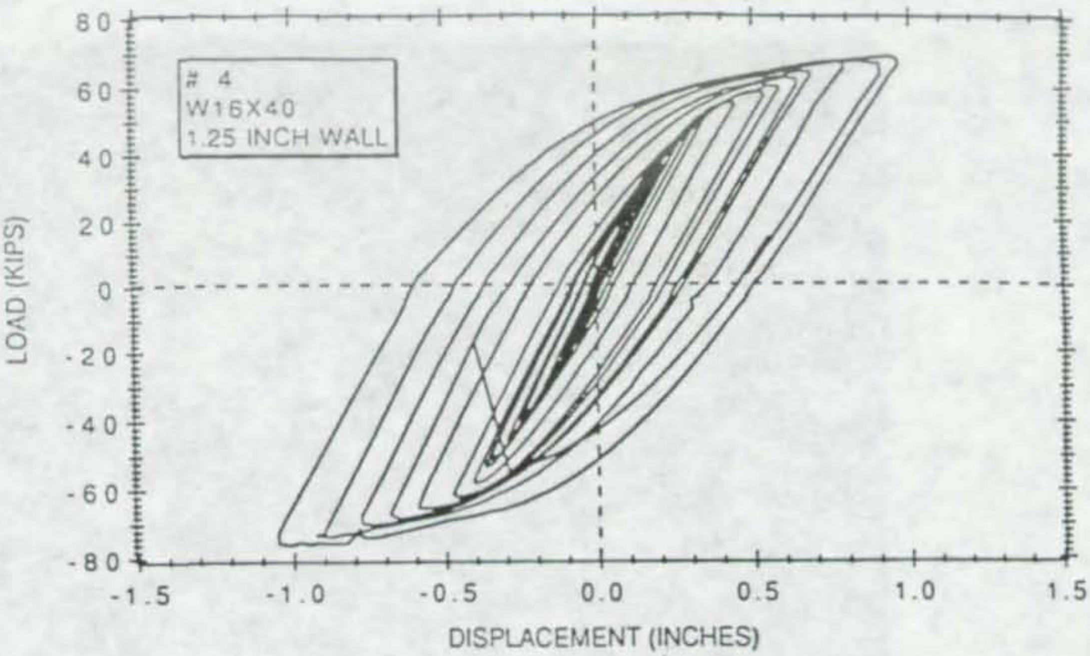

Figure 4.20 Beam Shear vs. Displacement, Specimen 4

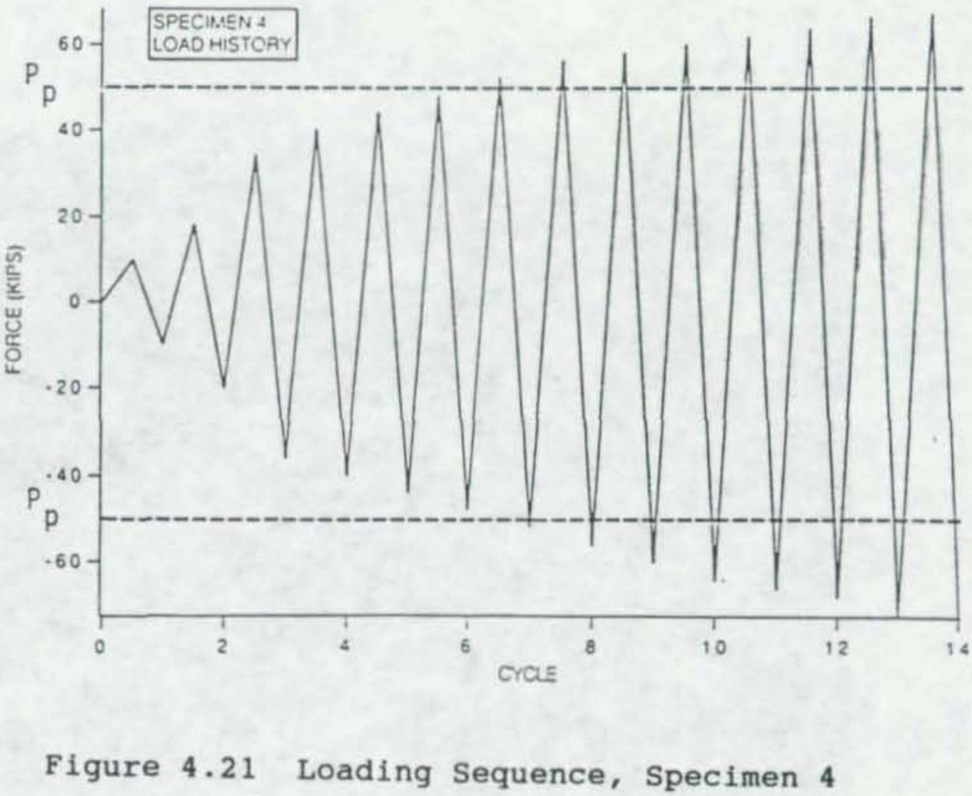

Figure 4.21 Loading Sequence, Specimen 4

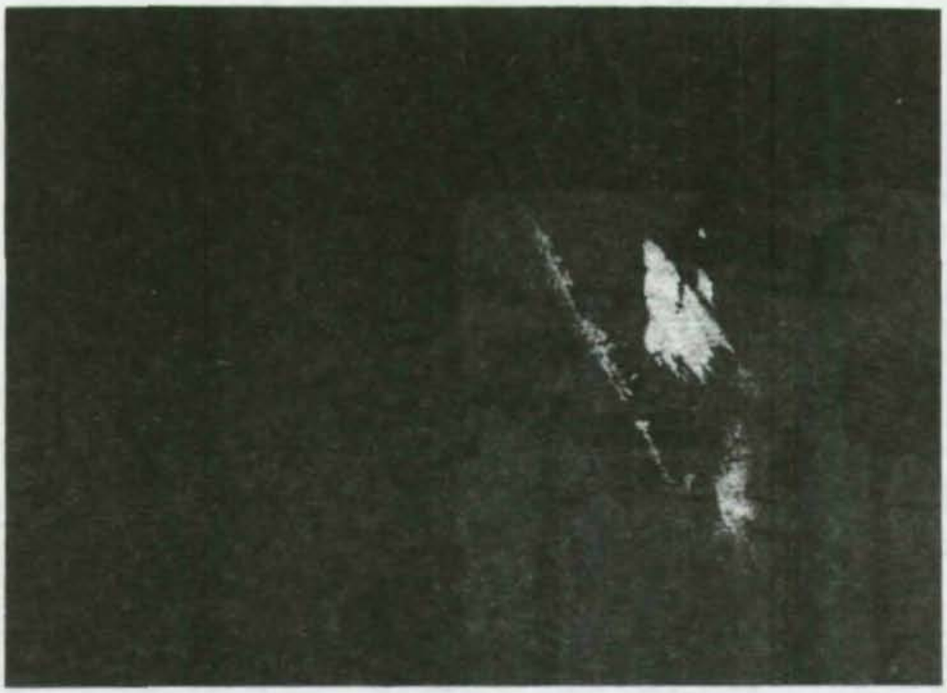

Figure 4.22 Whitewash Flaking on Beam Flange, Specimen 4

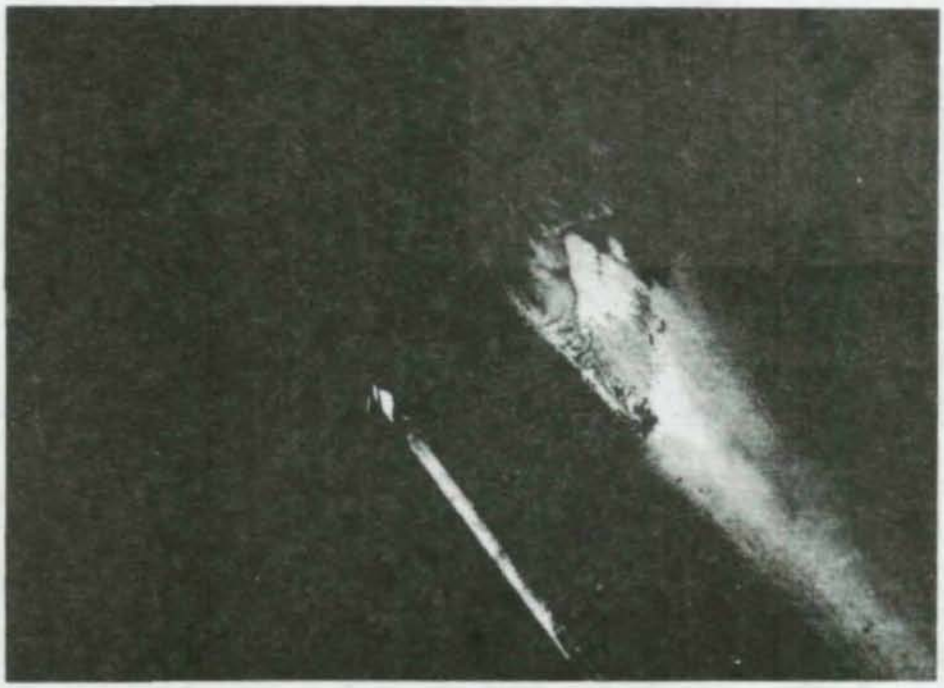

Figure 4.23 Whitewash Flaking, Specimen 4

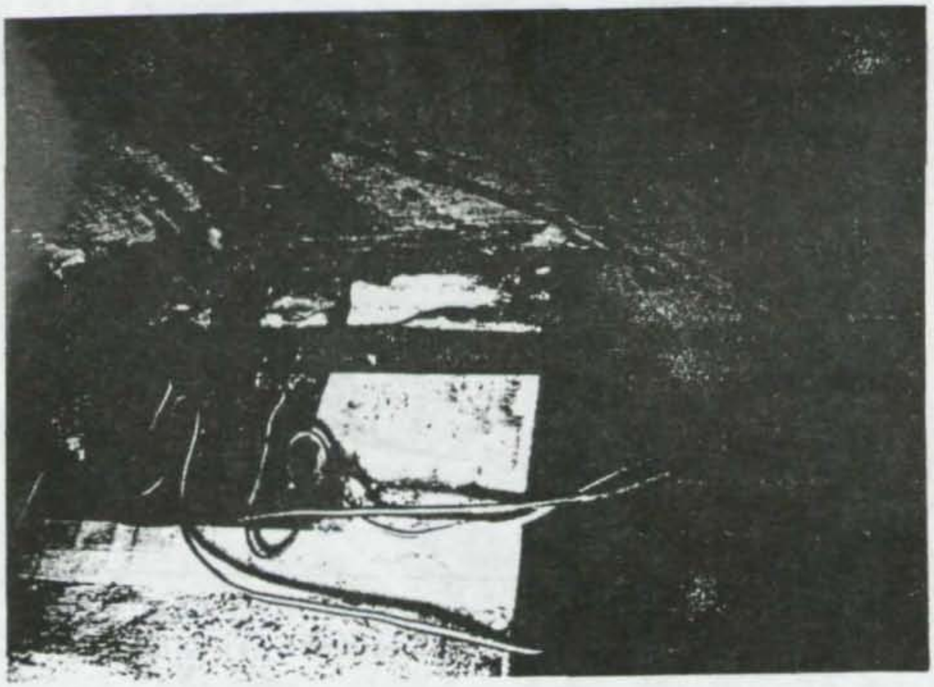

Figure 4.24 Crack in Top Flange, Specimen 4

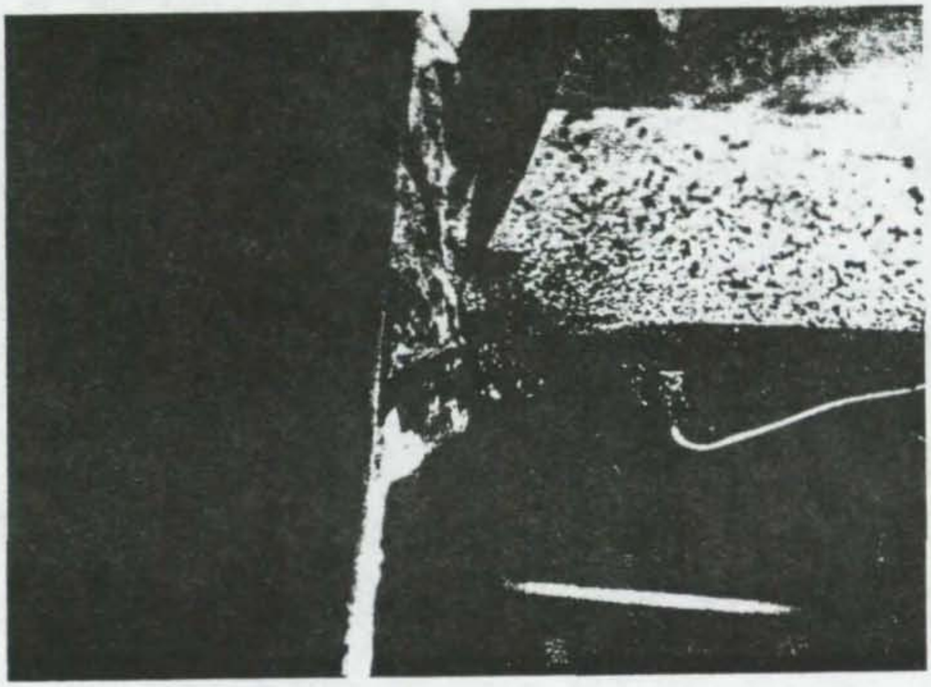

Figure 4.25 Crack in Bottom Flange, Specimen 4

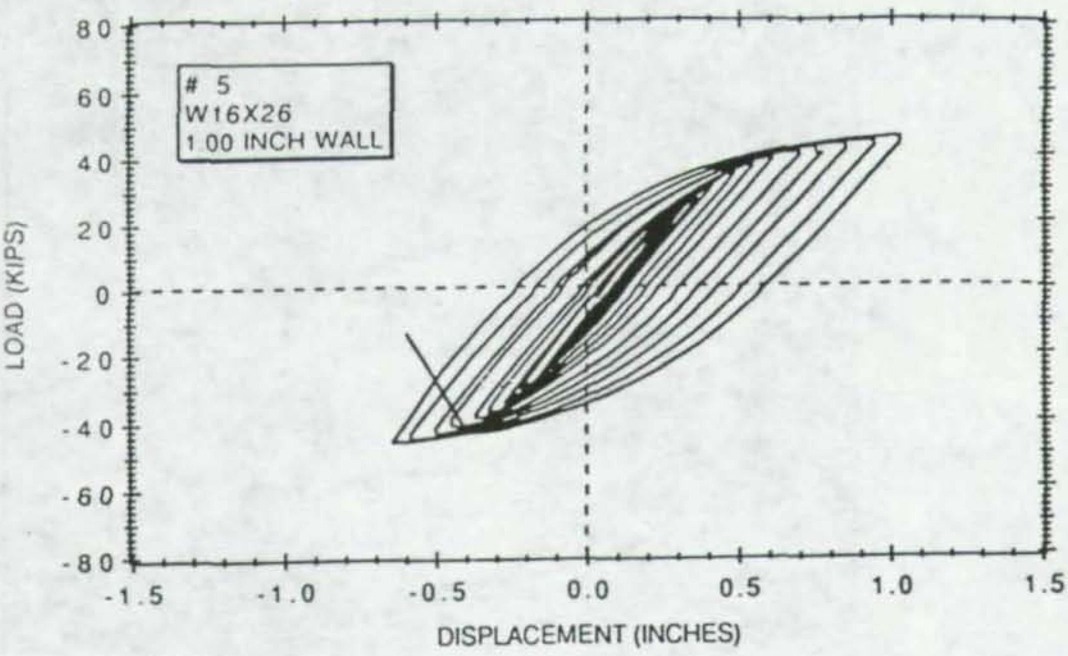

Figure 4.26 Beam Shear vs. Displacement, Specimen 5

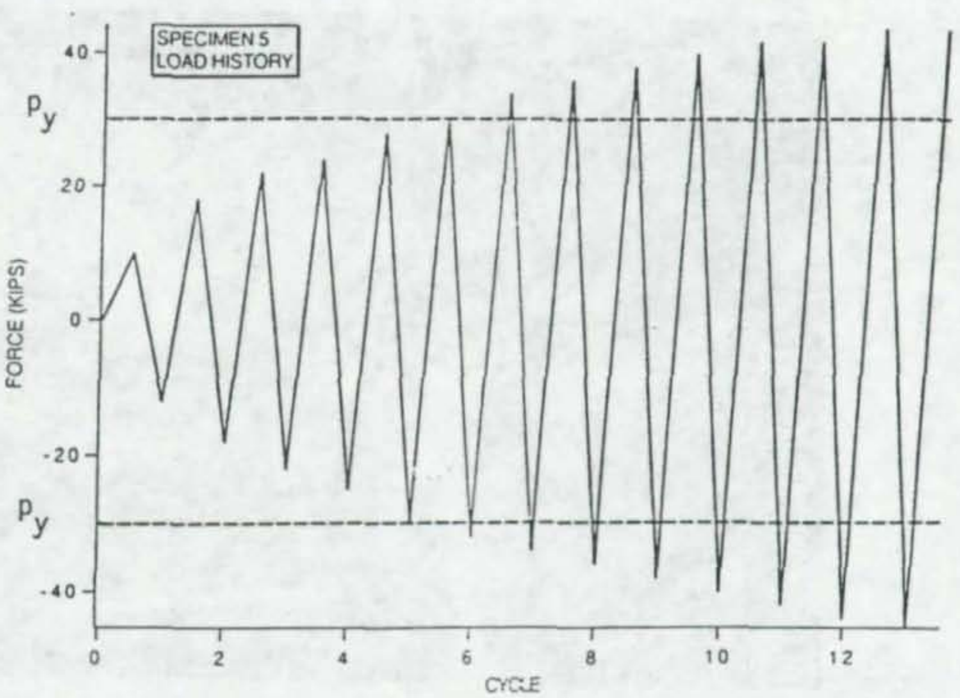

Figure 4.27 Loading Sequence, Specimen 5

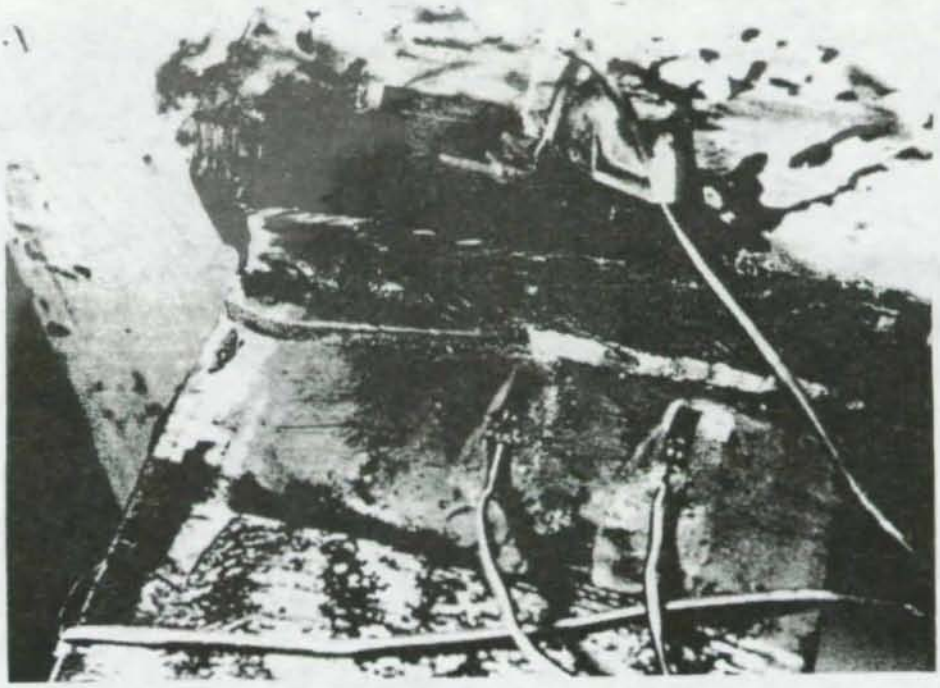

Figure 4.28 Failure Crack in Top Flange, Specimen 5

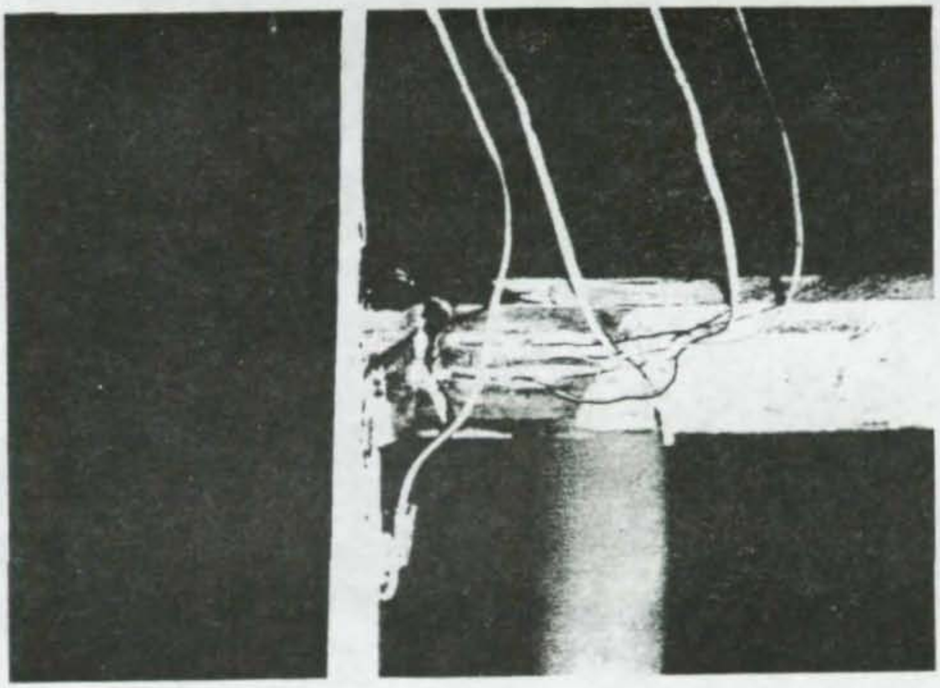

Figure 4.29 Crack in Top Flange, Specimen 5

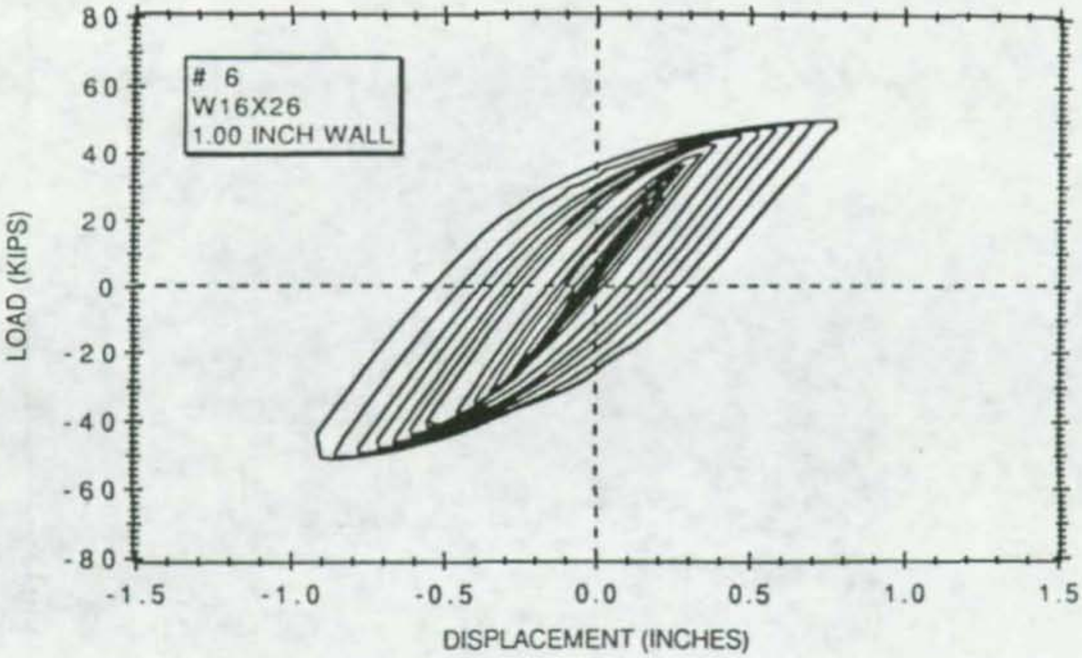

Figure 4.30 Beam Shear vs. Displacement, Specimen 6

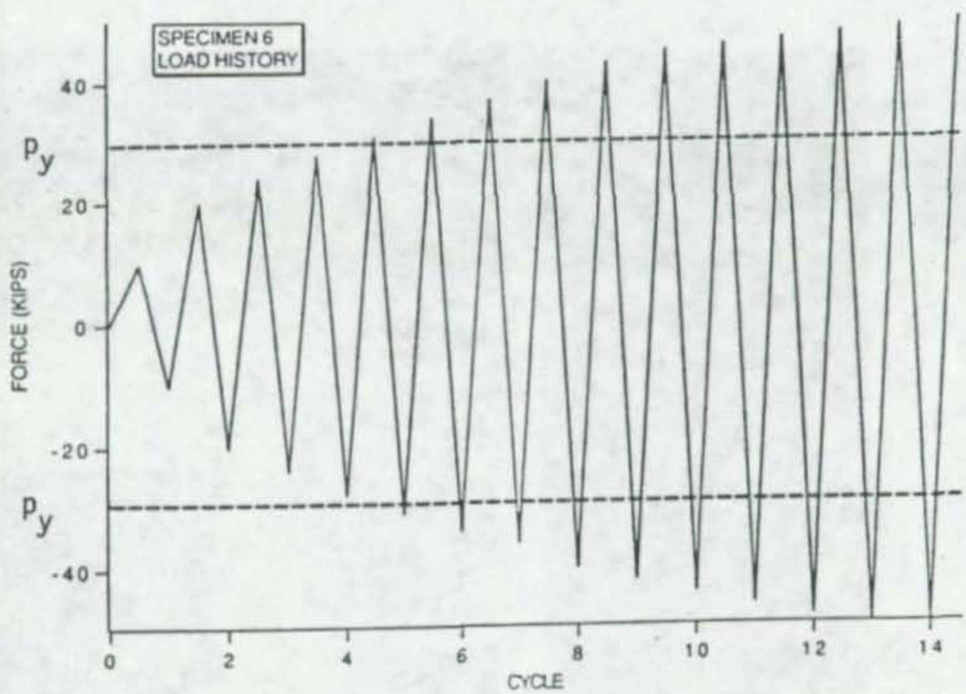

Figure 4.31 Loading Sequence, Specimen 6

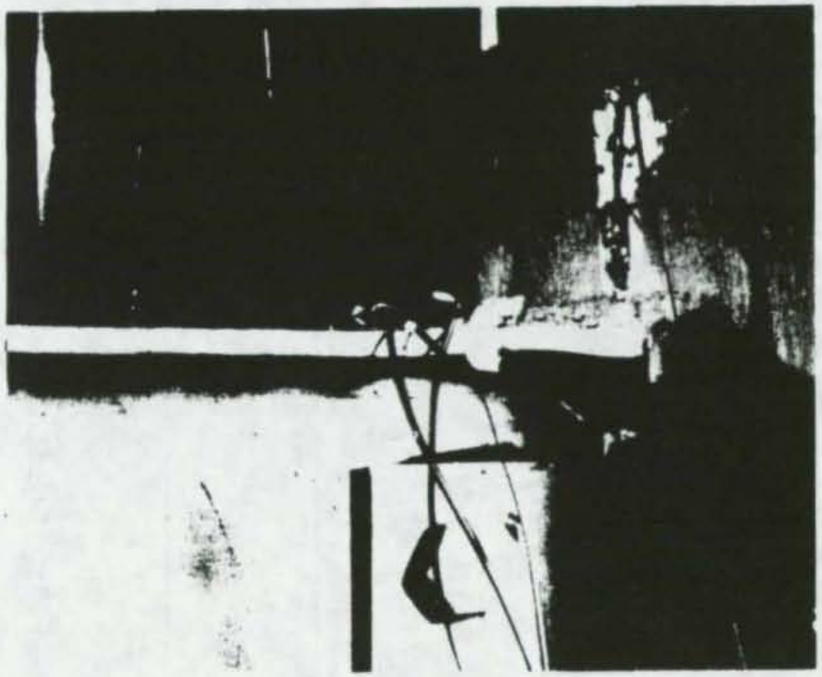

Figure 4.32 Buckle of Top Flange, Specimen 6

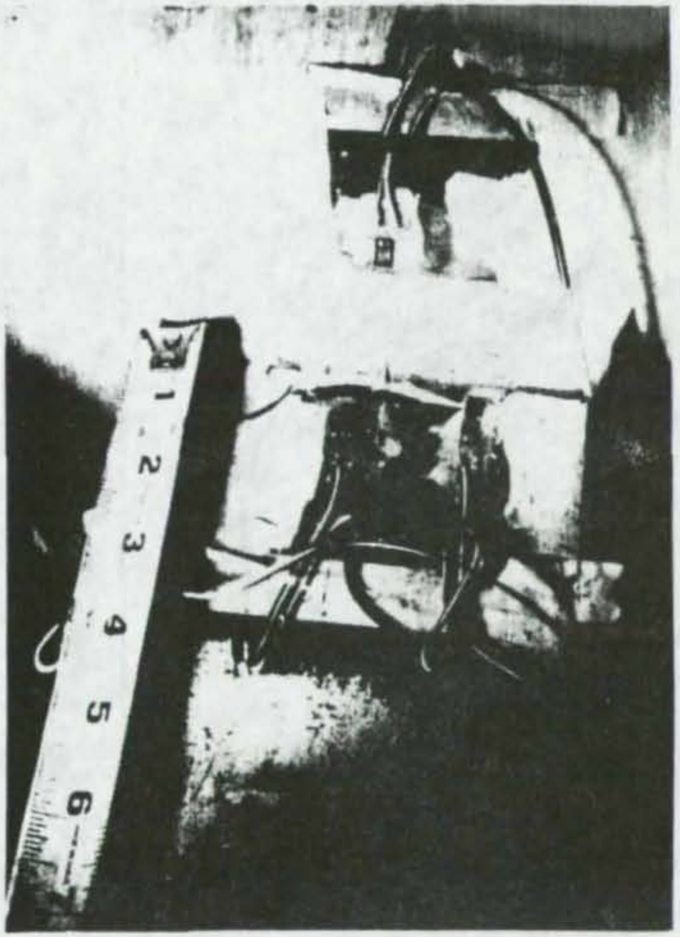

Figure 4.33 Failure Crack in Top Flange, Specimen 6

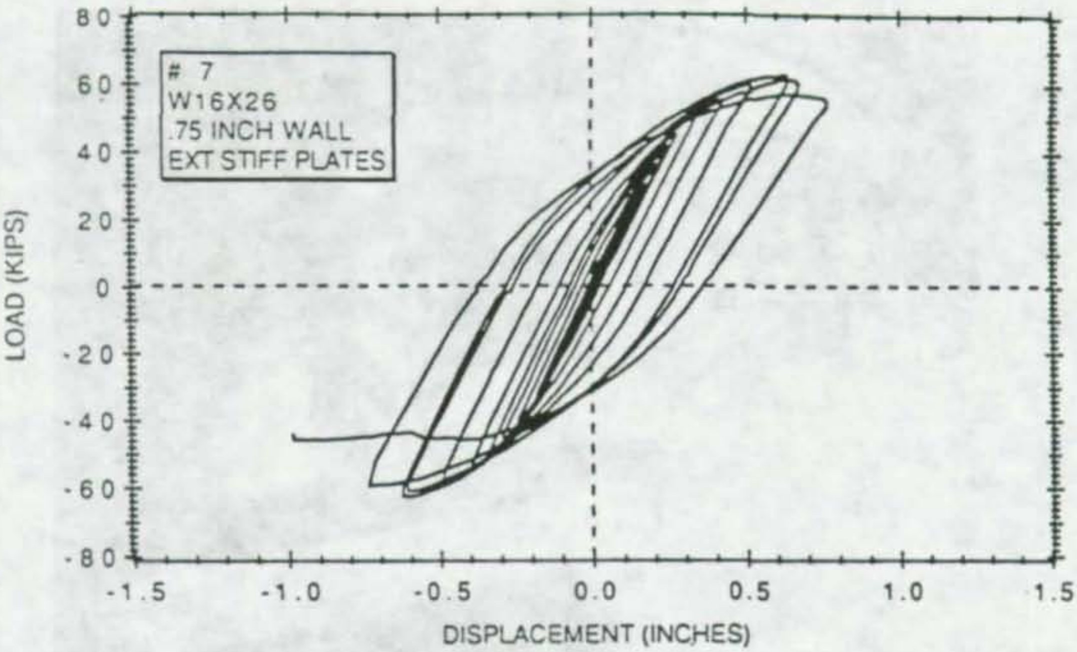

Figure 4.34 Beam Shear vs. Displacement, Specimen 7

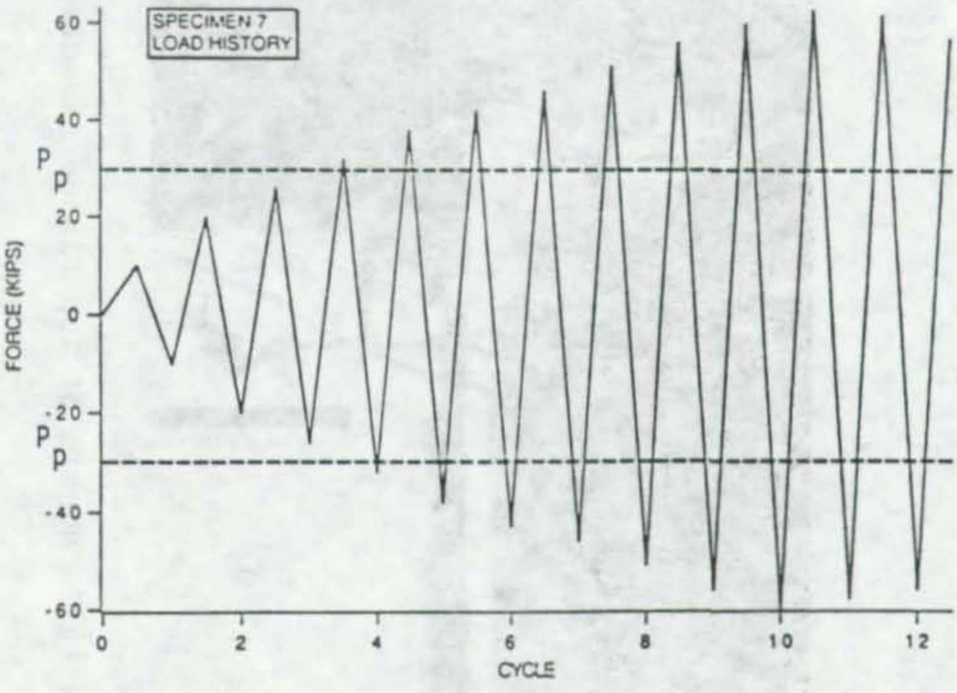

Figure 4.35 Loading Sequence, Specimen 7

Figure 4.36 Flaking at Bottom Flange,
Specimen 7

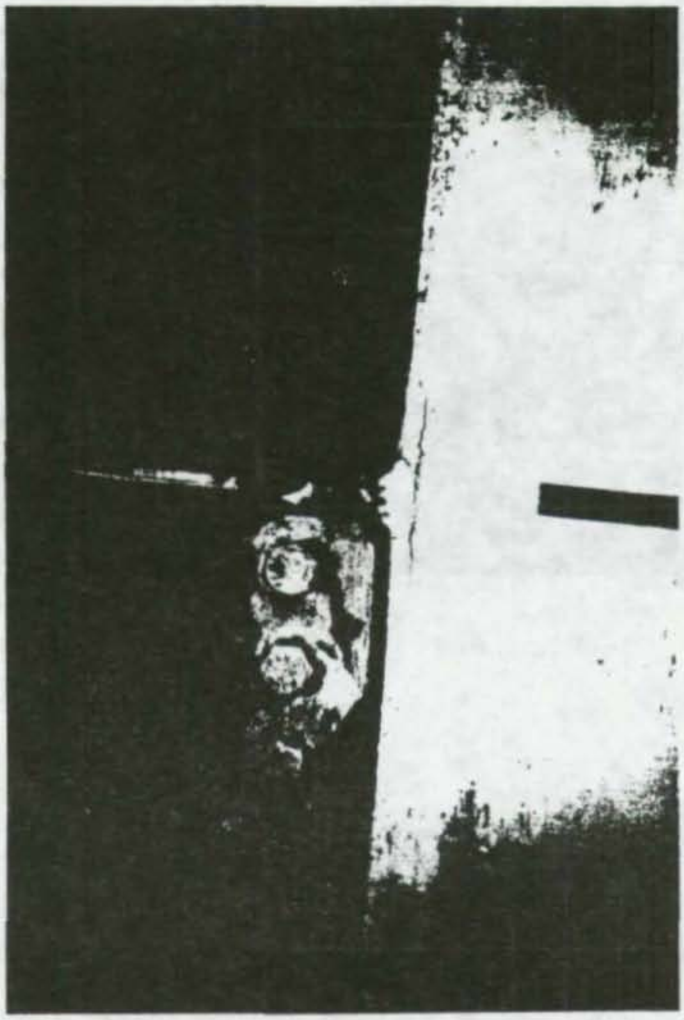

Figure 4.37 Longitudinal Crack, Specimen 7

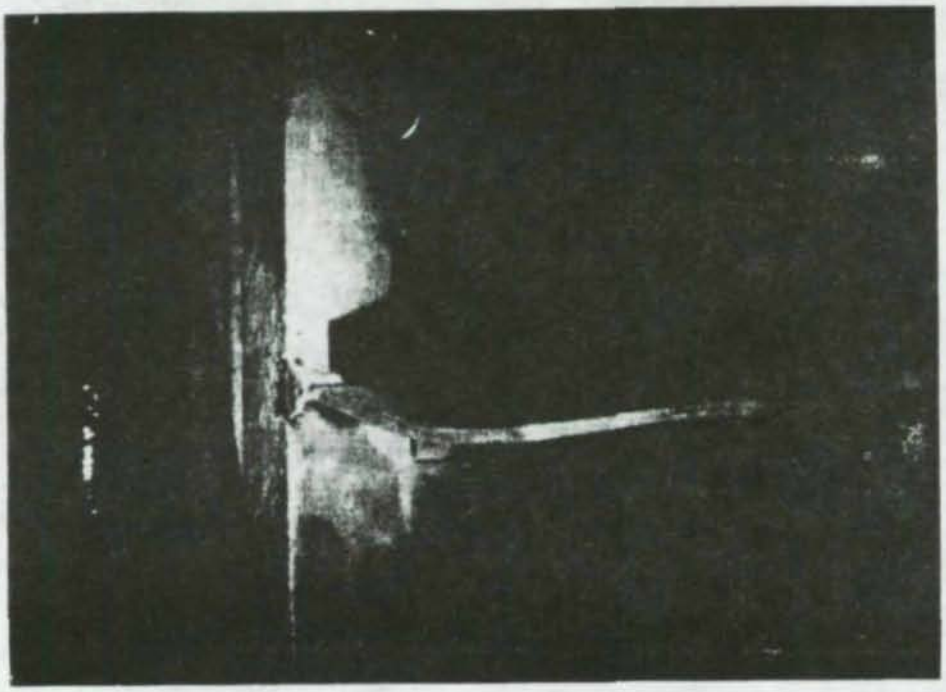

Figure 4.38 Buckling of Top Flange, Specimen 7

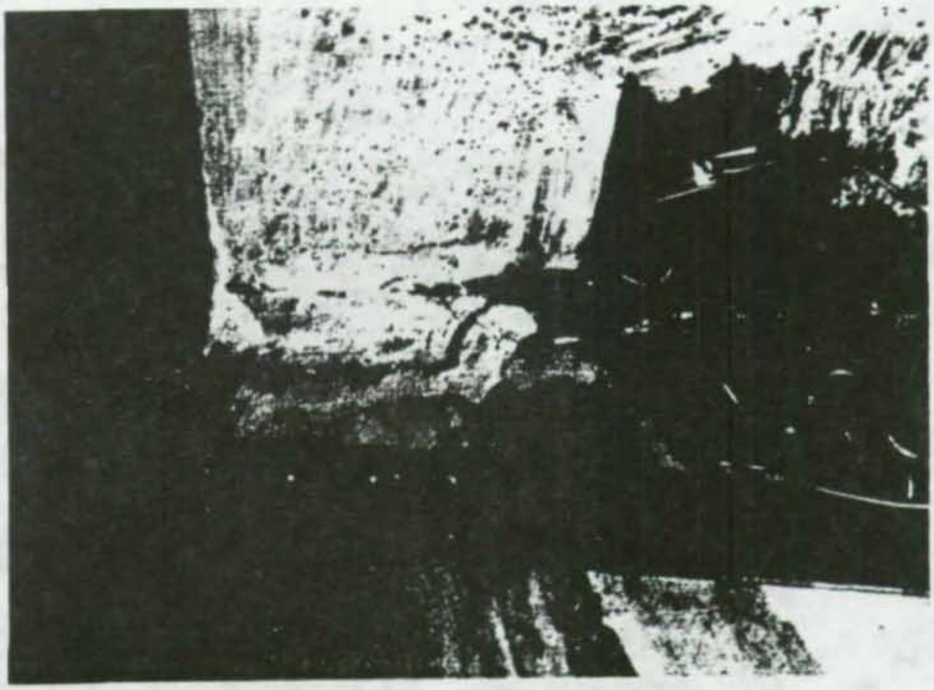

Figure 4.39 Failure Crack in Top Flange, Specimen 7

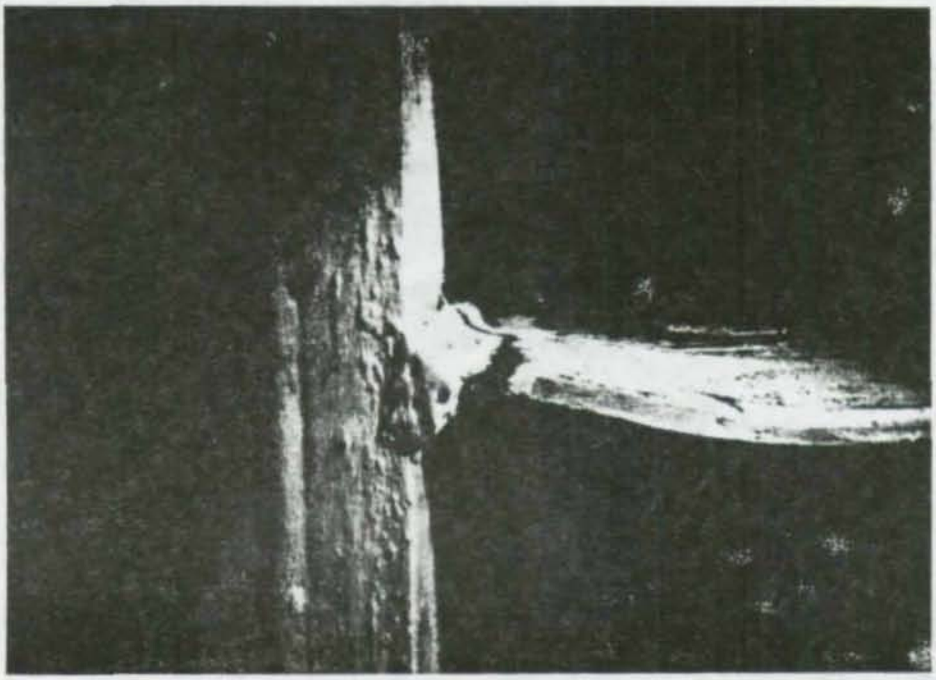

Figure 4.40 Top Beam Flange Crack, Specimen 7

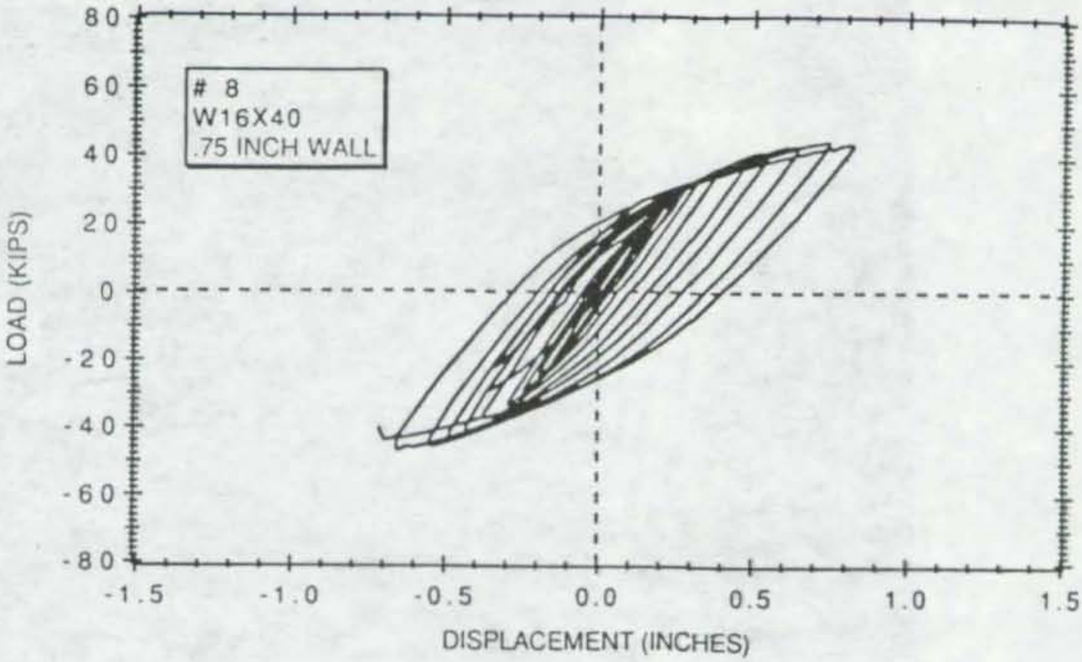

Figure 4.41 Beam Shear vs. Displacement, Specimen 8

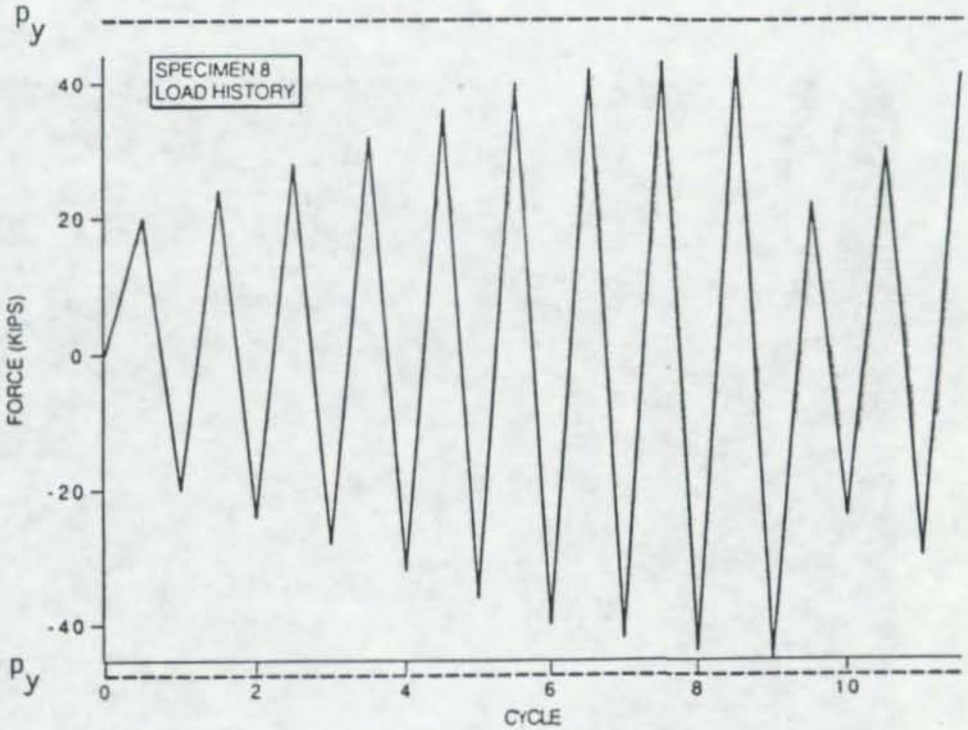

Figure 4.42 Loading Sequence, Specimen 8

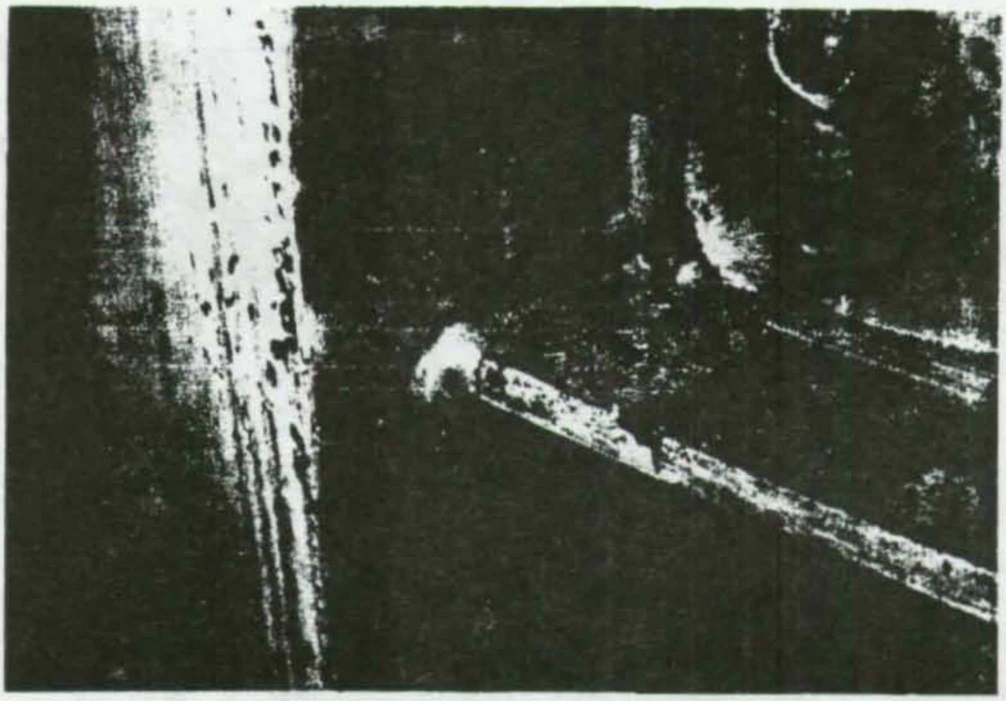

Figure 4.43 Crack in Bottom Flange, Specimen 8

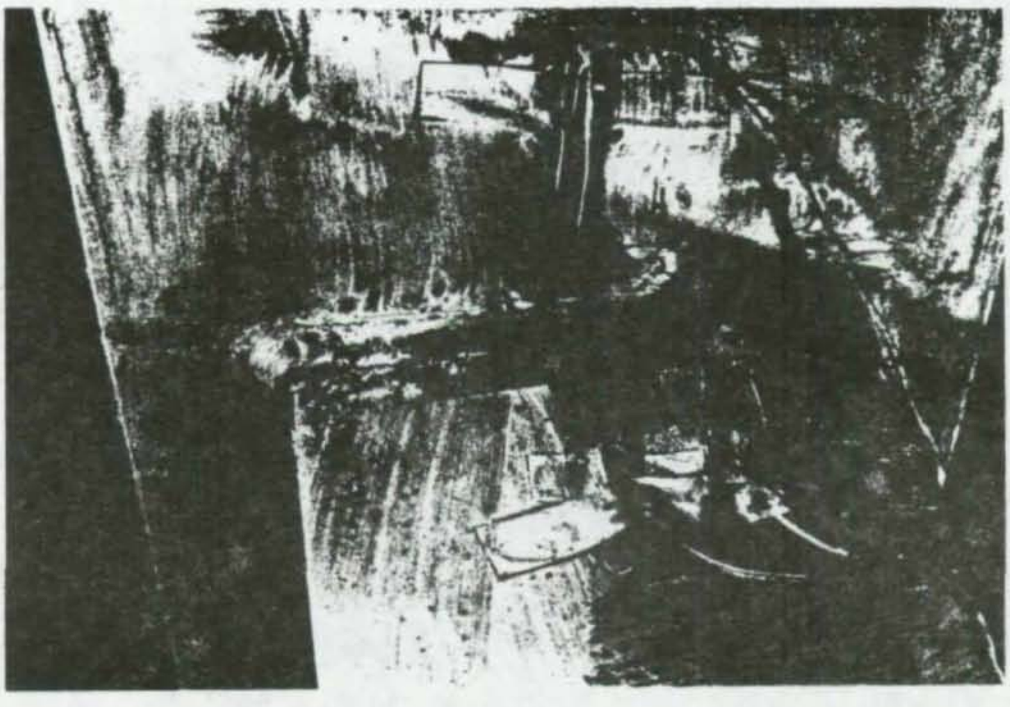

Figure 4.44 Failure Crack in Top Flange, Specimen 8

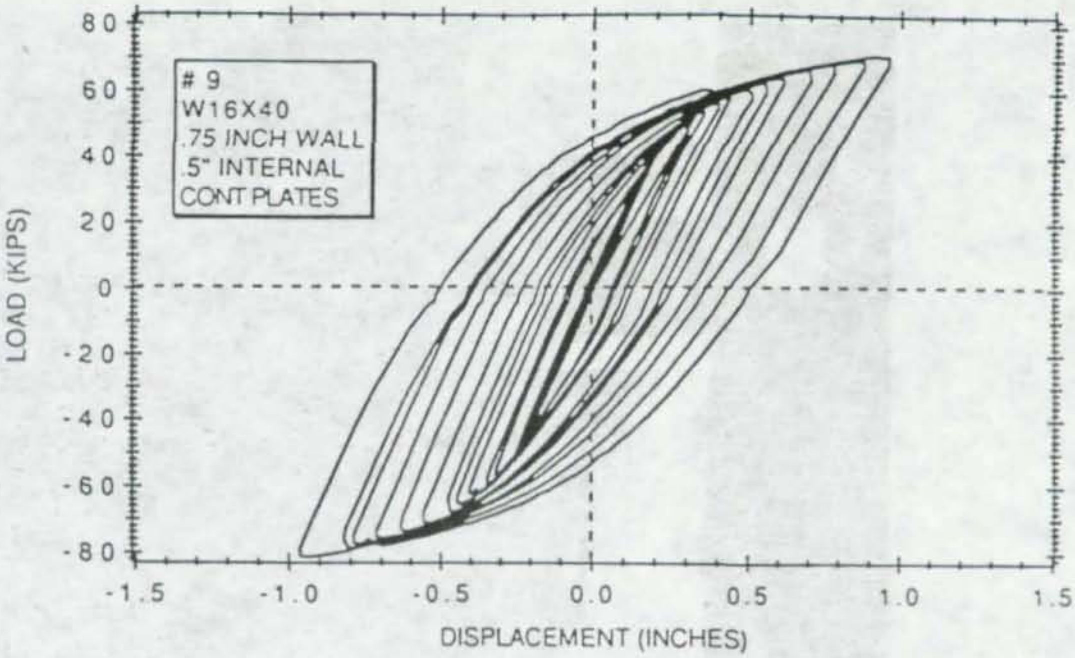

Figure 4.45 Beam Shear vs. Displacement, Specimen 9

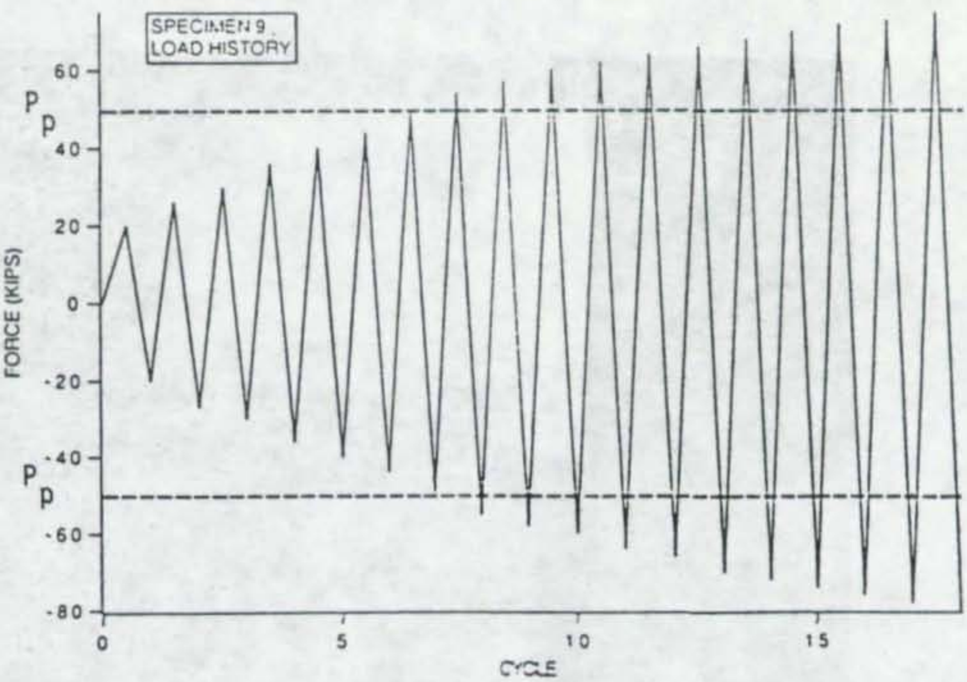

Figure 4.46 Loading Sequence, Specimen 9

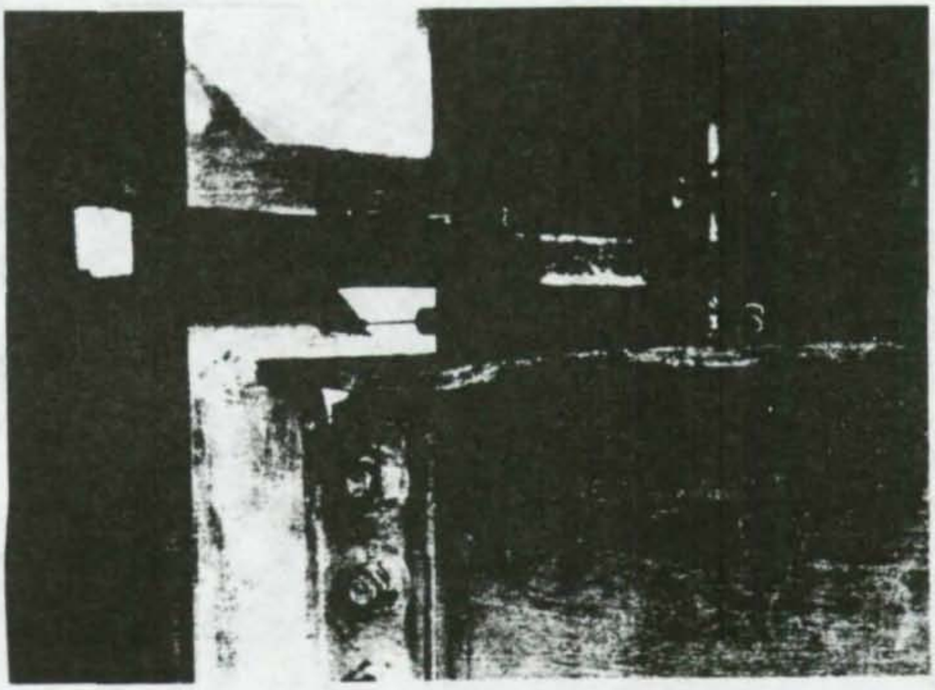

Figure 4.47 Buckling of Top Flange, Specimen 9

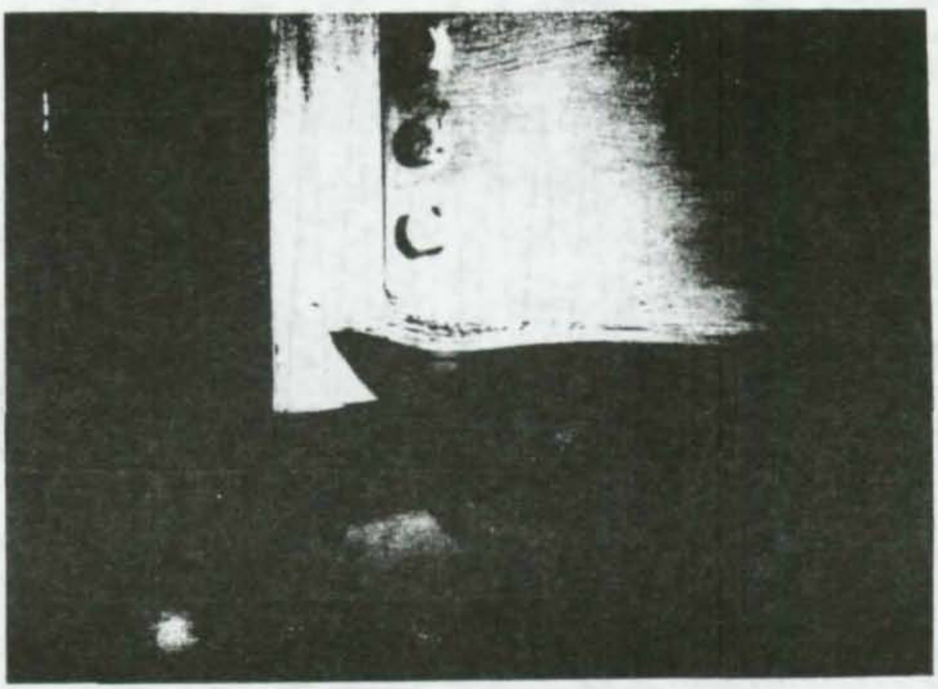

Figure 4.48 Buckling of Bottom Flange, Specimen 9

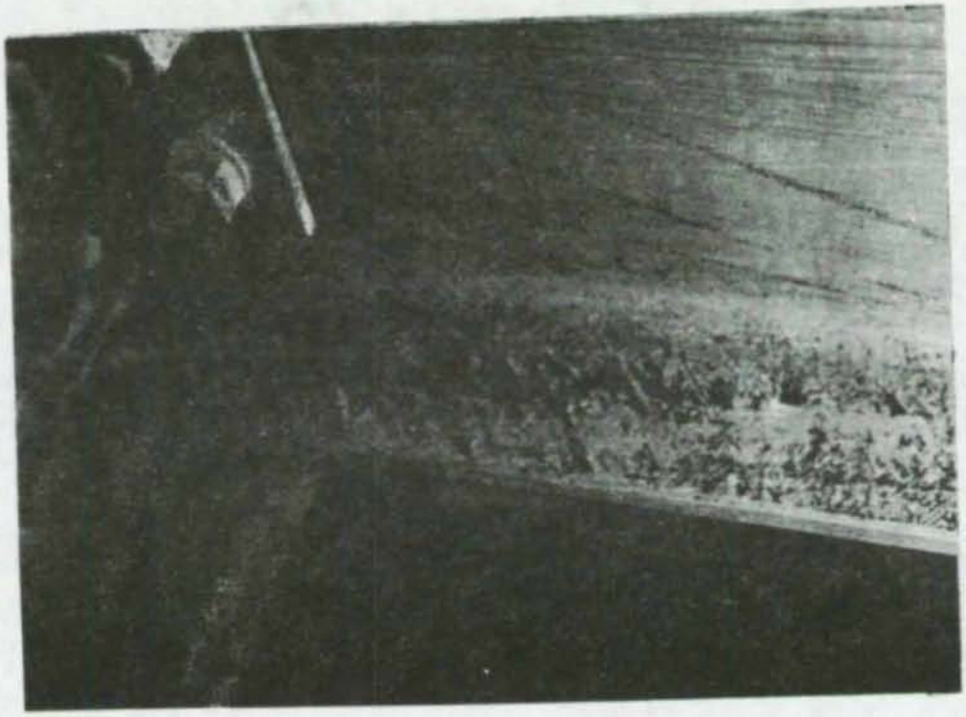

Figure 4.49 Yield of Bottom Flange,
Specimen 9

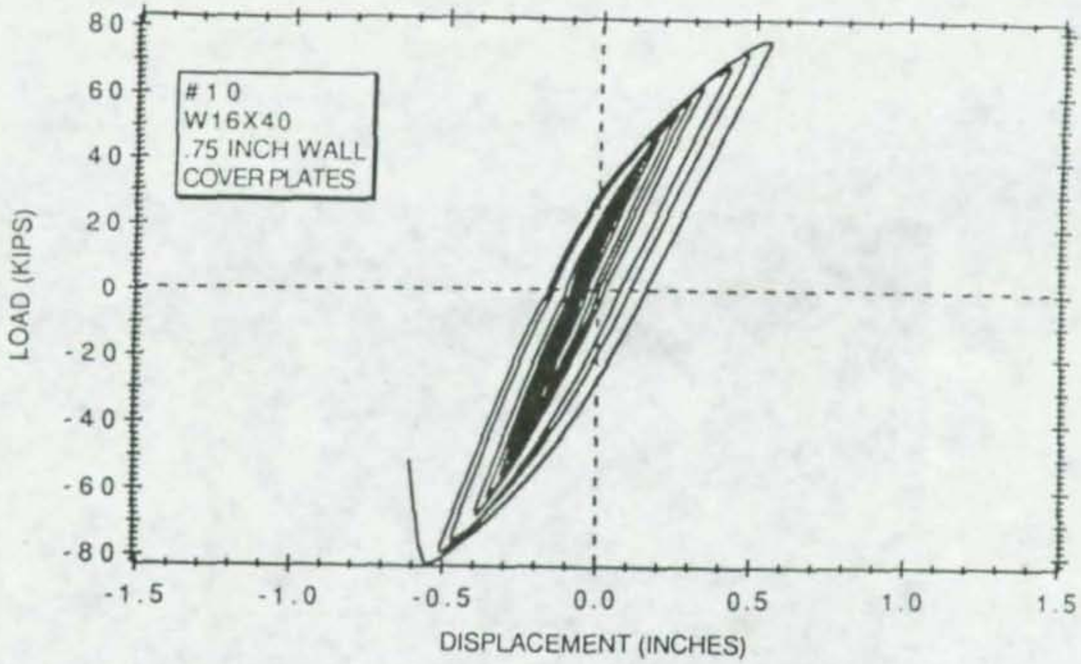

Figure 4.50 Base Shear vs. Displacement, Specimen 10

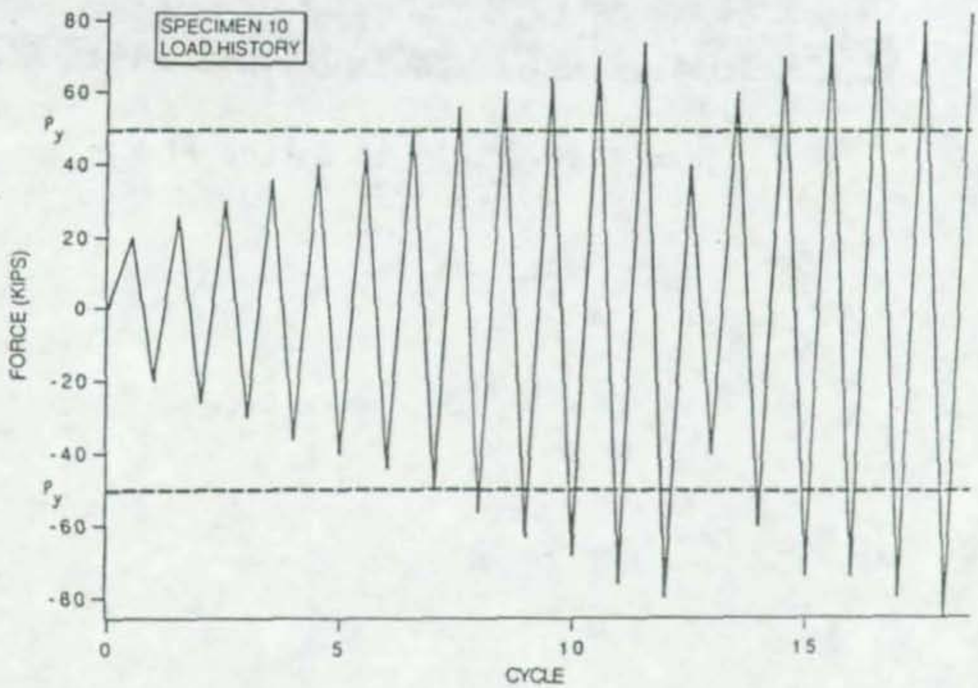

Figure 4.51 Loading Sequence, Specimen 10

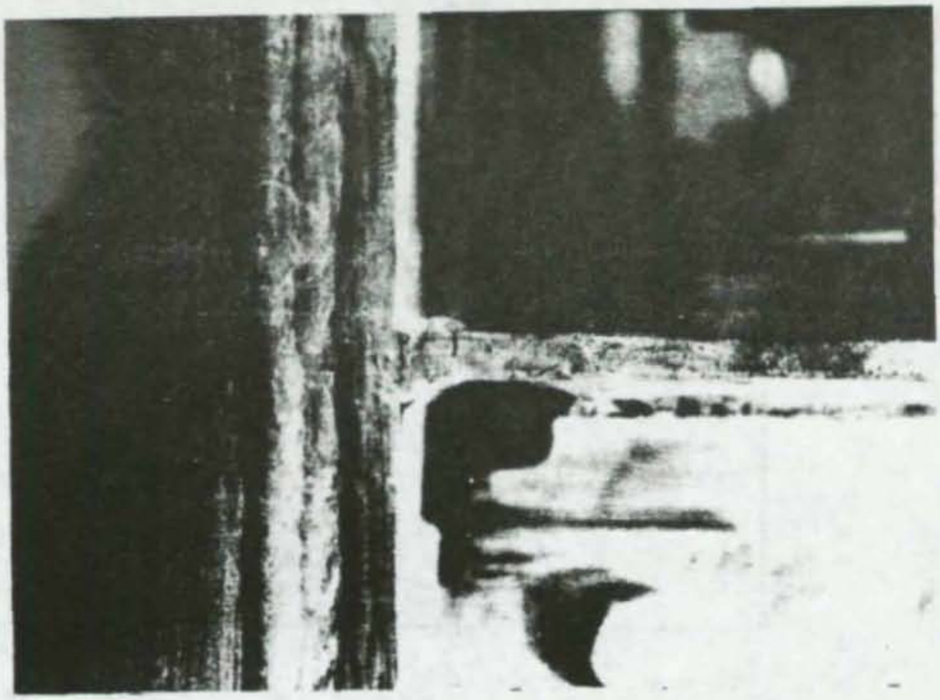

Figure 4.52 Crack in Top Flange, Specimen 10

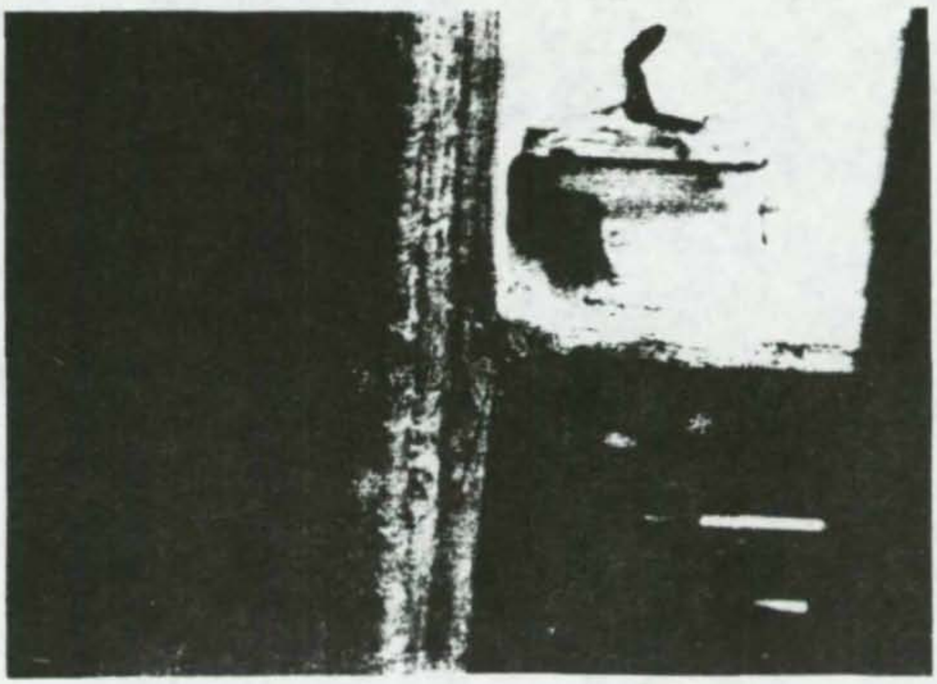

Figure 4.53 Split in Column, Specimen 10

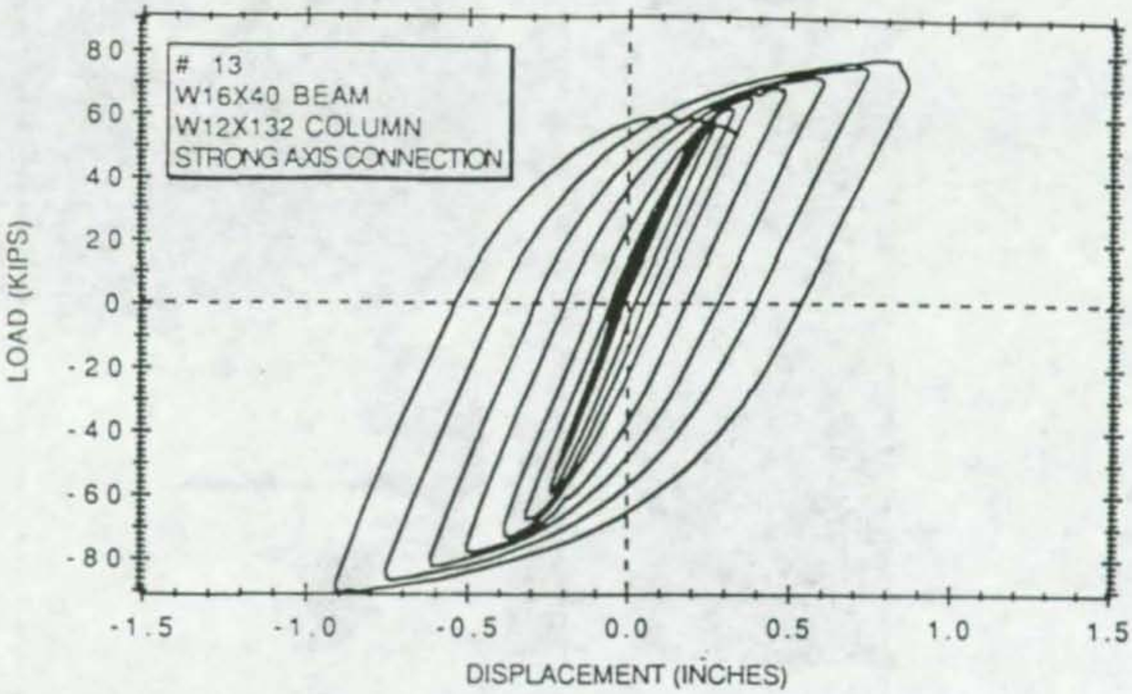

Figure 4.54 Base Shear vs. Displacement, Specimen 13

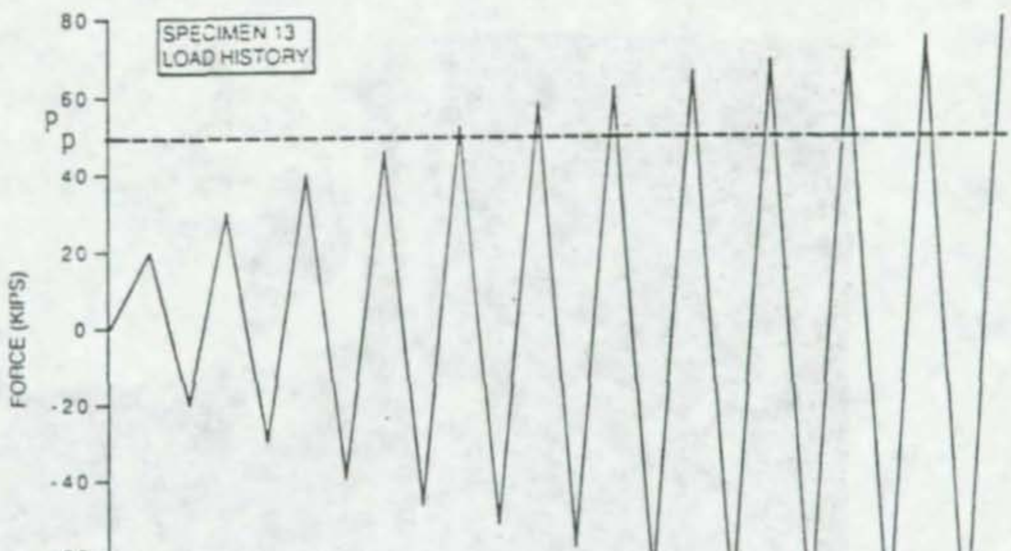

Figure 4.55 Loading Sequence, Specimen 13

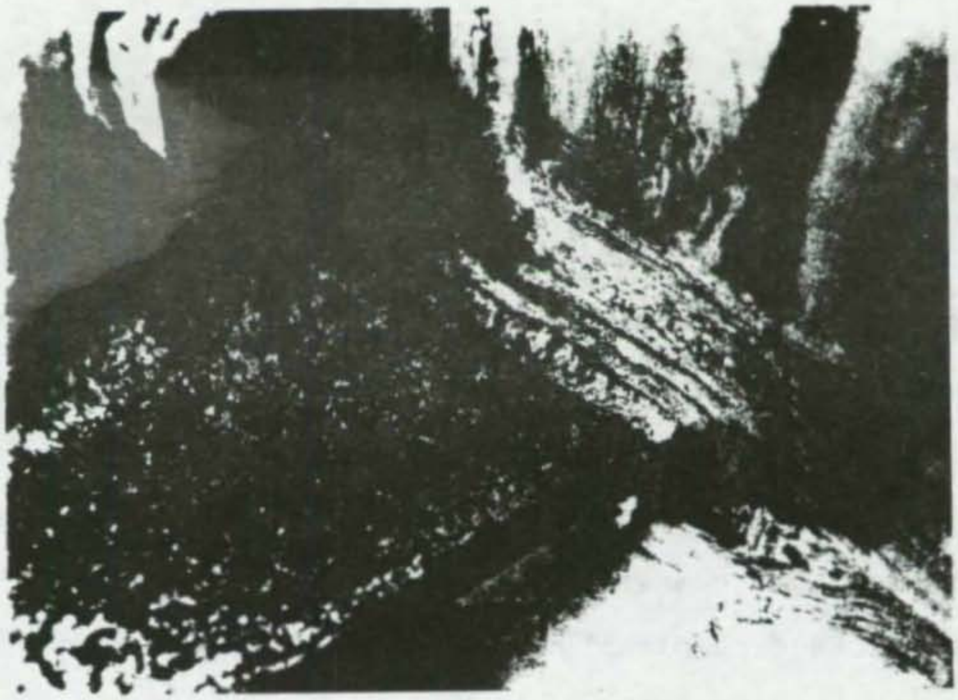

Figure 4.56 Crack at Web Cope, Specimen 13

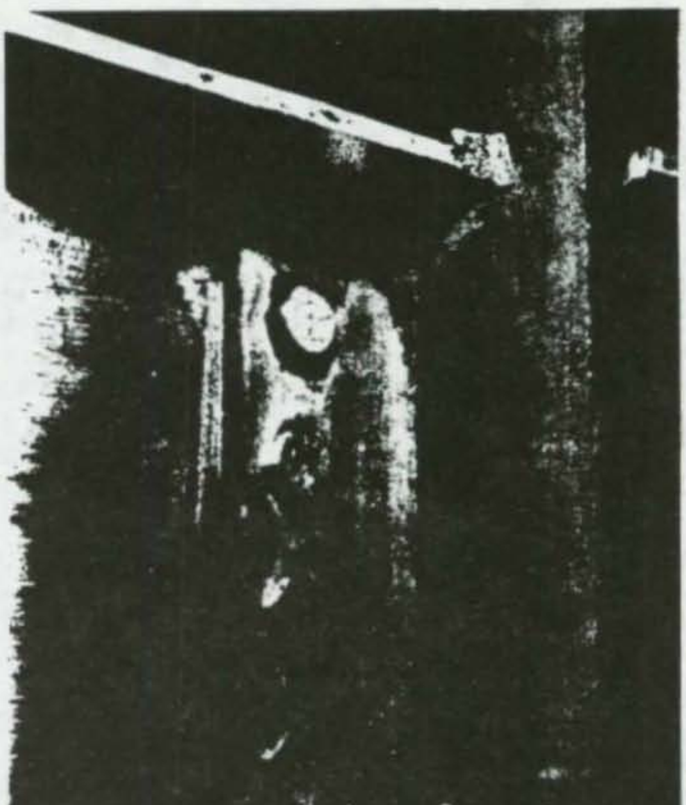

Figure 4.57 Plastic Hinge in Beam, Specimen 13

5.0 FINITE ELEMENT ANALYSIS

5.1 General

In order to gain better insight into the behavior of beam to box column connections a finite element analysis was undertaken concurrently with the experimental program. As stated in chapter one, the intent was to demonstrate that a finite element analysis using modern nonlinear finite element programs, coupled with an analytical model of sufficient complexity, can produce results that correlate well with those obtained from the experimental work. If this is possible, future work involving the variation of parameters can be undertaken using the finite element model, thus reducing the amount of expensive and time consuming experimental work.

However, it is recognized that a mathematical model can never incorporate all the complexities of a welded steel moment connection. Two experimental models of the same geometry and configuration will produce different results due to different workmanship during fabrication. Different crystalline structure of the steel caused by variations in rolling can also have an effect on the results. In this regard the finite element model has an advantage over the experimental model. The finite element method makes it easy to do parametric studies by allowing only one of the parameters to be varied while holding all others constant. On the other hand, the finite element model has limitations when it comes to predicting cracking and crack propagation.

Finite element programs are available which address the problems of crack initiation, propagation and fracture. They are expensive to run and are typically used only to model very small areas. The accuracy of the results they produce are very dependent on correctly modelling the residual stresses in the material due to rolling, welding and any flaws or weakness in the structure due to poor workmanship. For these reasons, tests of specimens where failure by fracture is expected are best done in the laboratory rather than relying on numerical solutions, or at least the results of finite element studies should be verified in the lab.

5.2 Discussion of Finite Element Program

The finite element program selected for use in this investigation was Nike3d, a fully vectorized, implicit, finite deformation, large strain, finite element code for analyzing the static and dynamic response of inelastic three dimensional solids, shells and beams. The program was developed at Lawrence Livermore National Laboratory (LLNL) by Hallquist [31] and interfaces with a preprocessor, Ingrid, also developed at LLNL, and a postprocessor, Post. For this study the program was run on a Convex C210 minisupercomputer. Nike3d uses the Hughes-Liu shell element [32] [33] which is considered a thick shell element because it includes shear deformations normal to the plane of the shell. The Hughes-Liu shell element is a four node element which uses a yield criteria based on the von Mises yield stress criterion. The model uses two by two quadrature in the plane of the element and a threepoint quadrature through the thickness of the element. The four node Hughes-Liu shell element was created by degenerating an eight node brick element. This is done by starting with an eight node brick element, adding in bending terms and then setting the normal stresses equal to zero.

Buckling is the result of nonlinear large deformation behavior and the large deformation characteristics of the shell element in Nike3d permit buckling to be captured. The main difference between Nike3d and other codes is the ability to look at post buckling behavior. Nike3d updates the system stiffness matrix at each load step to reflect the stiffness of the buckled geometry. In a linear finite element program, buckling is determined by checking the stiffness matrix for instabilities. The program must check each element to determine if buckling has taken place. However, once the program has determined that the model has buckled, it does not indicate the extent of the buckling or the magnitude of the nonlinear deflections. The large deformation characteristics of the shell element in Nike do not have this deficiency.

A complete discussion of the Nike code and the theory behind it are beyond the scope of this report. A much more complete discussion of the program and theory can be found in the references given above. The preprocessor Ingrid provides mesh generation and complete input file generation for Nike3d as well as for several other finite element codes developed at LLNL. Ingrid handles all materials data and geometry specifications with a minimum of input from the user and displays the geometry of the mesh as it is being created for the users benefit. After creation of the mesh and specification of boundary conditions, loads and material properties, Ingrid writes all files necessary to run Nike3d and Post.

5.3 Description of the Finite Element Model

The finite element mesh used for modelling Specimens 1, 2, 4, 5, 6, and 8 is shown in Fig. 5.1. The mesh is composed of 1395 nodes and 1312 shell elements. The mesh for Specimen 3 and Specimen 9 is shown in Fig. 5.2 and that for Specimen 7 in Fig. 5.3. The mesh for Specimen 3 and 9 included 1549 nodes and 1480 shell elements. The Specimen 7 mesh had 1467 nodes and 1384 shell elements.

The fineness of the mesh is increased in the beam and column near the area of the connection. The finest grid elements are sized one inch by one inch. Away from the connection the grid is coarsened by using elements of one inch by three inch dimension. Due to the symmetry of the problem it was decided to model only half of the specimen, slicing it down the middle in the plane of the web.

Modelling only half the specimen creates a few problems. The elements in the beam web are only half the thickness of the actual web. The nodes of the elements are slightly out of the plane of the web, where they would be if the full specimen was modelled. This offset of the element nodes allows for correct membrane stiffness in the model but leads to incorrect bending stiffness. However since the symmetry conditions constrain bending in these elements the problem does not affect the results of the analysis. The boundary conditions applied at the plane of symmetry are to restrain the motion along the axis perpendicular to the plane of symmetry and to restrain rotation around the two axes which define the plane of symmetry. In the current case, the plane of symmetry contains the X and Z axes. Therefore, the boundary conditions are to constrain axial motion along the Y axis and to constrain rotation about the X and Z axes.

The model is constrained against rigid body motion by fixing all degrees of freedom for each node at the base of the column. Fixing the base against both axial motion and rotation simulates the fully welded connection that was used in the experimental specimen. Motion along the X and Y axes is also prohibited for all nodes at the top of the column. This simulates the bracing of the experimental specimen against cantilever bending of the column. Because the symmetry constraints prohibit motion perpendicular to the plane of the beam web it was not necessary to further constrain the beam against out of plane buckling, which is provided in the real specimen by the tubular braces at the end of the beam.

There was a concern in the initial formulation of the model as to whether the top and bottom cap plates in the experimental specimen needed to be included in the finite element model. Because the nodes at the bottom of the column are constrained against all motion and rotation they react the same as if they were rigidly connected to an infinitely rigid plate. At the top of the specimen the nodes are free to rotate about any axis but are constrained in the x and y directions. This is equivalent to having a top plate which is infinitely rigid with respect to inplane forces but can bend freely. A computer run comparing a specimen with and without a top plate on the column showed that it made negligible difference as to the stresses in the column.

The model was loaded by applying a distributed load to the top of the column and at the end of the beam. The axial load to the column was figured by calculating the cross sectional area of the column and multiplying this area by a nominal stress of 12.5 ksi to give the total axial load in kips. This axial load was then divided by the number of nodes in the plane at the top of the column and this distributed force was applied to each node at the top of the column. The axial load was applied during the first load step and remained constant during each of the subsequent forty load steps. The beam loads were applied by dividing the maximum force in the last load step, 80 kips, by the number of nodes at the end of the beam. The initial load was set at zero and the load on the end of the beam was ramped from zero to eighty kips in two kip increments over forty load steps.

The size of the load step and its affect on the results of the study were considered. Several initial finite element runs were done using one, two, three and five kip increments. The force versus deflection curves at the end of the beam were then compared to determine the effect of the different size load steps. The five kip and to a certain extent the three kip load steps produced curves that were not completely smooth. The five kip curve was also slightly offset from the one kip curve. The one kip load increment resulted in very long run times. The two kip load increment seemed to provide the best compromise between accuracy of results and cost of computing time.

Applying an equal fraction of the beam load to each of the nodes on the end of the beam tended to cause the tips of the beam flange to bend at the higher loads. This could have been corrected by applying the distributed load only to the elements in the beam web. However, this would have complicated the input. In Ingrid there is a command which was used to apply the specified load at each point on a specified plane and it was this command which was used rather than specifying each node where the load was to be applied. Due to St. Venant's principle and the distance of the end of the beam from the area of interest it was decided that the bending of the beam flange tips at the end of the beam would not affect the results of the runs.

All of the finite element runs, except where otherwise noted, used the nominal material properties of A36 steel. The yield strength was taken as 36 ksi, the modulus of elasticity as 29,000 ksi and the tangent modulus for the nonlinear segment of the bilinear stress strain curve was taken as 300 ksi. As stated previously, the finite element runs were made on a Convex C210 with 64 megabytes of RAM and a clock cycle time of 40 nanoseconds. A run typically used 5.4 minutes of CPU time and a little over 8 minutes of combined CPU and I/O time. For specimens without stiffener plates (1,2,4,5,6,8), the model had 1395 node points and 1312 shell elements. For these specimens the stiffness matrix had a maximum column height of 342 and an average column height of 184.

5.4 Analytical/Experimental Comparisons

Several critical comparisons were made between results of the computer analyses and results of the experimental studies. This was done to evaluate the capability of the nonlinear computer program to represent the complicated inelastic behavior of a beam to column moment connection.

5.4.1 Moment Versus Rotation

The force versus displacement data from the finite element results were nondimensionalized and plotted on top of the nondimensionalized curves from the experimental data. The results are shown in Figs. 5.4 through 5.9.

The experimental data was nondimensionalized by converting beam displacements into rotations and the force applied at the end of the beam into a percentage of the nominal plastic moment capacity of the beam, M_p. Rotations were calculated by dividing the actual displacement by the distance from the point of measurement on the beam to the front face of the column, 36 inches, and taking the arcsine of this number.

Nondimensionalized moment is calculated by multiplying the load applied to the end of the beam as measured by the load cell on the Atlas cylinder by the distance from the application of the load to the face of the column, which was taken as 52 inches. The centerline of the hydraulic cylinder was actually 58 inches from the face of the column but it was assumed that only shear is transferred between the end plate of the beam and the clevis bracket plate on the cylinder. The moment calculated is then nondimensionalized by expressing it as a fraction of the full nominal plastic moment capacity of the beam.

The nondimensionalized hysteresis curve was then plotted against the nondimensionalized backbone or skeleton curve obtained from the Nike3d finite element runs. The skeleton curve was obtained from the finite element data by taking the deflection on the Z axis of a node corresponding to the location of the LVDT on the actual specimen and nondimensionalizing it. The loads to produce the displacement in the finite element model were similarly nondimensionalized. If there were perfect correlation between the finite element model and the experimental results, the skeleton curve should intersect the hysteresis loops at the point of load reversal of each loop.

The nondimensionalized curves and the backbone curves for specimen 3 are compared in Fig. 5.4. Here it can be seen that the backbone curve representing the finite element solution has a higher stiffness than the test specimen in both the elastic and inelastic regions. Among the factors that can contribute to these differences are the following: the residual stresses in the test specimen which arise as a result of rolling and fabricating the structural shape, the amount of fixity in the connection of the beam web to the column face by the bolted shear tab and the difference between the nominal yield stress of the material and the actual yield stress.

Similar results for specimens 4, 5, 6, 7, and 8 are shown in Figs. 5.5 thru 5.9. In all of these cases the agreement is much better in both regions and the backbone curve obtained from the finite element model gives a good estimate of the actual behavior.

5.4.2 Column Face Plate Bending

Bending of the column face plate has a direct effect on the stiffness and rotation of the connection. To better understand this behavior, bending plots of the column face profile were reprinted at 30 and 50 kips beam load. These are shown in Figs. 5.10 through 5.16. The profile was taken along the centerline of the column, coinciding with the plane of the beam web. In addition to the results of the finite element runs, the deflections of the column face during the experimental testing of the specimen, as measured by Linear Variable Differential Transformers (LVDTs), are shown with a black diamond on the column face profile. The measurements plotted for the actual experimental displacements were taken from the data, by reading displacements recorded by the LVDTs in the data block when the load cell on the beam end first recorded a force of 30 kips tension and first recorded a force of 30 kips compression. These two figures were then averaged, in order to account for zeroing errors, to find the displacement of the column face. The same was done for column face displacements at positive and negative 50 kips beam end force.

The data presented in tabular form in Table 5.1 shows the rotation of the beam column connection caused by the bending of the front face plate of the column at the centerline of the beam. These data are taken from the finite element runs. The average deflections of the column face plate at the centerline of the each beam flange for 30 and 50 kip cantilever beam loads are given in column three of the table. The degree of rotation of the connection is given by dividing the average horizontal deflection of the column face plate at the beam flange by the eight inch distance to the neutral axis of the beam and taking the arc tangent. Column four of the table gives this rotation in degrees. The rotation of the connection in percent (defined as hundredths of a radian) is given in column five of the table. The angle of rotation at the end of the beam is equal to the rotation of the connection and the rotation due to the elastic and plastic bending of the beam.

The results presented in this table clearly illustrate the influence of the face plate thickness and internal or external stiffeners on the stiffness of the connection. It can be seen that the smallest rotation occurs with specimen 9 which is representative of current design practice and that the largest occurs with specimen 1 which has an unstiffened 3/4 inch face plate. Specimen 6 which has a 1 inch face plate also has a relatively large rotation. There is a significant reduction in the face plate rotation between specimen 4 and specimen 6. Part of this is due to the thicker face plate, 1 1/4 versus 1, and part is due to the wider beam flange in specimen 4.

The profiles of the column face plate of Specimen 1 at 30 and 50 kips cantilever beam load as generated by the finite element runs are shown in Fig. 5.10. Experimental data from LVDTs showing actual displacement of the column face are 0.0148 inches at 30 kips and 0.1282 inches at 50 kips at a point one inch above the centerline of the top flange. This compares with displacements of 0.053 inches at 30 kips and 0.16 inches at 50 kips as calculated by the finite element runs. At a point 6 inches below the bottom flange of the beam, at the centerline of the column, the experimentally determined displacements of the column face plate were 0.0141 inches at a 30 kip cantilever load and 0.0293 inches at a 50 kip cantilever load. Rotations caused by faceplate deflection were calculated as 0.69% for a 30 kip load and 2.15% for a 50 kip load as shown in Table 5.1.

The displacement values obtained for Specimen 2, shown in Fig. 5.11, were 0.0186 inches for a load of 30 kips at a point one inch above the centerline of the top flange and 0.0093 inches at a point six inches below the bottom flange. The cantilever load on the end of the beam never reached 50 kips during the test and no displacement data is available at that level. Maximum force applied to the end of the beam as shown in Figs. 4.4 and 4.5 was about 40 kips.

For Specimen 3 at 50 kips the experimental displacement values from the LVDTs were 0.0132 inches, 0.0104 inches and 0.0087 inches at points below the centerline of the bottom flange of two inches, four inches and six inches, respectively. These experimental values are plotted on the profile of the column face displacement generated by the finite element program in Fig. 5.12. Column face plate rotations were calculated as 0.21% and 0.65% at 30 and 50 kips and are given in Table 5.1. Total rotation of the beam and connection at 50 kips from the experimental results was about 1.5% as shown in Fig. 5.4. Note that the nominal plastic moment capacity for the W16x40 is 2624 in-kips. Dividing by the moment arm of 52 inches gives a beam end load of 50.5 kips. Dividing 50 kips by the full plastic moment load of 50.5 kips results in a value of M/M_p of approximately one. Averaging the values for rotations obtained at the intersection of M/M_p equal to positive and negative one with the backbone of the hysteresis curves in Fig. 5.4 gives an approximate rotation of 1.5%. This suggests that the column face plate accounted for just under half the rotation of the connection.

As shown in Fig. 5.13, Specimen 4 had experimental displacements of the column face plate at points two, four and six inches below the centerline of the bottom flange of 0.0147 inches, 0.0166 inches and 0.0116 inches for a cantilever load on the end of the beam of 30 kips. For a 50 kip load the values were 0.0243 inches, 0.0323 inches and 0.0185 inches. Rotations due to deflections of the column face plate, as presented in Table 5.1, were 0.28% and 0.55% at 30 and 50 kips. From Fig. 5.5 the actual rotation for the entire subassembly at 50 kips was approximately 0.85% suggesting that the column face plate accounted for about two thirds of the rotation of the connection.

As discussed in Chapter 3, Specimens 5 and 6 shared the same geometry and nominal material properties. The experimental results differ based on the change in axial load applied to the two different specimens (400 kips for Specimen 5 and 800 kips for Specimen 6) and variations in actual material properties and workmanship. Due to the similarity of the two specimens, a finite element model was not run for Specimen 5.

Results for Specimen 6, shown in Fig. 5.14 indicate experimental displacement values at 30 kips of 0.0303 inches at two inches below the bottom flange, 0.0190 inches at four inches below and 0.0138 inches at six inches below the bottom flange. The corresponding displacements for a 50 kip load were 0.070 inches, 0.0393 inches and 0.0274 inches at two, four and six inches. In Table 5.1 the rotations calculated from column face deflections at 30 and 50 kips are 0.69% and 1.72% Average experimental rotation at the end of the beam was on the order of 1.8% at 50 kips as shown in Fig. 5.7.

For Specimen 7 the column faceplate displacements as measured by LVDTs at points 2 inches and 4 inches below the centerline of the bottom flange were 0.0135 inches and 0.0102 inches at a beam end load of 30 kips and 0.0308 inches and 0.0210 inches at 50 kips. These displacements are plotted in Fig. 5.15 against the column face profile generated by the finite element program. Rotations of the column face as shown in Table 5.1 are 0.34% and 0.86% at a cantilever beam load of 30 and 50 kips respectively.

Specimen 9 had LVDTs at points four inches and one inch above the centerline of the top flange of the beam and two inches, four inches and six inches below the centerline of the bottom flange of the beam. For a beam end load of 30 kips the respective column face plate deflections were 0.0143 inches, 0.0155 inches, 0.0064 inches, 0.0059 inches and 0.0052 inches. For a beam end load of 50 kips the displacements at the locations given above were 0.0289 inches, 0.0281 inches, 0.0113 inches,0.0104 inches and 0.0093 inches. Fig. 5.16 shows these experimental results plotted on the finite element generated displacement plots. Table 5.1 gives column faceplate rotations of 0.13% for a 30 kip load and 0.26% for a 50 kip load. The average rotation of the beam end was determined to be approximately 0.75% at 50 kips.

One can observe from the plots that in almost every instance the deflections of the column face recorded during the experiments were less than those predicted by the finite element models. Given that the finite element models often predicted smaller beam rotations for a given moment, this would imply that the finite element attributed more of the rotation of the connection to displacement of the column wall than actually took place and less deflection and rotation due to bending and hinging of the beam. This can be explained by noting that in the finite element model the beam is under emphasized and the faceplate of the column is over emphasized due to the rigid connection in the model at the web to face plate connection. In the analytical model the beam web and the column face plate shared common nodes and were rigidly connected at the joint. In the experimental specimen the beam webs were connected to the column face plate by a bolted web shear plate connection which had some slippage at higher loads, whereas the finite element model did not allow for this slippage. As would be expected, the model of Specimen 9 showed the least amount of column face deflection. It is interesting to note that Specimen 3, with the half thickness internal continuity plates, showed about twice the displacement of Specimen 9.

5.4.3 Yield Line Theory

The yield line theory assumes that plastic hinges form a distance six times the thickness of the plate (6t) above and below the beam flange. For the case of Specimen 1 it would appear that the hinge is about six to ten inches above the flange. In the area above the bottom flange and below the top flange the influence of the beam web allows only a linear deflection of the column face. Because of the beam web, the hinge below the top flange forms right at the beam flange rather than 6t below it. Observing the plots of Specimens 2, 4 and 7, one could argue that instead of four hinges forming, one above and below each flange, only two plastic hinges form in the column face, one at each flange. The only time that it appears that the column face under the web can even bend is in Specimens 3 and 9, both of which had continuity plates. The assumption in yield line theory that one can analyze the effect of a single beam flange on the column face, neglecting the influence of the web may not be entirely valid. It may be necessary to assume a mechanism about the whole beam, as Stockwell [14] has done for beam-column web connections, with hinges at each flange and a distance above the top flange and below the bottom flange. Stockwell also uses the figure of six times the column web thickness for determining the location of the hinge above and below the flange, but a larger number may be more appropriate, based on the few profiles considered in this test. It should be pointed out that in the model used in this analysis the elements of the beam web and the elements of the column wall share a common node in the wall of the column. This would correspond to a fully welded beam web which is not often the case. The finite element model did not have web copes, a shear tab or account for slippage of the bolts between the shear tab and the beam web, all conditions normally encountered practice.

In addition the finite element model used nominal material properties. The actual material yield strengths, as shown in Table 4.1, were in every case greater than the nominal. Each of these conditions would allow for additional flexibility in the column face plate under the beam web in the finite element model and would explain the smaller displacements of the column face plate obtained from the experimental results as compared to the finite element results.

5.5 Parametric Studies

In the course of the finite element studies of the beam to box column connections, several runs were made varying the size of only one parameter to determine how the particular parameter in question influenced the stiffness of the connection.

The curves plotted in Fig. 5.17 show how the behavior of the beam column connection varies as the ratio of the beam flange width to column width is varied. The dimensions and thickness of the column walls remain constant as does the thickness of the beam flanges and web and the height of the beam. Only the width of the beam flange is allowed to vary. In this case an eleven inch column with three quarter inch column walls was used with the beam having the dimensions of a W16x26. The rotation of the connection in percent (hundredths of a radian) is plotted against the moment applied at the column face. The lowest curve corresponds to a beam flange to column width of 0.5, giving a 5.5 inch flange width for an eleven inch wide column. This is the actual width of the W16x26 beam flange. The middle curve, noted as Run B, is for a flange to column width ratio of 0.7, which corresponds to an actual flange width of 7.7 inches. The uppermost curve, shown as Run C, was for a ratio of 0.9, which is a 9.9 inch flange width. As would be expected, increasing the flange to column width ratio increases both the stiffness of the connection and the plastic moment capacity of the beam. In order to develop the nominal plastic moment capacity of the beam, the narrow beam flange requires a connection rotation of 2% whereas the wide beam flange requires a rotation of only 1.4%. This indicates that for the 3/4 inch column wall, the width of the beam flange can have a significant effect on the moment rotation characteristics.

In Fig. 5.18 the ratio of beam flange to column width is again varied from 0.5 to 0.9 and the other dimensions of the beam correspond to that of a W16x26. The column retains an eleven inch width but the thickness of the column face has been increased to one inch. Comparing the curves in Fig. 5.18 with those in Fig. 5.17 illustrates the results of varying only the thickness of the column wall. In this case, the narrow beam flange can develop the nominal plastic moment capacity of the section with a rotation of 1.03% compared to the wide beam flange requirement of 0.93%. It can be readily seen that as the thickness of the column wall is increased, the effect of the width of the beam flange on the moment rotation characteristics of the connection has been reduced substantially.

The curves shown in Fig. 5.19 are for a column with wall thickness of 1 1/2 inch with all other parameters being the same as the two previous cases. In this case it can be seen that both the narrow beam flange and the wide beam flange develop the nominal plastic moment capacity of the section at a connection rotation of 0.57%.

In Figs. 5.20 and 5.21 the dimensions of the column and the beam are held constant and only the thickness of the column face plate is varied from three quarters inch thick to one and one half inch thick material. The data presented in Fig. 5.20 differs from Fig. 5.21 only in the size of the beam used and the horizontal line is used to indicate the nominal plastic moment capacity of the beam section. For the W16x26 beam, shown in Fig. 5.20, the data indicates that a rotation of 1.6% will be required to develop the nominal plastic moment with the 3/4 inch column wall compared to a value of 0.35% for a 1 3/4 inch wall. It would appear from the test results discussed previously that this range of connection rotation can be developed and that all column face plates should work with the W16x26 beam. Similar data for the W16x40 beam is shown in Fig. 5.21. Here it can be seen that if the 3/4 inch column face plate is used, a connection rotation of 2.6% is required in order to develop the nominal plastic moment capacity. For the 7/8 inch face plate the rotation requirement drops to 1.8% but both of these values are considered to be high. If the plate thickness is increased to one inch or above, the rotation requirement drops to 1.3% and below. These results indicate that for the W16x40 beam, a column face plate thickness of 1 inch or greater should be used.

5.6 Element Stress and Strain versus Load

The predominance of cracking of the beam flanges as the failure mechanism prior to either the development of a full plastic hinge in the beam or buckling of the beam flange indicates very large stresses and strains in the beam flange tips as a result of the flexibility of the column wall. In order to gain insight into the magnitude of the increase in stresses above those predicted by customary beam bending equations, the effective von Mises stress and the effective plastic strain were plotted against the applied beam load for the beam flange elements directly adjoining the column face. These curves were calculated by the finite element program Nike3d, using nominal material properties with a yield strength of 36 ksi. The numbering of the elements in the tension flange for all Specimens except 7 and 10 is shown in Fig. 5.22. As stated before, because of the symmetry of the problem, only half the column and beam were modeled. Fig. 5.22 shows the model reflected on itself, thus showing the entire width of the tension flange. Element 833 is at the tip of the beam flange, element 869 is at the plane of symmetry and elements 845 and 857 are located between 833 and 869 on the flange.

Specimen 7 had extension plates welded onto the sides of the beam flanges to increase the width of the flanges to the full width of the box column. The extension plates were the same thickness as the beam flange. Because of the extra width of the beam flange extra elements were included in the model. The preprocessor, Ingrid, which automatically numbered the elements therefore used a different element numbering sequence for Specimen 7. Fig. 5.23 shows the element numbers used for the tension flange of the beam. It should be noted that in this figure the model is not reflected and thus only half the beam flange is shown.

The stress versus load and strain versus load curves are shown in Figs. 5.24 through 5.39. The units along the horizontal axis are the load steps used in the finite element solution. Each load step was equal to two kips. Thus the units on the horizontal scale are in tons. The units on the vertical axis are in pounds per square inch for the stress curves and nondimensional units of strain (inches/inch) for the strain curves. These units apply for all the curves in this series. It can be seen that the stresses in the elements are not zero at time zero, but appear to have an initial prestress. This is because of the initial compressive axial load applied to the column prior to the first load step, which remained constant throughout the 40 load steps. The initial prestress causes an elastic compressive strain in the column. This compressive strain causes the distance between the beam flanges to shorten slightly causing an initial stress in elements of the beam connected to the column face which can be seen in the curves.

It can be observed in comparing the stress and strain curves for the same element and specimen that there are elements in which the curves never reach an effective stress of 36 ksi, the material yield stress, and yet show some plastic strains on the strain versus cantilever force curves. The explanation for this can be found in the way the finite element handles the stress and strain data from each of the integration points in the element. Each element has four in plane integration points on three separate planes through the thickness of the element, for a total of twelve integration points per element. Because of the nature of the problem it is quite probable that each of the elements on the beam flange next to the column wall experiences both in plane and out of plane bending. This would result in the integration points on different planes in the element showing large variations in stress at the same load step with some integration points undergoing stresses greater than the yield strength of the material at the same time as other integration points in the material are experiencing stresses well below yield. The program Nike averages across the four integration points on a plane in the element and stores a value for each through thickness plane in the element. The postprocessor, Post, then averages the values for each of the three planes to arrive at an average value for stress and strain for each element. If just one of the integration points has reached a level of plastic strain then that level will be averaged with the other integration points, which are zero, which will give a non zero plastic strain for the entire element. For this reason, the strain curve can show plastic strain in the element while the stress curve shows and effective stress of less than yield stress for the material. It was also be noted that the stresses and strains vary slightly between the tensile and compressive flanges, however, only the tensile flange will be discussed.

The von Mises stresses in the tension flange for Specimen 1 are shown in Fig. 5.24. Here it can be seen that the element at the edge of the flange reaches initial yield at a beam force of approximately 14 kips (7 tons). Using simple beam theory, first yield in the beam is calculated to occur at a load of 45 kips. For this specimen first yielding has occurred at approximately 31% of the nominal yield value. It can also be noted that at initial yield there is a very high stress gradient across the elements of the beam flange. The post yield increase in stress in the outside flange element, 833, indicates considerable strain hardening and associated large plastic strains. The allowable beam load based on the column capacity as calculated using Blodgett's equation is 14 kips which is a close approximation to initial yield.

The plastic strains for this specimen are shown in Fig. 5.25. Here, the high plastic strains in the outside flange element are readily apparent. Recall that for A36 steel, the nominal yield plateau, plastic strain at constant force, extends to a strain of approximately 1.5% at which point strain hardening of the material commences. The experimental specimen reached a maximum load of 48 kips (24 tons) which would indicate a plastic strain of 2.3% which is well into the strain hardening region. It should also be noted that in the experimental specimen failure occurred by the formation of a crack at the tip of the beam flange.

The stresses in the tension flange elements of Specimen 2 are shown in Fig. 5.26. In this case, initial yield occurs at approximately 15 kips which is 57% of the calculated value of 26.5 kips. However, it can be seen from the figure that at this load, the gradient of the stresses across the flange is much less than in the previous case. The experimental specimen reached a maximum load of 40 kips which represented a moment capacity which was 31% greater than the nominal plastic moment capacity of the beam. Allowable capacity of the column according to the Blodgett equation is 35 kips. At the force level of 40 kips (20 tons), it can also be seen that the stress distribution across the elements of the tension flange is close to uniform and that no significant increase in stress due to strain hardening has occurred.

This result can also be seen in the plastic strains which are shown in Fig. 5.27. At the maximum load of 40 kips (20 tons), the maximum plastic strain is approximately 0.8% which is well within the nominal yield plateau of the A36 steel.

Specimen 2 has a thicker column wall than Specimen 1 and a smaller beam. The curves show that the thicker column wall allows the beam to distribute the bending stresses across the entire width of the flange in a more uniform manner. The thin column wall in Specimen 1 causes more of the stress to be concentrated in the outer edge of the flange.

The stress versus load curves for Specimen 3 are shown in Fig. 5.28. This specimen had an internal stiffener plate which was half the thickness of the beam flange and a W16x40 beam. The calculated force at yield is 45 kips, while the finite element analysis shows initial yielding in the outer element of the flange to occur at approximately 58% of this value (26 kips). The maximum load attained in the experimental specimen was 73 kips (36.5 tons) which resulted in a plastic moment capacity which was 45% above the nominal capacity. At this level of loading, stress increase due to strain hardening has just begun to occur in the outside element (833). Although not as uniform as Specimen 2, the stresses at ultimate load are much more uniform across the beam flange than for Specimen 1.

The plastic strains in the beam flange elements of Specimen 3 are shown in Fig. 5.29. The reduction in strain in the elements, particularly the element located at the edge of the beam flange, compared with the strain experienced in the unstiffened connections is quite apparent. At the ultimate load of 36.5 tons, the plastic strain in the outermost beam flange element is 1.8% which places it at the beginning of the strain hardening region.

Strains in the other elements are well within the yield plateau.

A comparison of stresses in the beam flange of Specimen 4, is shown in Fig. 5.30. Initial yield occurs at approximately 16 kips which is 36% of the nominal yield. The experimental specimen attained a maximum beam load of 74 kips (37 tons) which represents a moment capacity 47% greater than the nominal plastic moment capacity of the beam. At this load, there is a considerable spread (12,000 psi) in the stress curves representing a substantial stress gradient across the beam flange.

This is reflected in the curves of plastic strain shown in Fig. 5.31. Here, it can be seen that at maximum load the outer flange element has a maximum strain of 2.4% which places it well into the strain hardening region. Other flange elements have strains less than 1.5% and are therefore still in the material yield plateau.

The stress curves for Specimen 6 are shown in Fig. 5.32. The only difference between this specimen and specimen 2 is the 1/4 inch reduction in the thickness of the column face plate. Comparing the results presented in Figs. 5.26 and 5.30, it can be seen that there is a significant change in the pattern of all four stress curves. The curves for Specimen 2 are more closely spaced, representing a more uniform distribution of stress across the full width of the beam, whereas those of Specimen 6 are more widely spaced and are representative of higher stress gradients. The maximum load attained in the experimental specimen was 50 kips which is representative of a plastic moment capacity which is 63% above the nominal. At this load level, the outer flange element shows considerable strain hardening.

The plastic strain distributions for specimen 6 are shown in Fig. 5.33. Comparing the element strains in Figs. 5.27 and 5.31, it can be seen that at maximum load, the plastic strain in the outside flange element of Specimen 6 reaches a value of 2.6% which is well into the strain hardening region. Plastic strains in the other flange elements are within the nominal yield plateau. At 50 kips beam load the strain in the outermost flange element Specimen 2 is approximately 1.5% which represents the end of the nominal yield plateau.

The finite element study indicates that there is a considerable difference in the performance of Specimen 2 and Specimen 6 showing that the change in thickness of the column faceplate of 1/4 inch has a significant effect. Referring to the experimental results in Tables 4.2 and 4.3 and the discussion in Section 4.3 of the previous chapter one does not observe this difference.

Stresses in the beam flange elements of specimen 7 which has the flange extension plates are shown in Fig. 5.34. The curves representing the stresses in the tension flange have a uniform spacing. Yield in the outermost beam flange element occurs at about 10 kips cantilever beam load which is 38% of that calculated using simple beam theory. At the maximum load of 63 kips (31.5 tons) the stresses are well distributed across the beam flange with some increase in stress due to strain hardening occurring in the outer element.

The plastic strain curves shown in Fig. 5.35 indicate the presence of large plastic strains in the outer two elements of the beam flange. The plastic strains in the outer element reach 3.5% and those in the next element reach 2.0%. Both values are well into the strain hardening region. This indicates a concentration of stress in the beam flange extensions opposite the column web walls which are much stiffer than the column face. Recall that this specimen failed by the development of a vertical crack in the weld connecting the column face plate to the side plate. This failure was most likely due to the high stresses in this region.

Specimen 9 is representative of current design practice, having internal stiffener plates the full thickness of the connecting beam flange. The stress curves are shown in Fig. 5.36. Here it can be seen that initial yield occurs at approximately 30 kips which is 67% of that calculated using beam theory. The experimental specimen reached a maximum load of 80 kips (40 tons) representing a plastic moment capacity which is 59% above the nominal plastic moment capacity of the beam. At this load level, it can be seen that the stress distribution across the beam flange is very uniform.

The curves representing the distribution of plastic strain are shown in Fig. 5.37. Here it can be seen that the plastic strains in all elements of the beam flange are in the yield plateau of the material and are therefore less than 1.5%.

Specimen 13 is a typical wide flange beam to wide flange column connection which is used as a benchmark for evaluating the other connections. The stress curves for this specimen are shown in Fig. 5.38. It can be seen that the element stress curves for this specimen are very similar to those of the previous specimen having a relatively close spacing across the width of the flange and therefore indicating low stress gradients. Initial yield in the outermost element occurs at approximately 40 kips which is 89% of the nominal yield value. The maximum load attained in the experimental specimen was 91 kips (45.5 tons) which represents a plastic moment capacity which is 80% above the nominal and is beyond the scope of the analytical study. However, at 40 kips, it can be seen that the stress curves are closely spaced indicating an almost uniform stress distribution across the beam flange.

The curves representing plastic strain are shown in Fig. 5.39. It is readily apparent that for this type of connection, the plastic strains at ultimate load are all small being less than 0.5% which is well within the nominal yield plateau.

TABLE 5.1

COLUMN FACEPLATE ROTATIONS

Specimen Number	*Load Kips*	*Deflection Inches*	*Rotation Degrees*	*Rotation* % (0.01*Radians*)
1	30	0.0552	0.3951	0.69
1	50	0.1724	1.2345	2.15
2	30	0.0276	0.1605	0.34
2	50	0.0655	0.4734	0.83
3	30	0.0172	0.1232	0.21
3	50	0.0517	0.3704	0.65
4	30	0.0224	0.1605	0.28
4	50	0.0441	0.3156	0.55
6	30	0.0482	0.3457	0.69
6	50	0.1379	0.9878	1.72
7	30	0.0276	0.1976	0.34
7	50	0.0690	0.4939	0.86
9	30	0.0103	0.0741	0.13
9	50	0.0207	0.1482	0.26

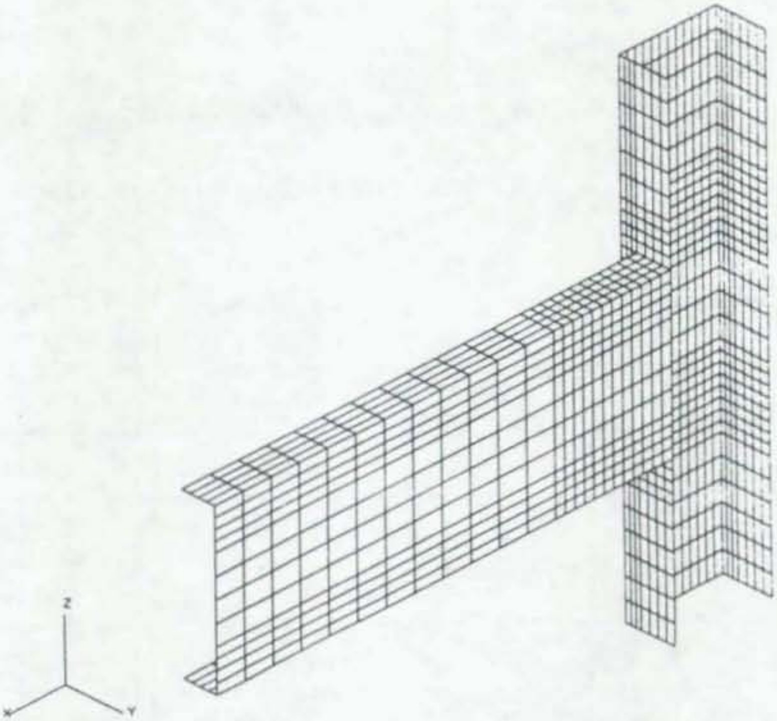

Figure 5.1 Typical Finite Element Mesh

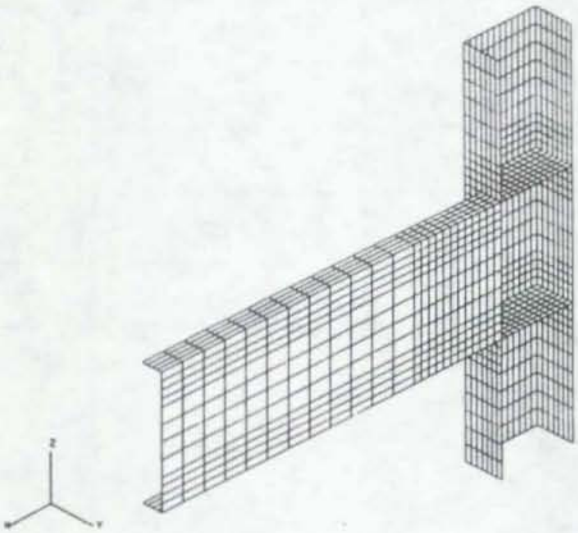

Figure 5.2 Finite Element Mesh,
Specimens 3 and 9

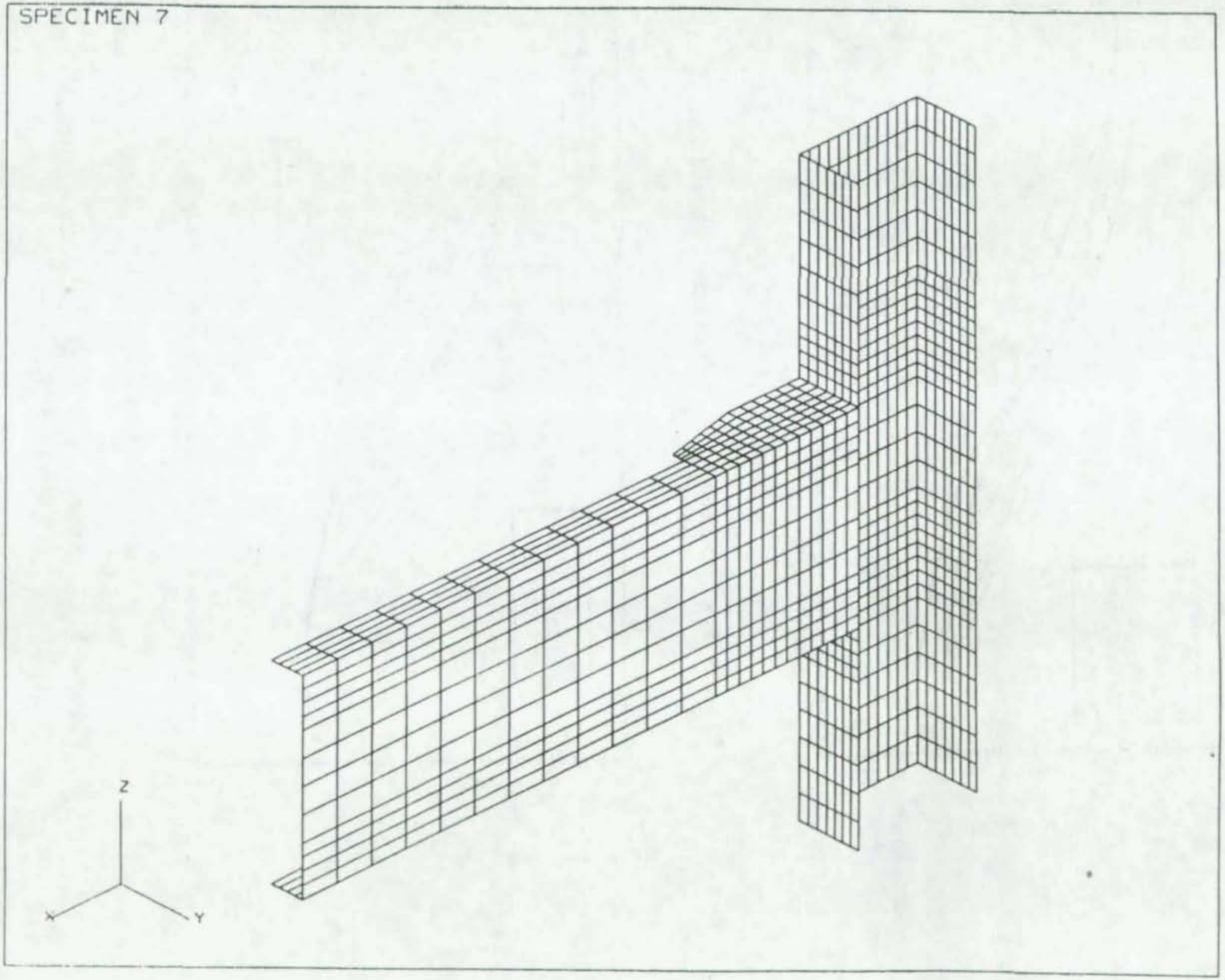

Figure 5.3 Finite Element Mesh, Specimen 7

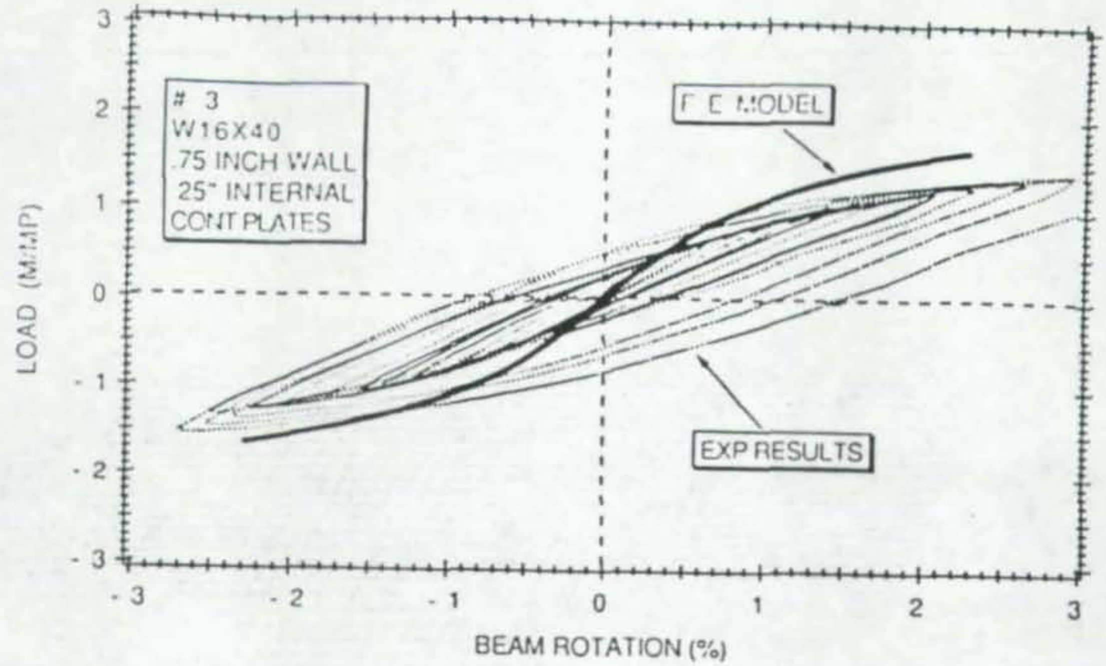

Figure 5.4 Moment vs. Rotation Comparison, Specimen 3

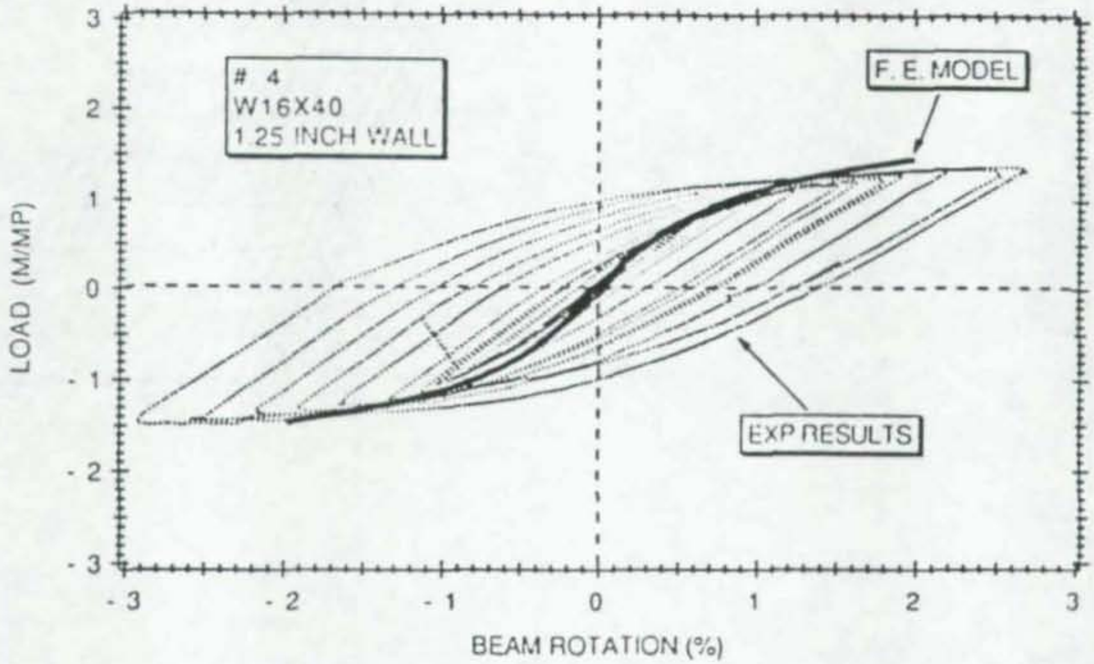

Figure 5.5 Moment vs. Roataion Comparison, Specimen 4

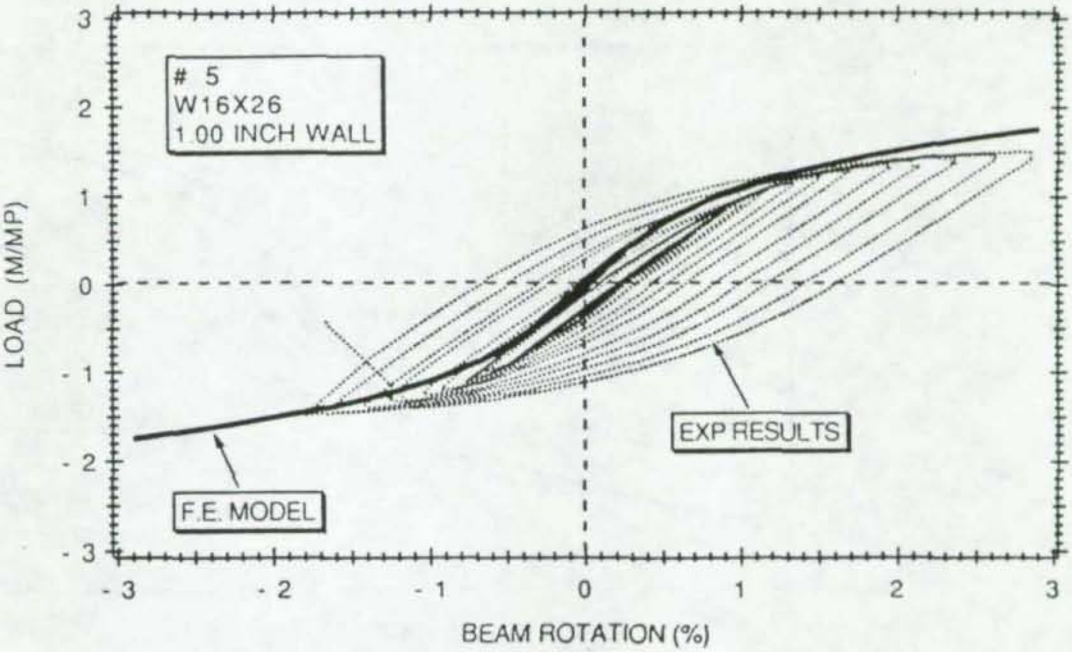

Figure 5.6 Moment vs. Rotation Comparison, Specimen 5

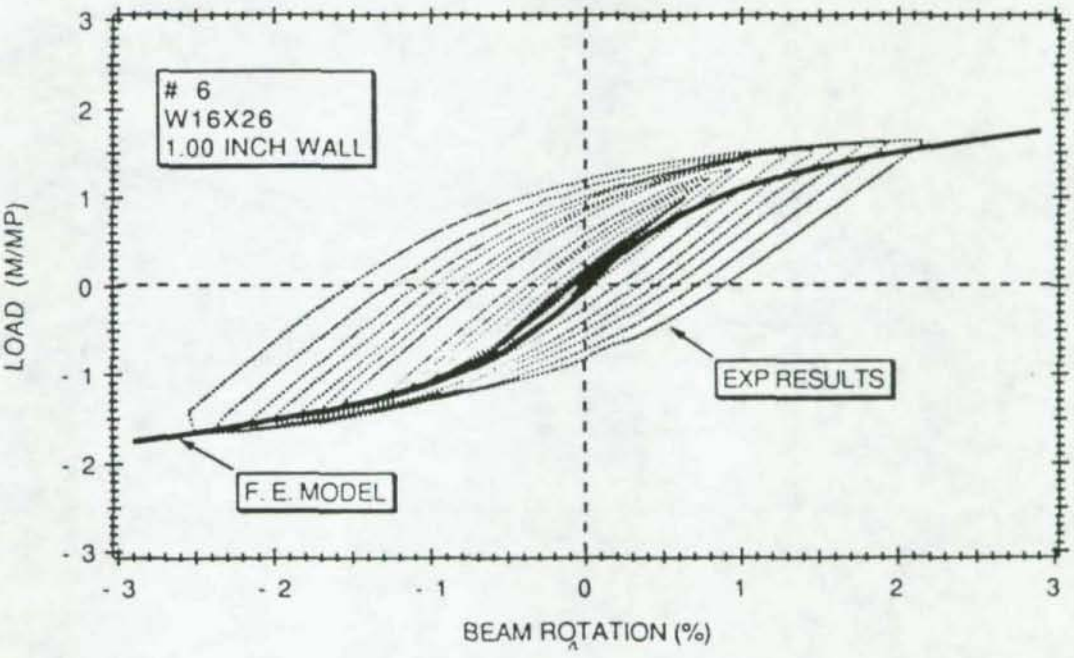

Figure 5.7 Moment vs. Rotation Comparison, Specimen 6

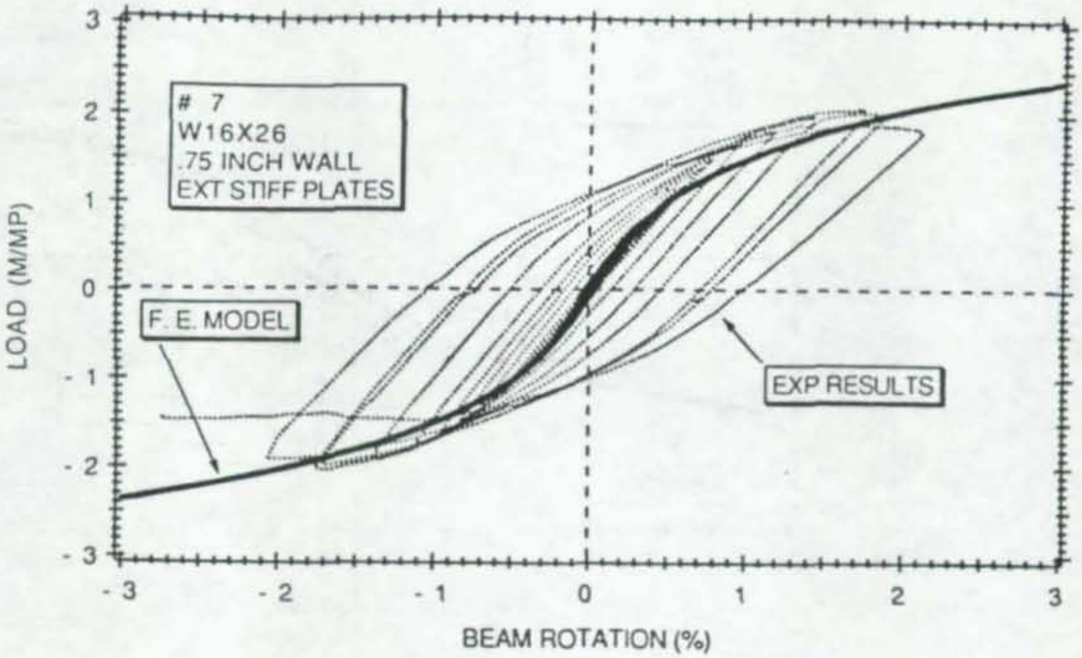

Figure 5.8 Moment vs. Rotation Comparison, Specimen 7

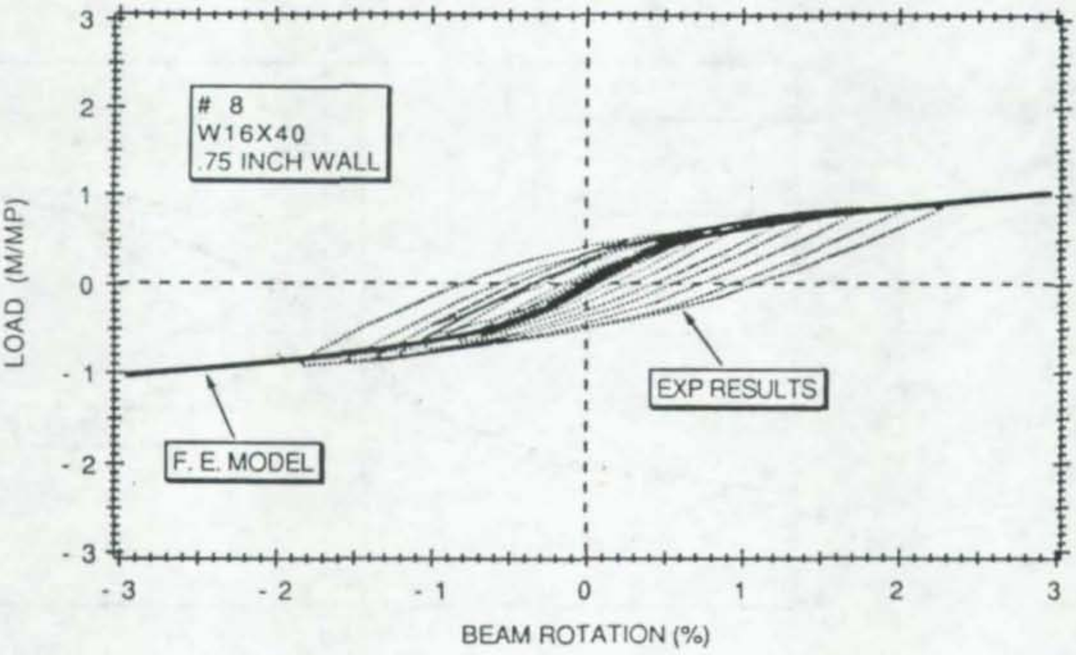

Figure 5.9 Moment vs. Rotation Comparison, Specimen 8

Column Face Displacement (Specimen 1)

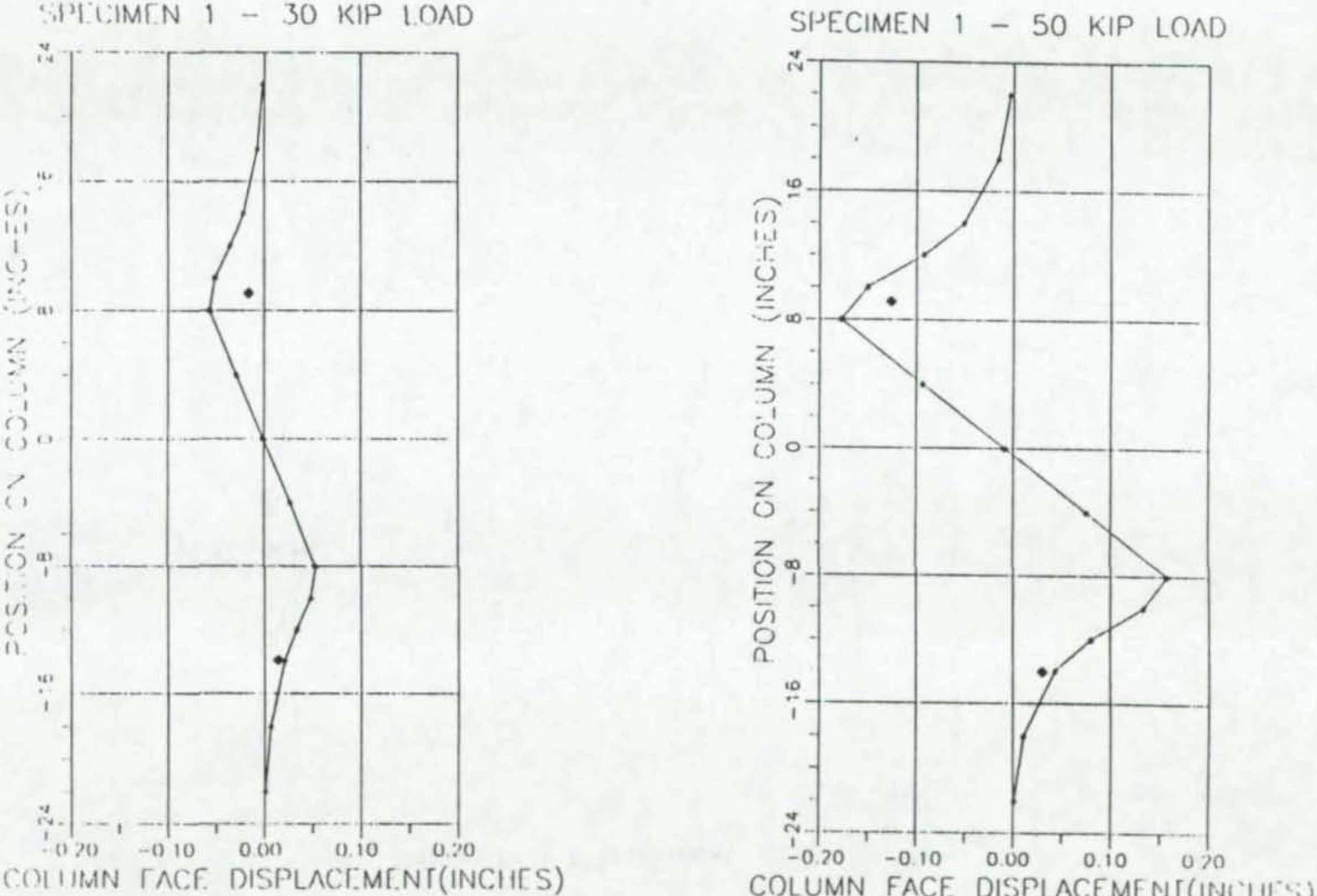

◆ Experimental Results

Figure 5.10 Column Face Plate Displacement, Specimen 1

Column Face Displacement (Specimen 2)

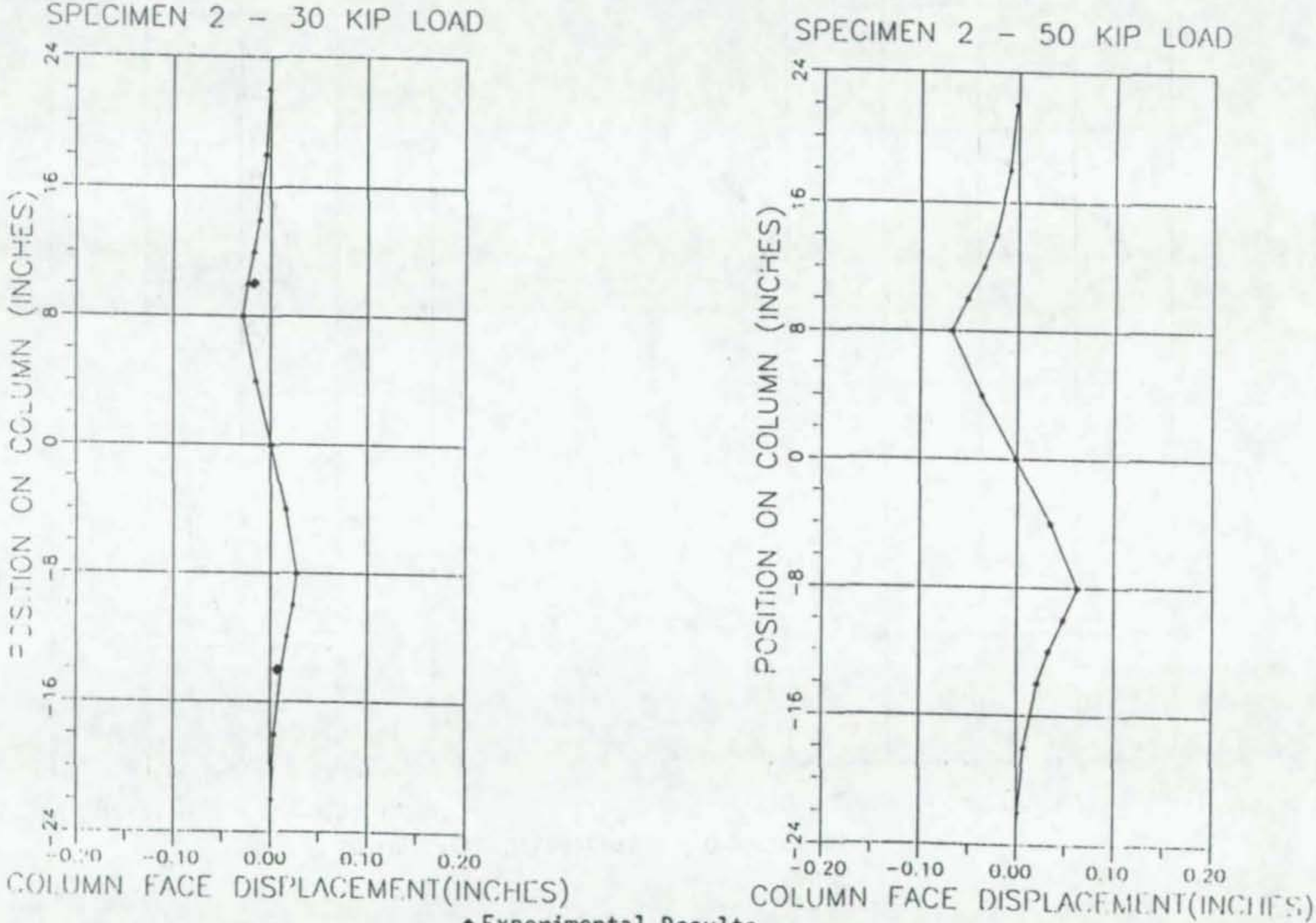

• Experimental Results

Figure 5.11 Column Face Plate Displacement, Specimen 2

Column Face Displacement (Specimen 3)

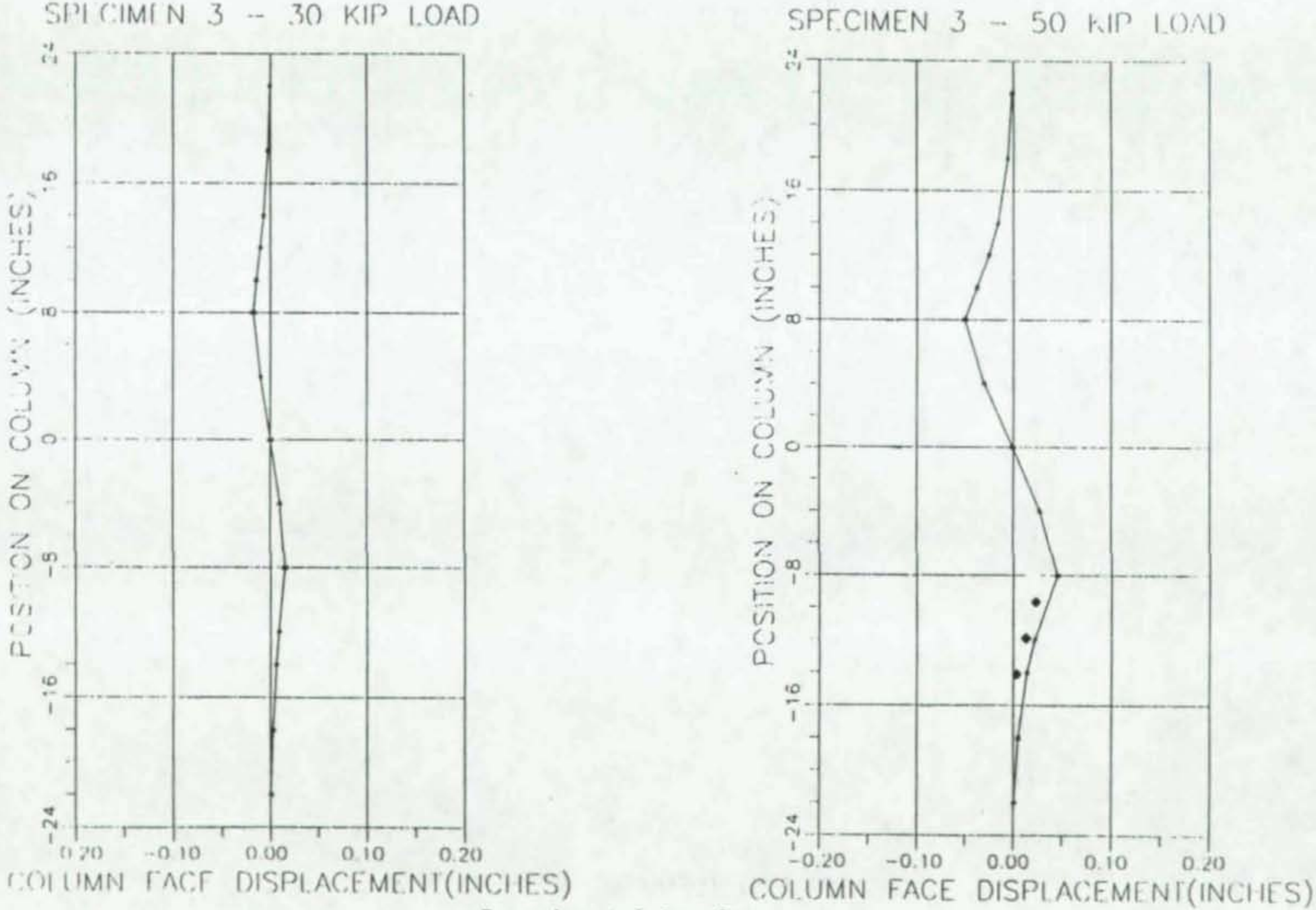

• Experimental Results

Figure 5.12 Column Face Plate Displacement, Specimen 3

Column Face Displacement (Specimen 4)

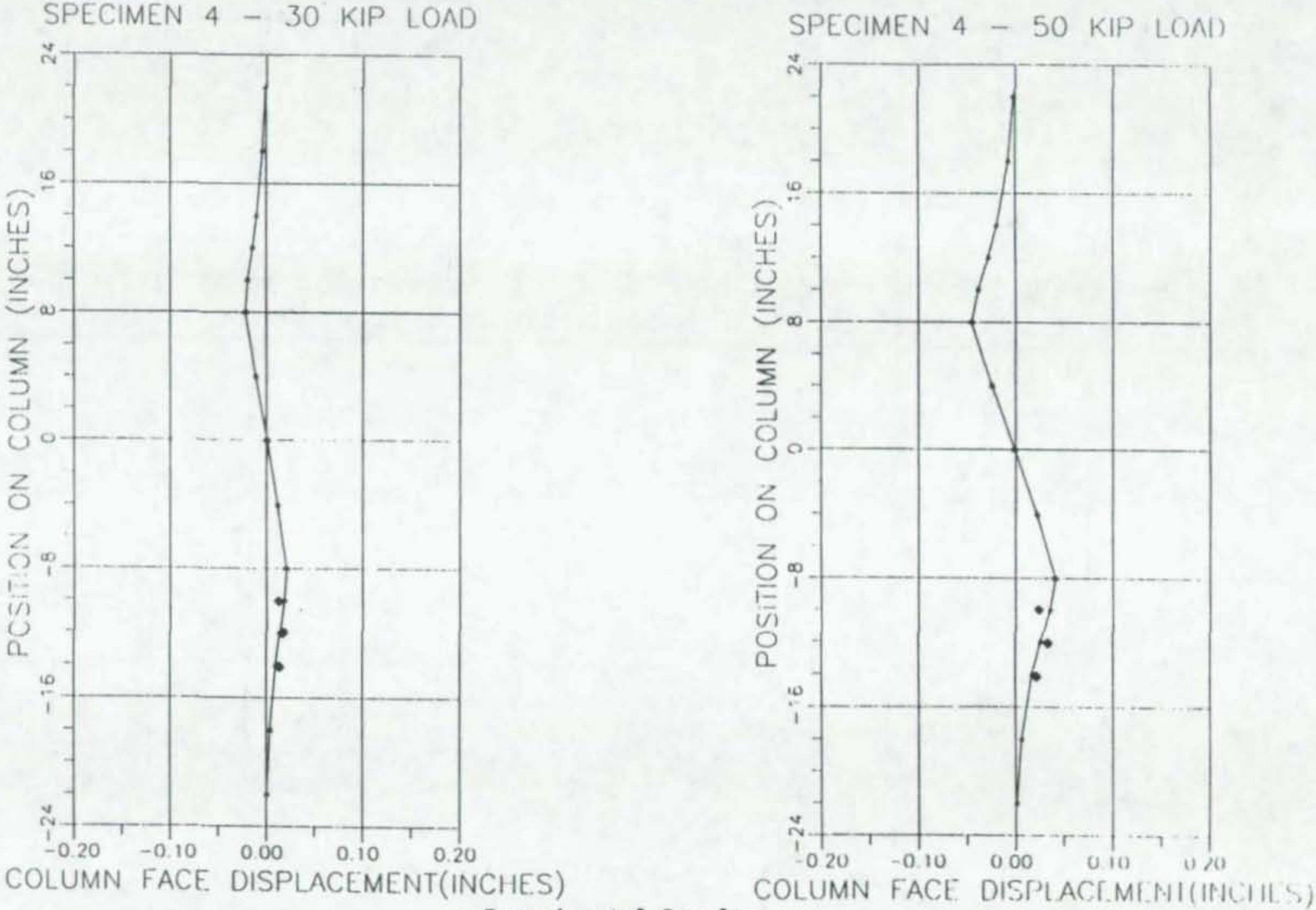

• Experimental Results

Figure 5.13 Column Face Plate Displacement, Specimen 4

Column Face Displacement (Specimen 6)

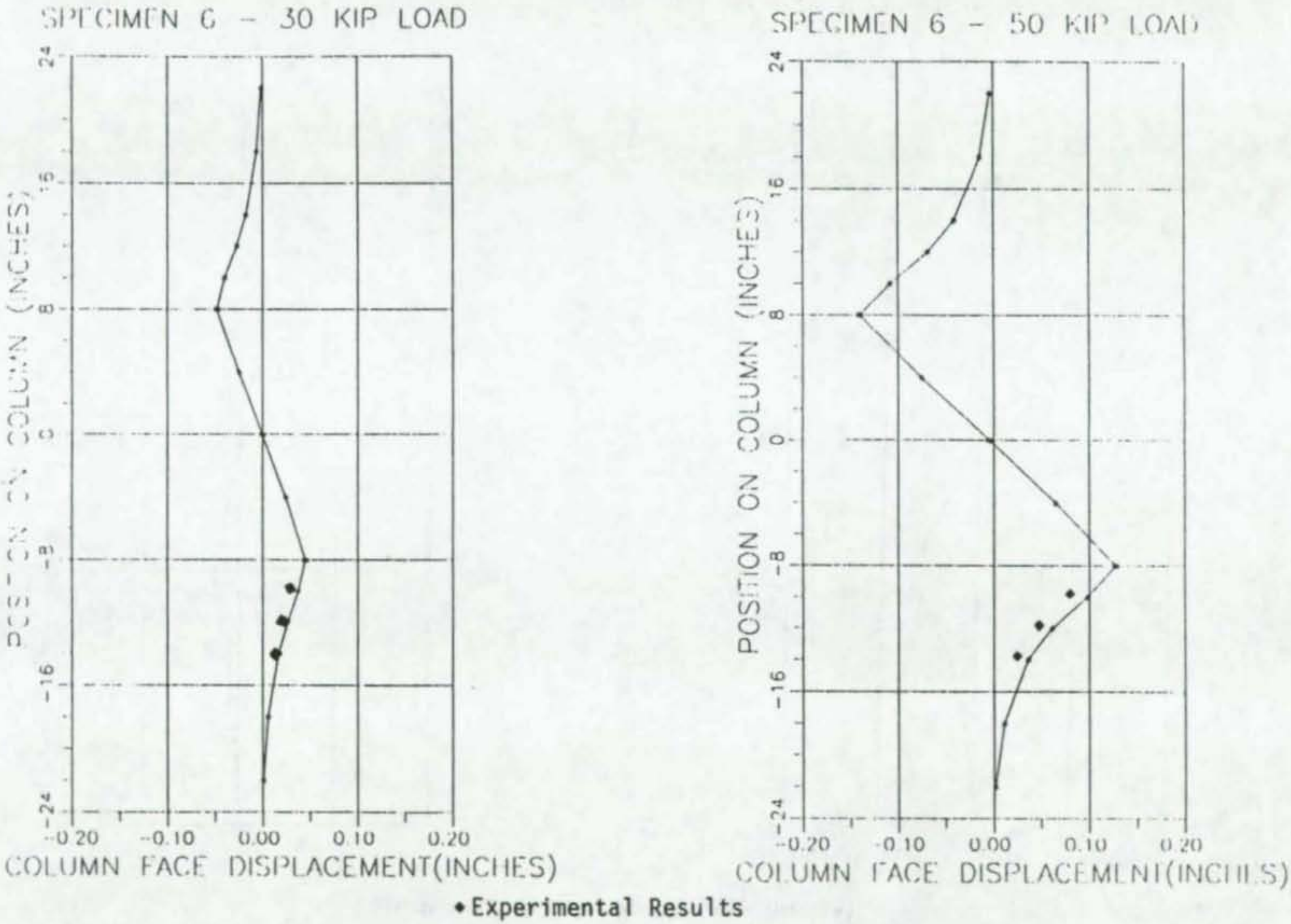

Figure 5.14 Column Face Plate Displacement, Specimen 6

Column Face Displacement (Specimen 7)

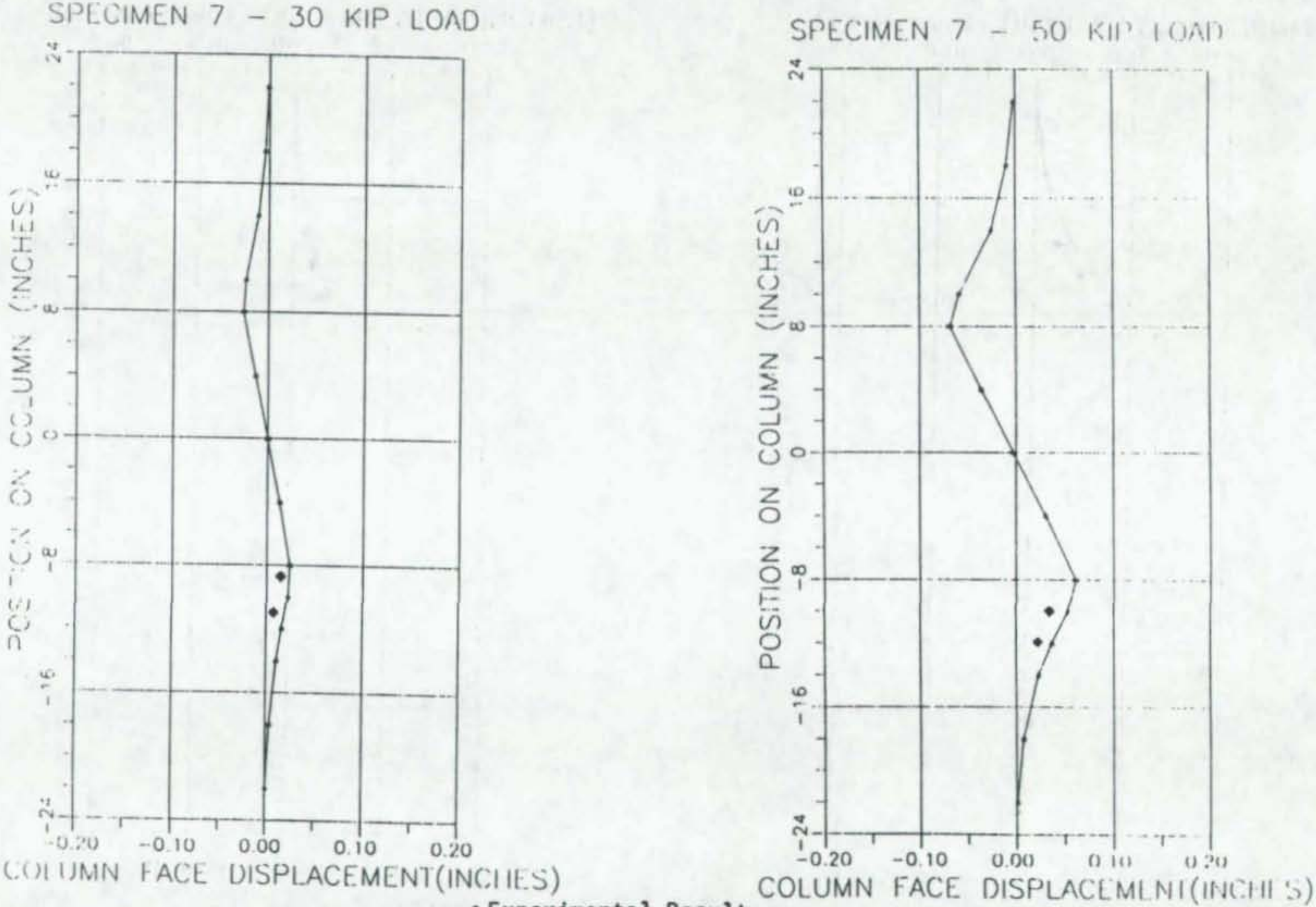

• Experimental Results

Figure 5.15 Column Face Plate Displacement, Specimen 7

Column Face Displacement (Specimen 9)

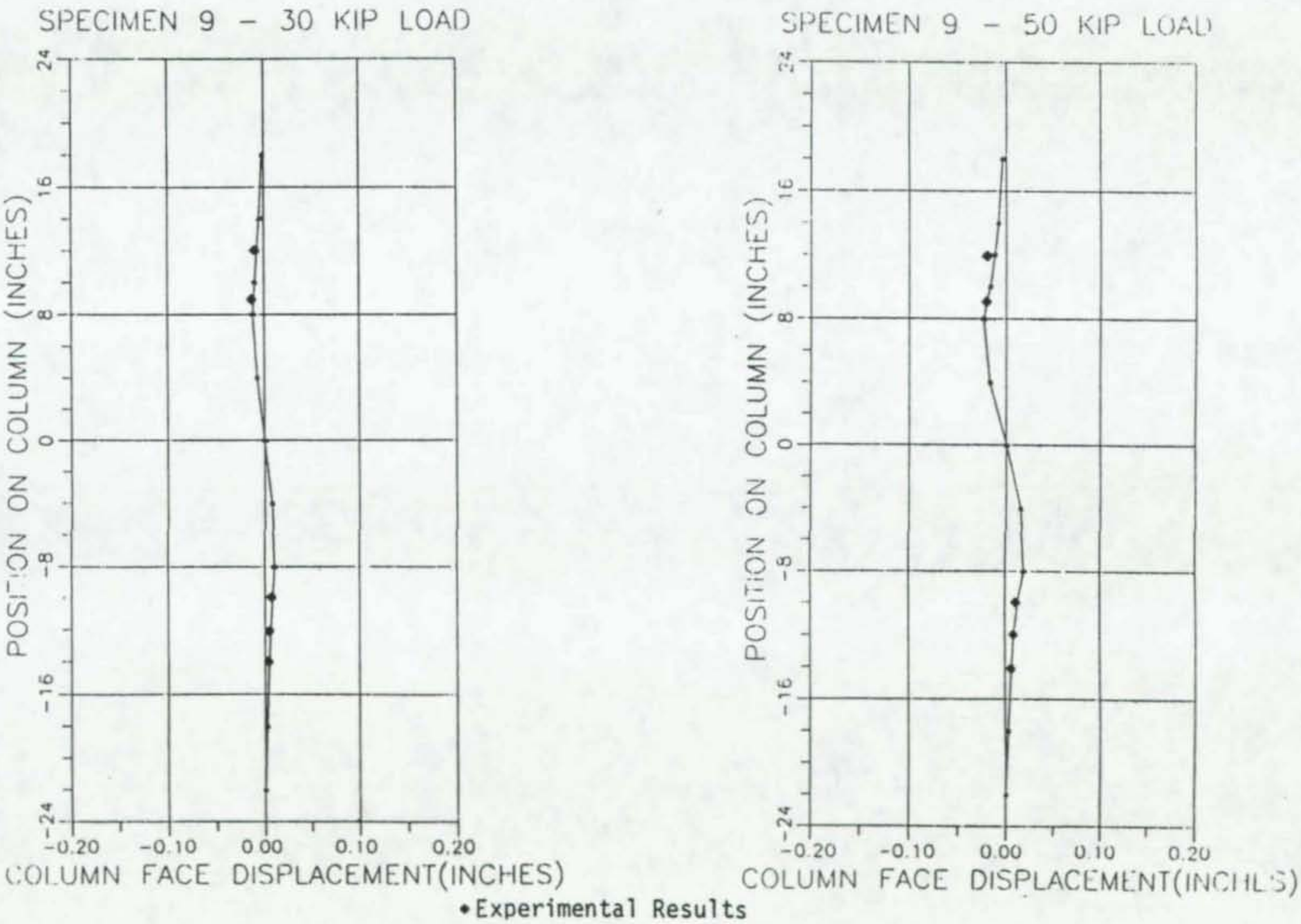

Figure 5.16 Column Face Plate Displacement, Specimen 9

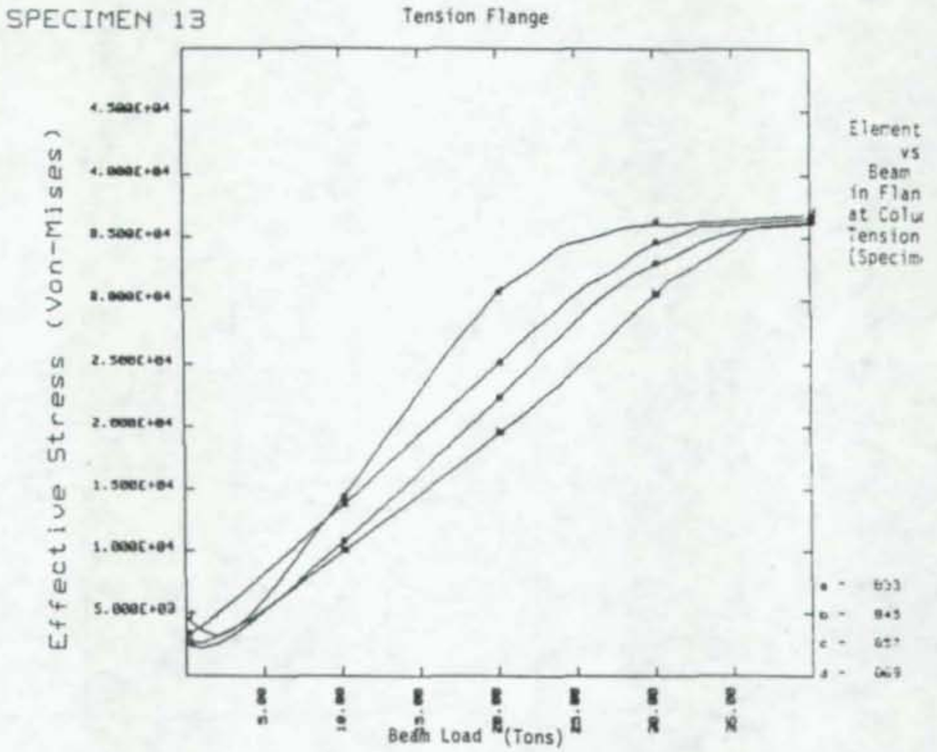

Figure 5.38 Element Stress vs. Beam Shear, Specimen 13

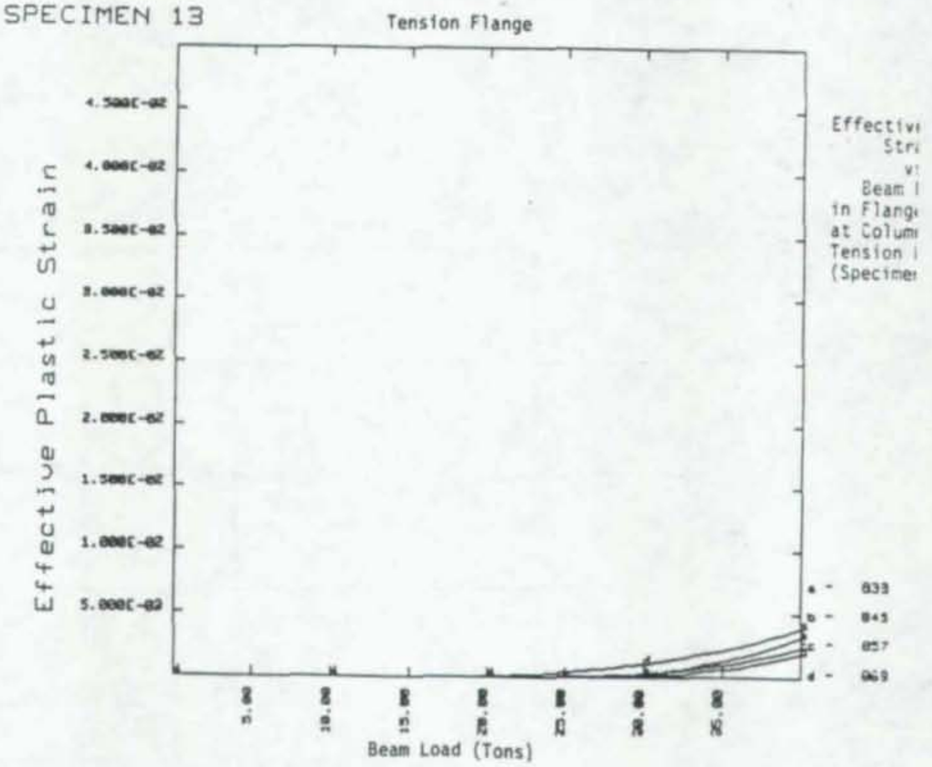

Figure 5.39 Element Strain vs. Beam Shear, Specimen 13

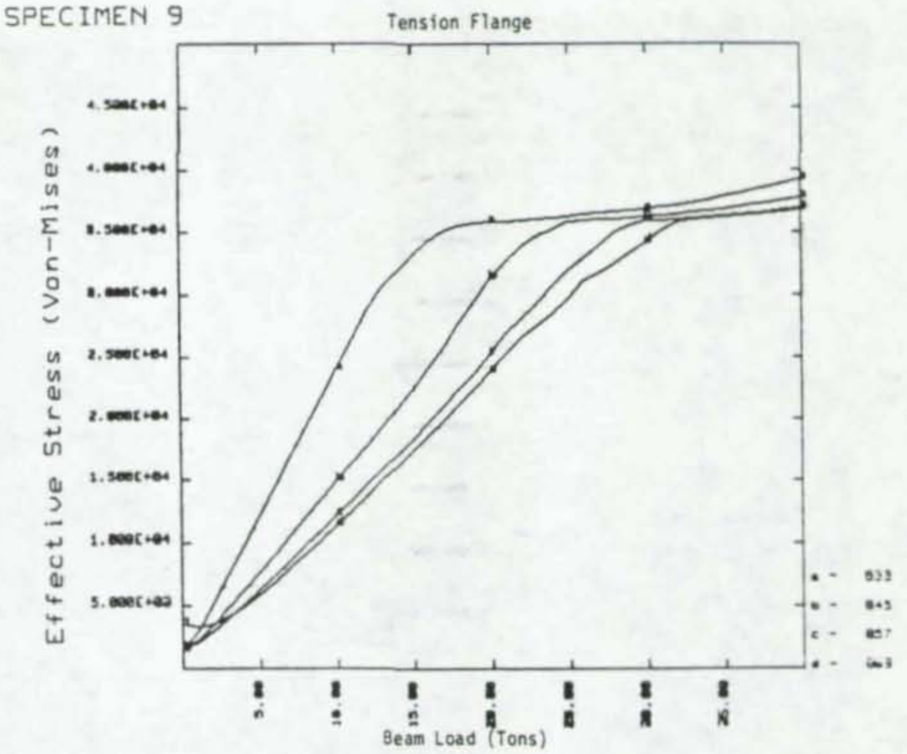

Figure 5.36 Element Stress vs. Beam Shear, Specimen 9

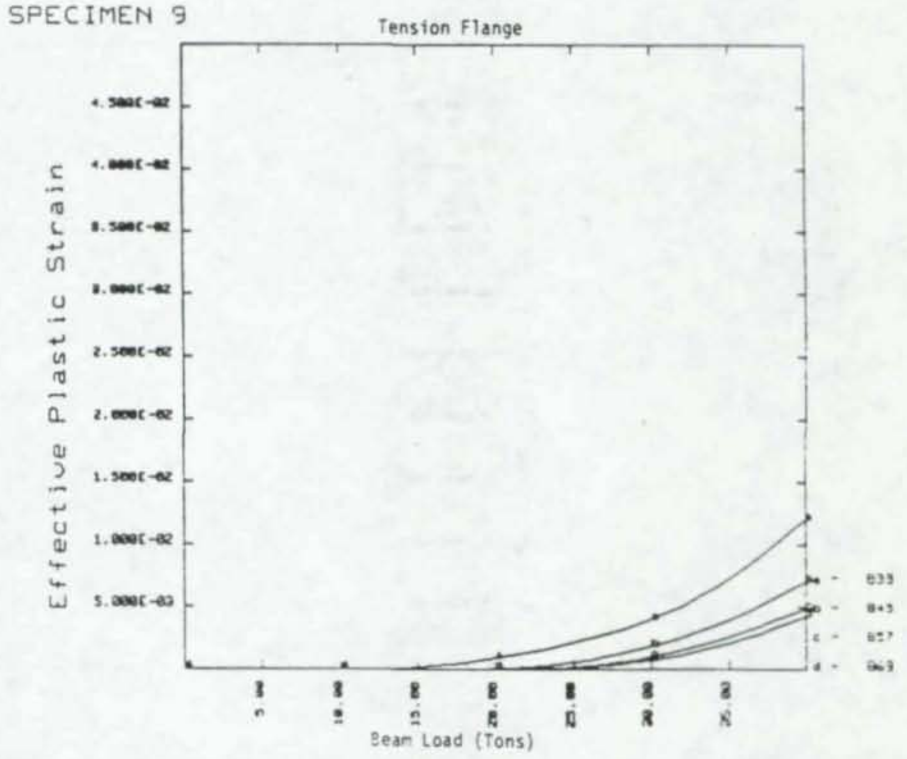

Figure 5.37 Element Strain vs. Beam Shear, Specimen 9

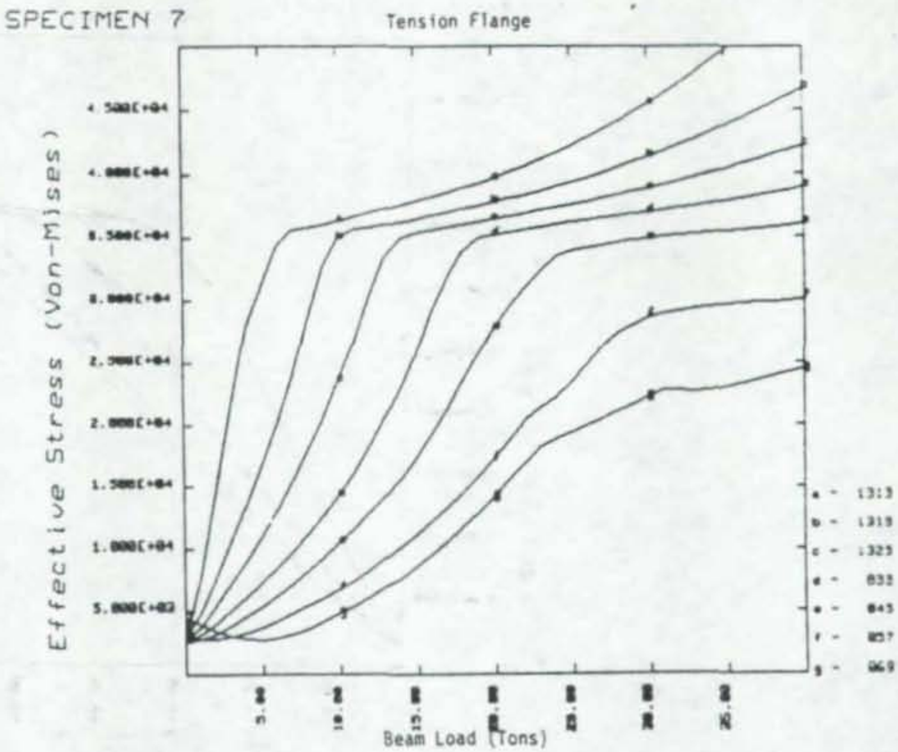

Figure 5.34 Element Stress vs. Beam Shear, Specimen 7

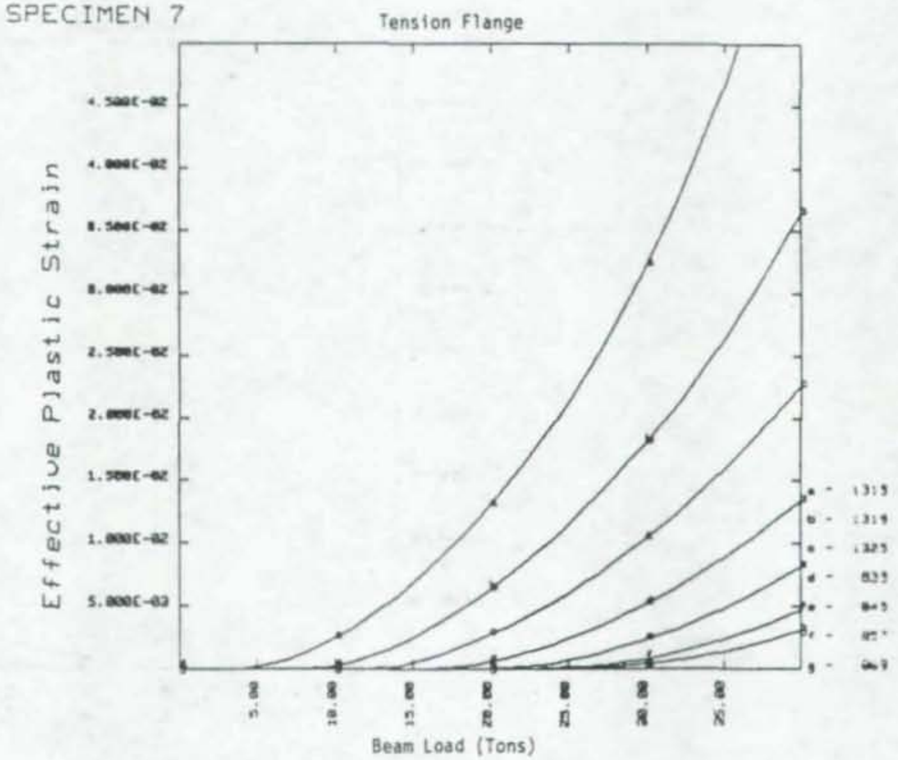

Figure 5.35 Element Strain vs. Beam Shear, Specimen 7

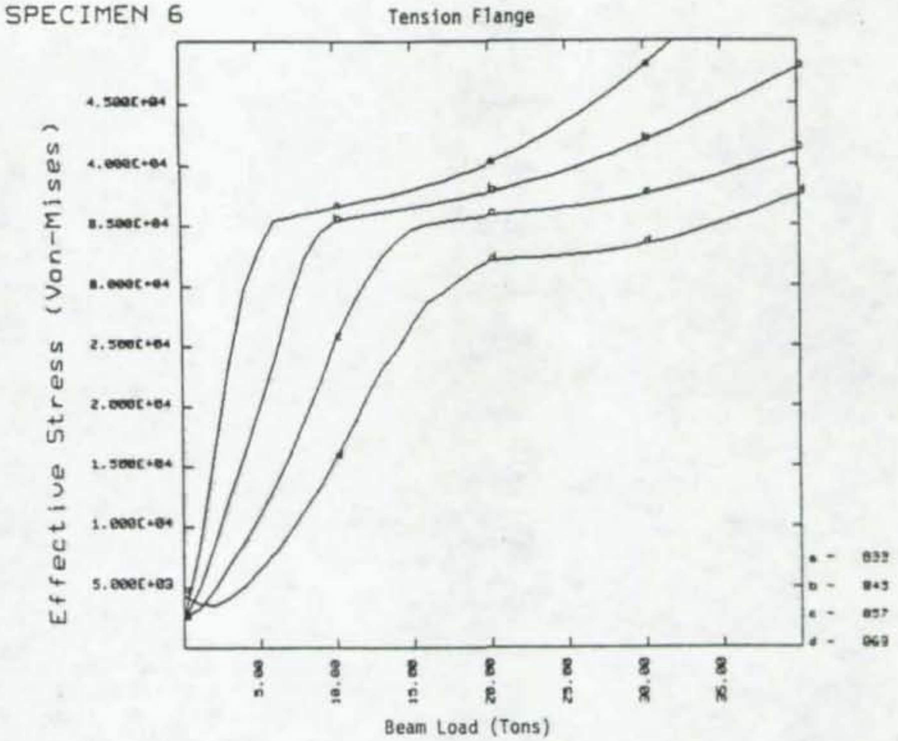

Figure 5.32 Element Stress vs. Beam Shear, Specimen 6

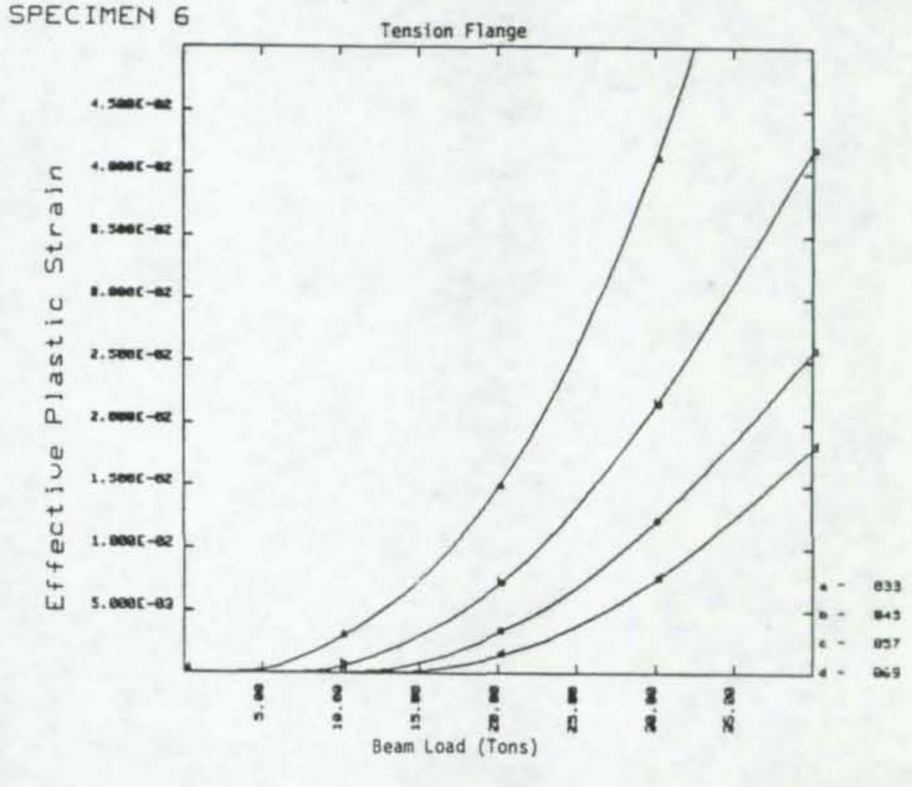

Figure 5.33 Element Strain vs. Beam Shear, Specimen 6

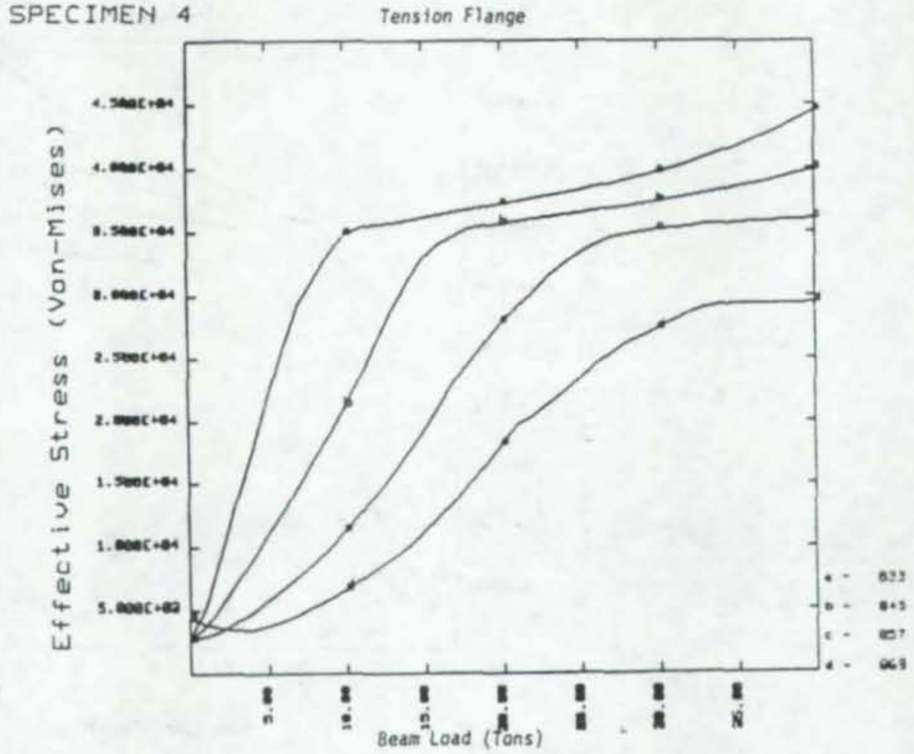

Figure 5.30 Element Stress vs. Beam Shear, Specimen 4

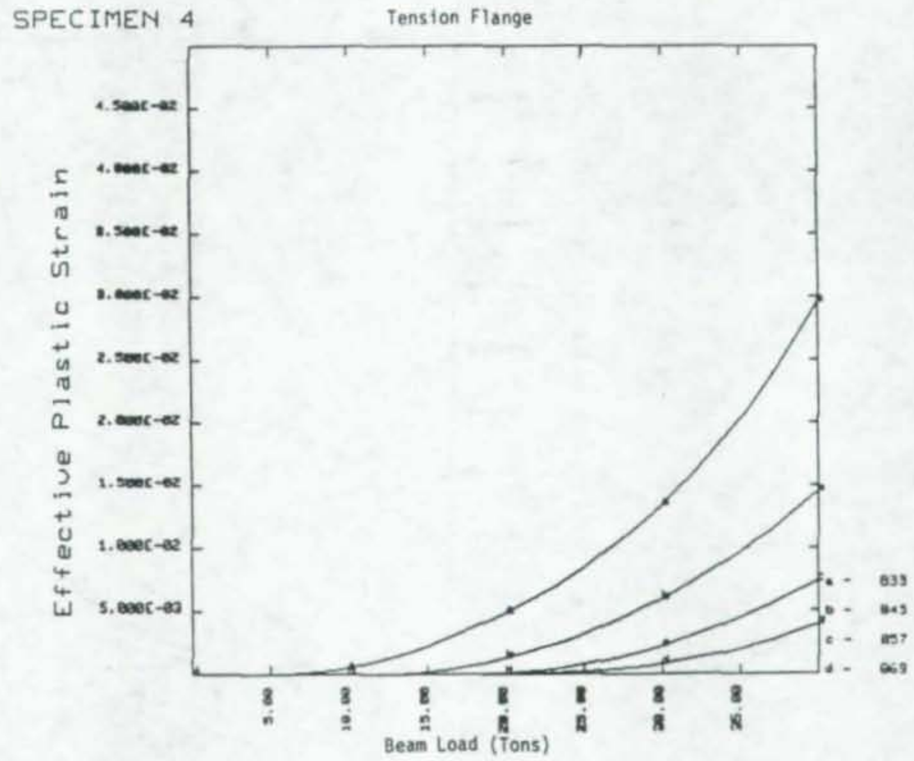

Figure 5.31 Element Strain vs. Beam Shear, Specimen 4

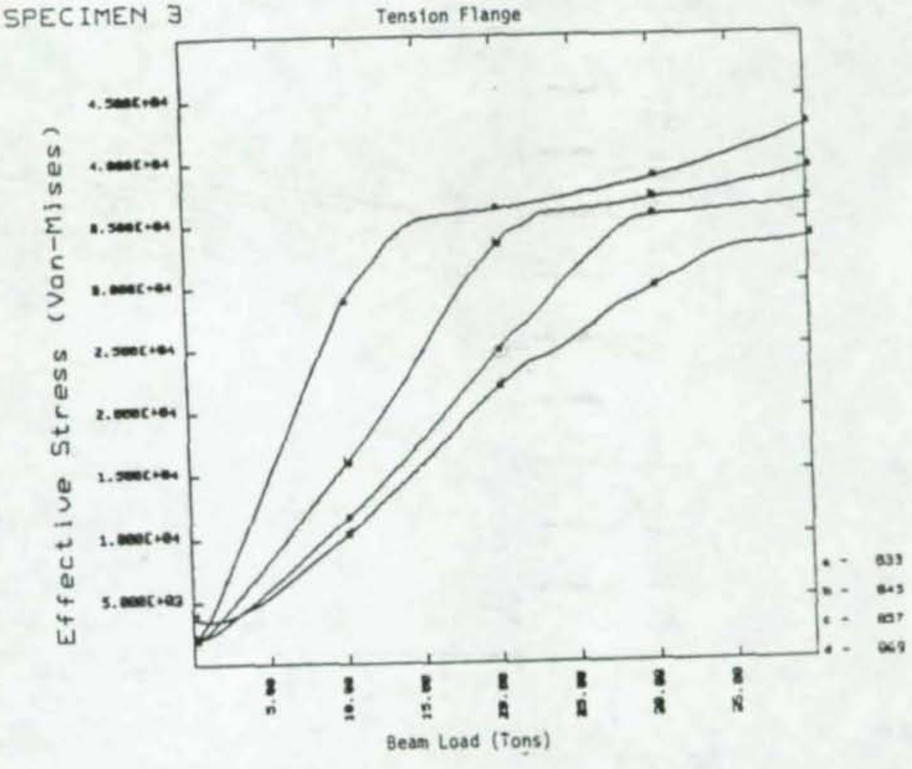

Figure 5.28 Element Stress vs. Beam Shear, Specimen 3

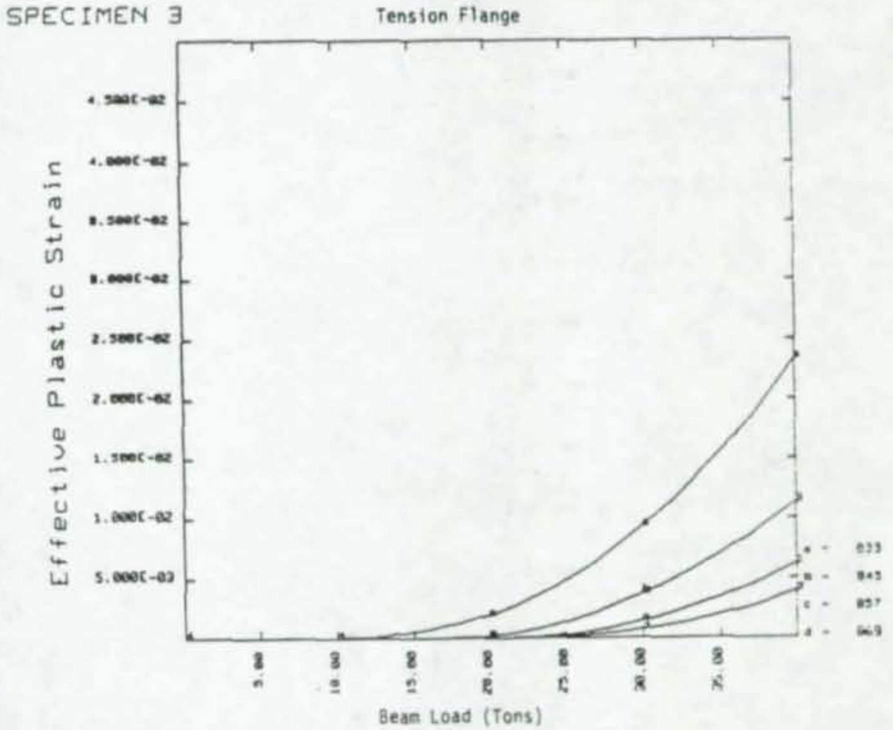

Figure 5.29 Element Strain vs. Beam Shear, Specimen 3

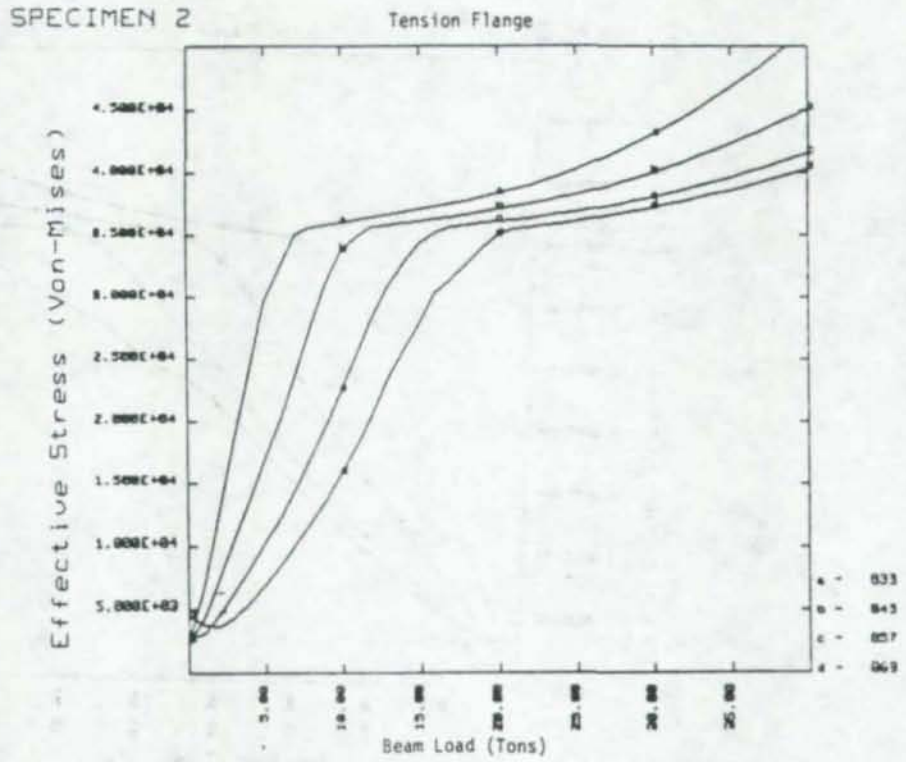

Figure 5.26 Element Stress vs. Beam Shear, Specimen 2

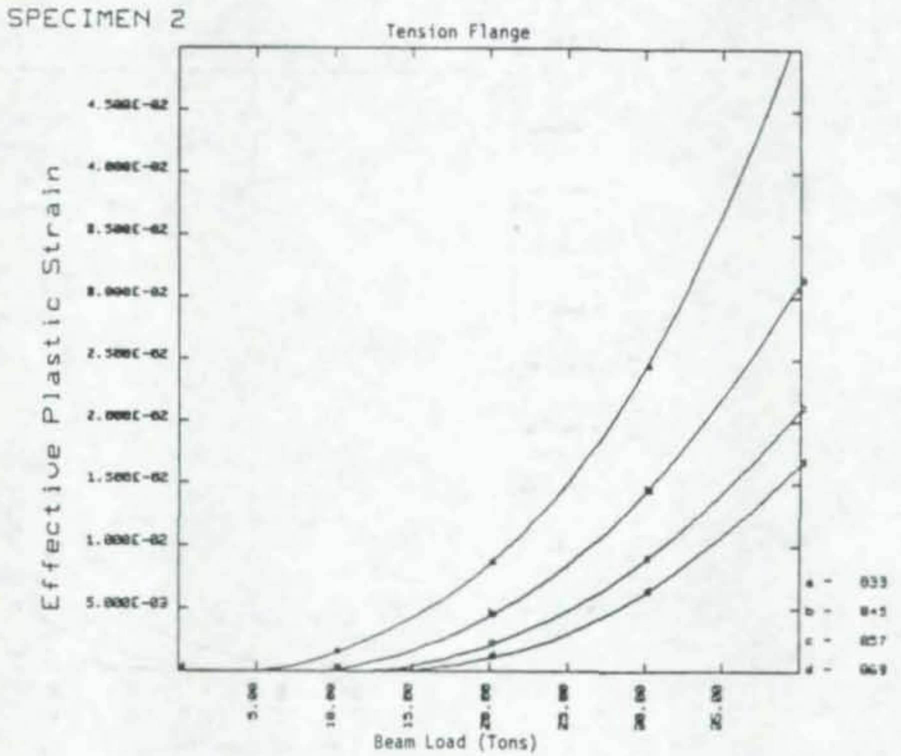

Figure 5.27 Element Strain vs. Beam Shear Specimen 2

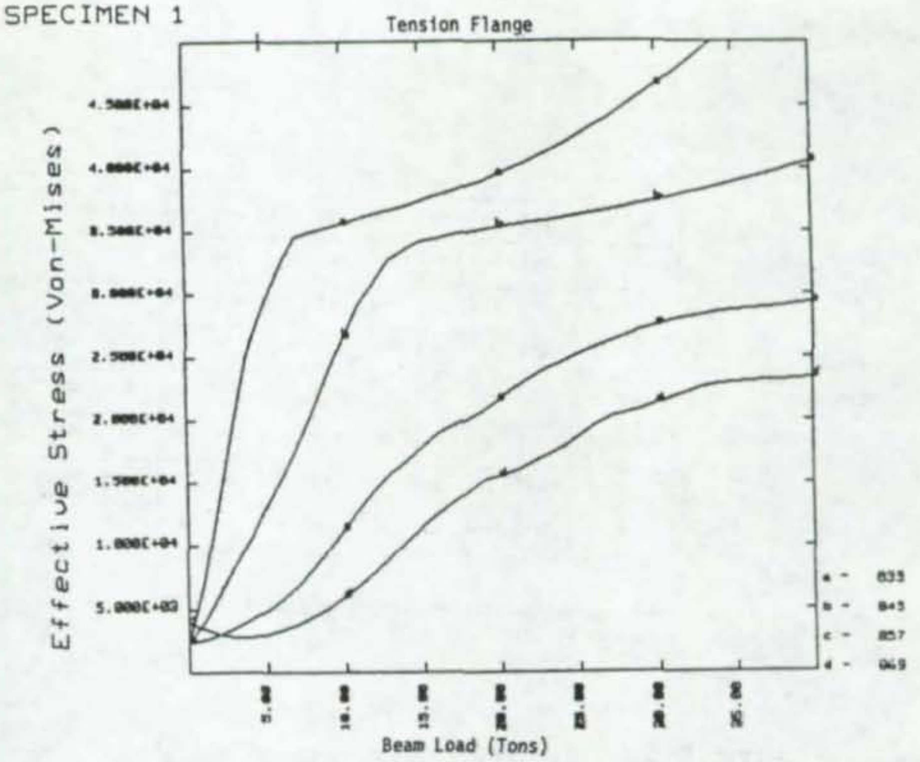

Figure 5.24 Element Stress vs. Beam Shear, Specimen 1

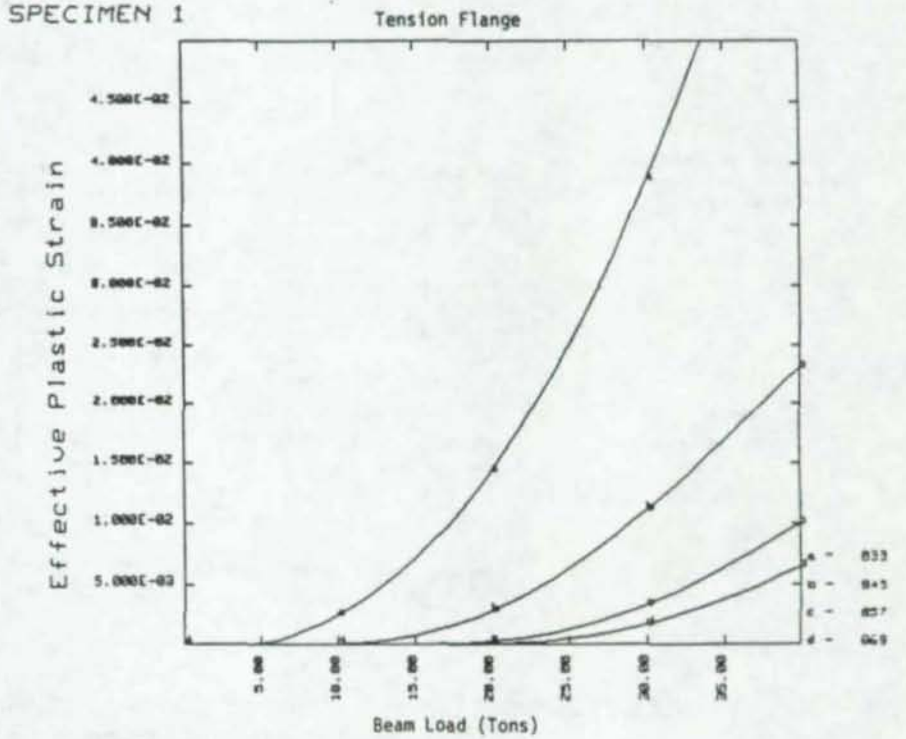

Figure 5.25 Element Strain vs. Beam Shear, Specimen 1

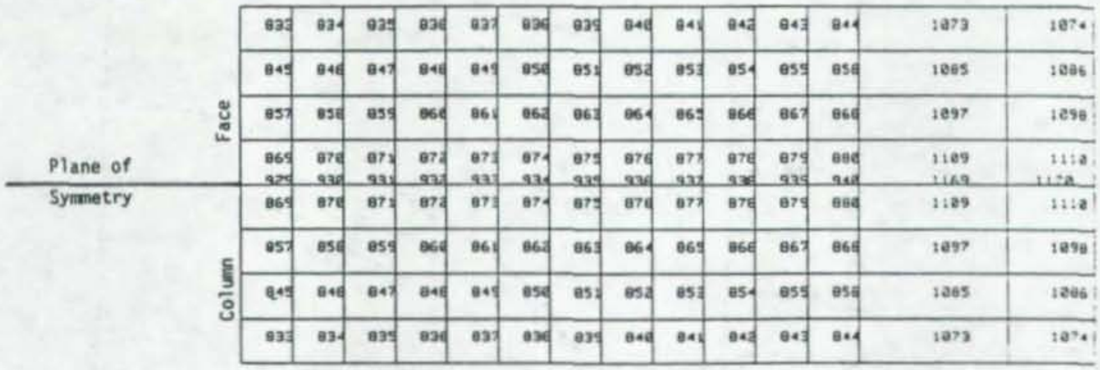

Numbering of Finite Elements on Tension Flange
(Specimens 1, 2, 3, 4, 6, 9, 13)

Figure 5.22 Typical Element Numbering, Tension Flange

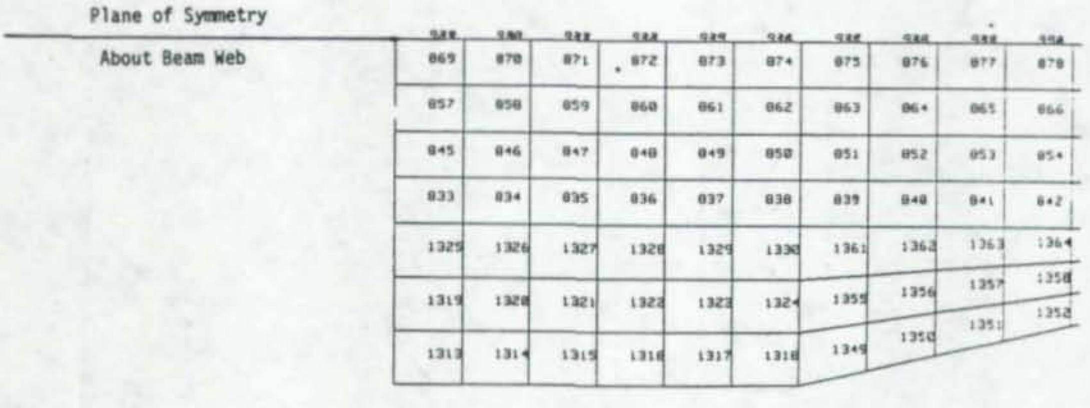

Numbering of Finite Elements on Tension Flange
(Specimen 7)

Figure 5.23 Element Numbering for Specimen 7,
Tension Flange

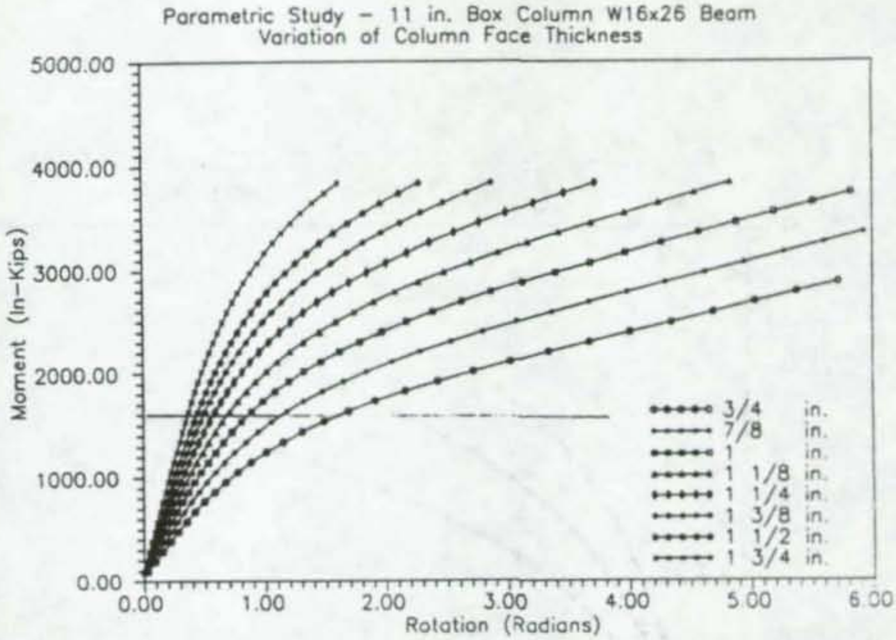

Figure 5.20 Effect of Column Face Plate Thickness W16x26 Beam

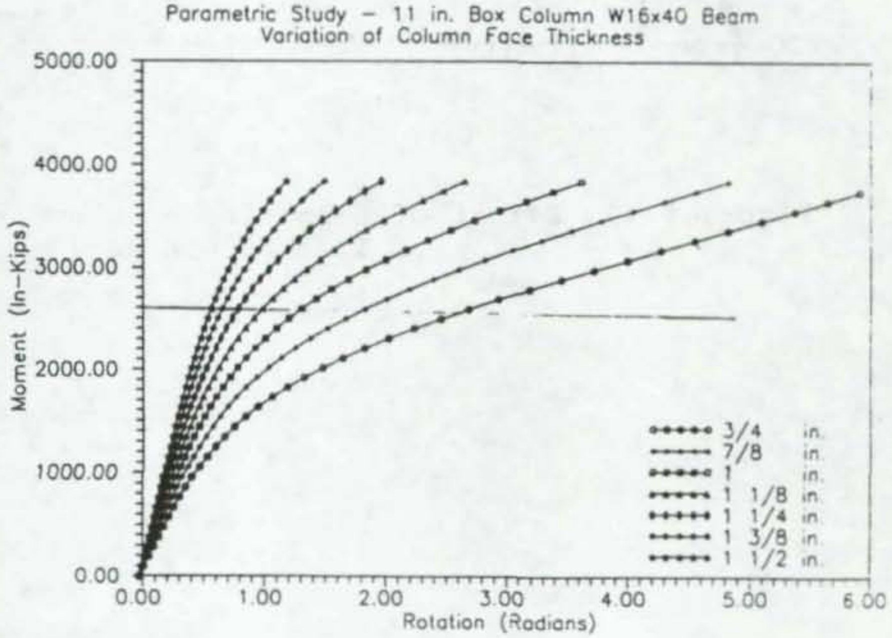

Figure 5.21 Effect of Column Face Plate Thickness W16x40 Beam

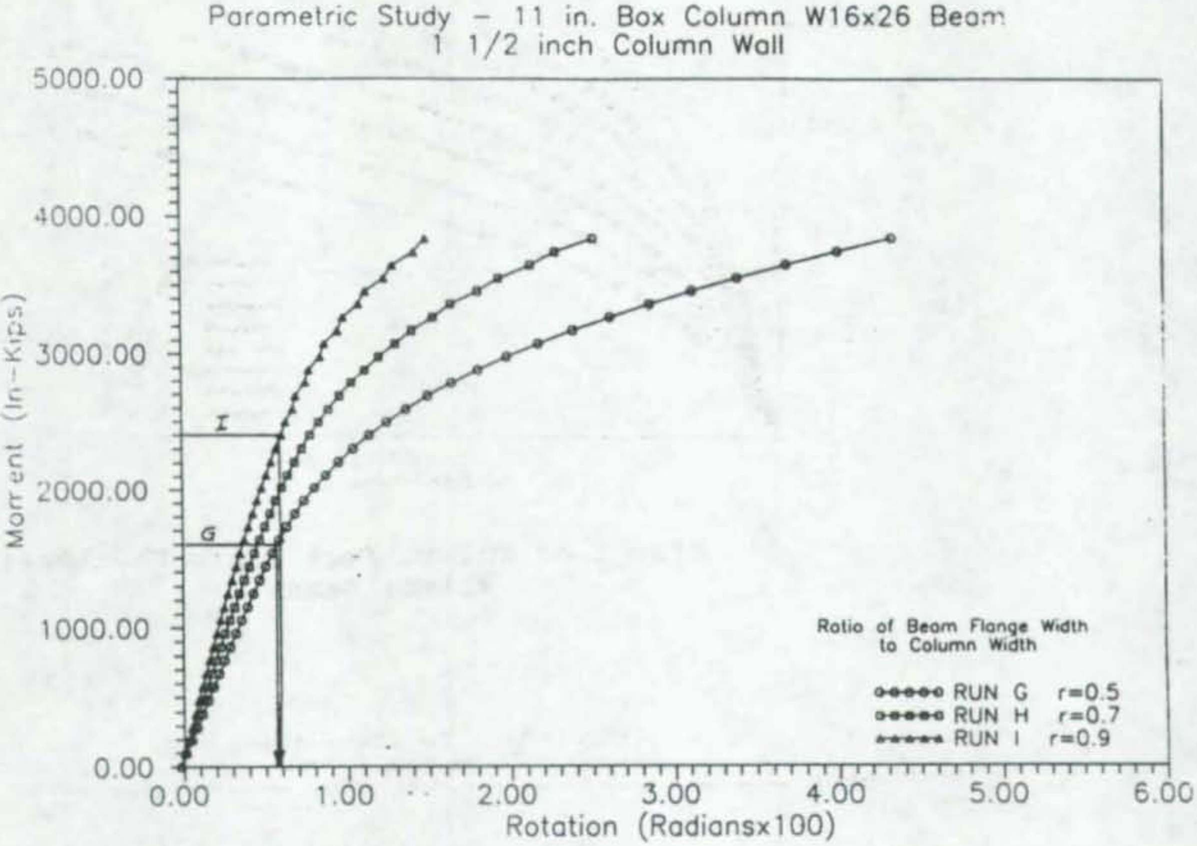

Figure 5.19 Effect of Beam Flange/Column Width Ratio 1 1/2" Column Wall

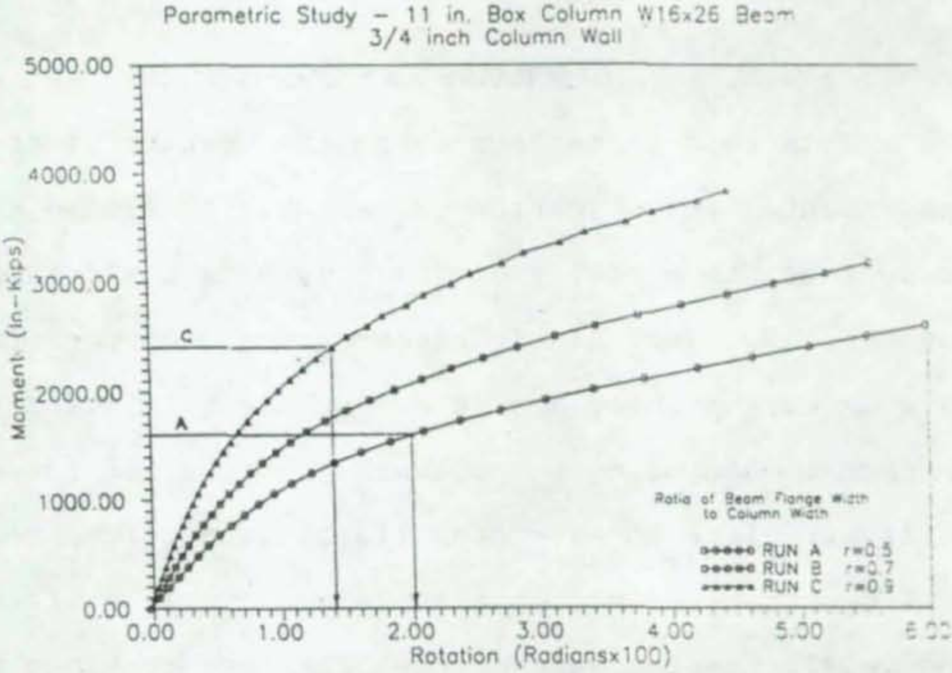

Figure 5.17 Effect of Beam Flange/Column Width Ratio 3/4" Column Wall

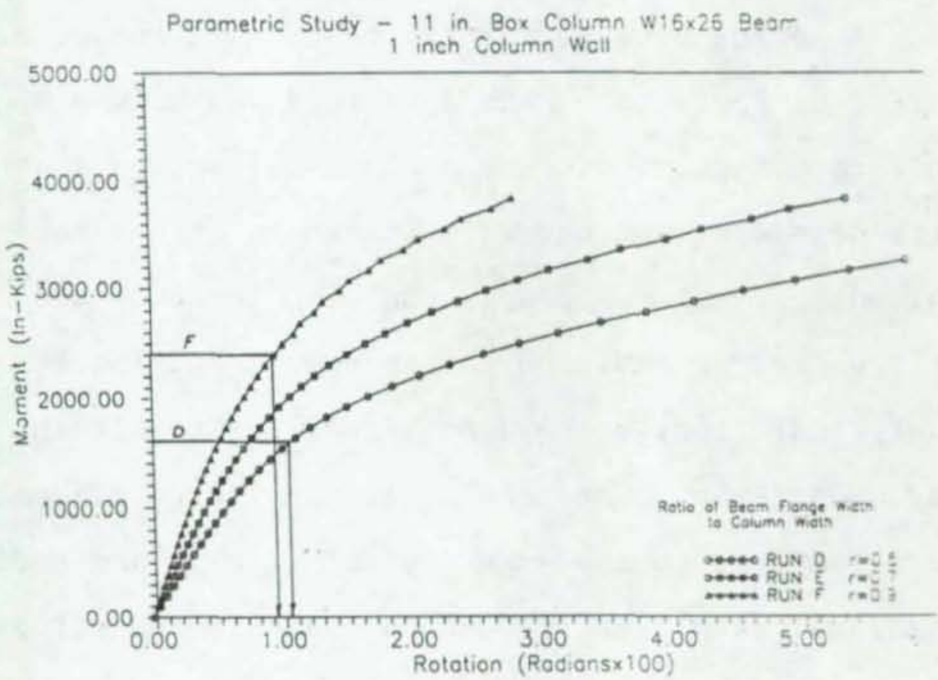

Figure 5.18 Effect of Beam Flange/Column Width Ratio 1.0" Column Wall

6.0 SUMMARY AND CONCLUSIONS

This report has documented the results of an experimental investigation and associated finite element study into the behavior of steel beam to box column connections. Very little research has been performed to date on this problem and as a result, it is standard design procedure when using box columns to detail an interior stiffener plate at each beam flange connection, requiring a full penetration weld on three sides of the stiffener plate and an electroslag weld on the backplate to close the column. The cost and difficulty of fabrication of these connections along with the lack of previous research provided the motivation for this study.

A series of experimental tests were run on eleven different specimens. The specimens had column segments of uniform height, width and depth. The two parameters varied were beam size and the wall thickness of the face of the column. Several tests were run with internal and external stiffeners. In addition to the experimental tests a parallel analytical study using a nonlinear finite element program was undertaken. The results of the finite element studies were compared to the experimental results and additional numerical studies were done to evaluate the effect of certain critical parameters.

The following conclusions are drawn from the experiments and analytical studies performed for this investigation:

1. Box columns with internal stiffeners the same thickness as the connecting beam flange perform in a manner which is similar to moment connections to wide flange columns. The internal stiffeners tend to make the stresses across the connecting beam flange more uniform. If the thickness of the stiffener plates is reduced, the connection becomes more flexible with increased rotation and increased stress gradients and plastic strain in the beam flange. Both connections are able to develop the plastic moment capacity of the connecting beam.

2. If the stiffener plates are inside the column, it is difficult to detect failures in the internal welds and impossible to perform a repair. In such a case it may be necessary to use external beam flange cover plates or flange extension plates to return the connection to its full strength.

3. Internal stiffener plates having a thickness less than the beam flange are subject to buckling at ultimate load, as evidenced in this investigation. This behavior must be considered in the design. The design criteria given in Section 2.7 of the AISC Specification specifying minimum width to thickness ratios for flange plates in box

sections and cover plates can be used as a guide. The maximum width to thickness ratio in this case is given as $190/\sqrt{F_y}$. One problem that may occur in using internal stiffeners less than the full thickness of the connecting beam flange is that the stresses in the internal welds can be higher than the beam to column weld. Should a weld failure take place, the larger stresses can lead to an increased probability of having weld failure occur inside the column, with the problems discussed in item one above.

4. Flange cover plates or flange extender plates which increase the width of the beam flange to the full width of the column face appear to be a possible substitute for internal stiffener plates. One problem identified with their use is an increase in the stresses at the edge of the plates which cause either a tearing of the column steel or a weld failure of the full penetration weld at the corner of the two column plates. The connection with the beam flange would also have to be properly designed in order to transfer the stresses to the cover or extender plates. One advantage of this approach is the tendency of the beam to form two plastic hinges, one at the column face and the other at the point where the cover or extender plates terminate. Two plastic hinges at a joint should increase the energy dissipation characteristics of the connection. A further advantage is

the relative ease of inspection and repair after a seismic event or fire.

5. The thickness of the column face plate can be increased sufficiently to provide a workable connection without the addition of stiffener plates. The thicker column face plate tends to distribute the stresses in the beam flange and make them more uniform. The required column thickness depends on the plastic moment capacity of the beam which frames into the column.

6. Box columns with face plate thickness which is thin relative to the beam cannot be designed without internal or external stiffener plates as evidenced in the poor performance of Specimens 1 and 8. The connection fails before the beam reaches its full plastic moment even when using nominal values for yield stress in the beam. The flexibility of the column face concentrates the beam flange stresses in the tips of the flanges leading to very high strains in these locations and high stress gradients across the beam flange. This can lead to premature failure of the beam due to the formation of a crack which usually occurs in the heat affected zone of the full penetration welds. The flexibility of the column walls also leads to unacceptably large rotations of the connection which make it impossible to develop the plastic moment capacity.

7. Nonlinear finite element analysis shows reasonably good correlation between the analysis and the experimental results. Nonlinear finite element programs can be used to produce moment rotation curves which can be used for connection design.

8. Current design practice for moment connections to the strong axis of wide flange column sections results in plastic strains at ultimate load which are on the order of 0.5% (.005 in/in). Current design practice for box columns appears to limit the plastic strain at ultimate to the yield plateau of the steel. For A36 steel, this is a strain of 1.5%. From the results of this study it would appear that any box column connection which limits the plastic strain in the beam flange to the yield plateau will perform satisfactorily. Problems appear to occur when high stress gradients appear and when the maximum plastic strain enters the strain hardening region of the stress-strain curve for the material.

In closing, it should be emphasized that the above observations and recommendations are based on a very limited amount of experimental test data. It is hoped that this initial investigation will provide guidance to other investigators performing analytical and/or experimental studies on beam to column connections. It is recognized that many of these recommendations and conclusions will change in time as further research on beam to box column connections is conducted and the results become available.

REFERENCES

[1] O. W. Blodgett, "Design of Welded Structures," The James F. Lincoln Arc Welding Foundation, Cleveland, Ohio, 1966.

[2] R.M. Richard and D.B. Rosenbaum, Letter to James Marsh, Western Regional Director, American Institute of Steel Construction, El Monte, California, dated 19 July 1985.

[3] R.M. Richard and D.B. Rosenbaum, Unpublished Report to Western Regional Office, American Institute of Steel Construction, El Monte, California, 1986.

[4] G. C. Driscoll and L. S. Beedle, "Suggestions for Avoiding Beam-to-Column Web Connection Failure," Engineering Journal, AISC, January 1982.

[5] J.O. Halquist, "NIKE3D: An Implicit, Finite Deformation, Finite Element Code for Analyzing the Static and Dynamic Response of Three Dimensional Solids," University of California, Lawrence Livermore National Laboratory, Rept. UCID-18822, 1981.

[6] F. B. Kahn and N. R. Amin, "Analysis and Design of Framed Tube Structures for Tall Concrete Buildings," Structural Engineering, London, Vol. 51, No. 3, March, 1973.

[7] J.W. Peters and G.C. Driscoll, "A Study of the Behavior of Beam to Column Connections," Fritz Laboratory Report 333.2, Lehigh University, Bethlehem, Pennsylvania, 1968.

[8] E. P. Popov, N. R. Amin, J. J. C. Louie and R. M. Stephan, "Cyclic Behavior of Large Beam-Column Assemblies," Earthquake Spectra, EERI, Vol.1, No. 2, February 1985.

[9] V.V. Bertero and E.P. Popov, "Effect of Large Alternating Strains on Steel Beams," ASCE, Journal of the Structural Division, Vol 91, No. ST1, February, 1965.

[10] E.P. Popov and R.B. Pinkney, "Cyclic Yield Reversal in Steel Building Connections," ASCE, Journal of the Structural Division, Vol. 95, No. ST3, March 1969.

[11] H. Krawinkler and E. P. Popov, "Seismic Behavior of Moment Connections and Joints," Journal of the Structural Division, ASCE, Vol. 108, No. ST2, February 1982.

[12] E.P.Popov, N.R.Amin, J.J.C. Louie and R.M. Stephen, "Cyclic Behavior of Large Beam-Column Assemblies," AISC, Engineering Journal, January, 1986.

[13] D.J. Fielding and J. S. Huang, "Shear in Beam to Column Connections" Welding Research Supplement, Welding Journal, Vol. 50 No. 7, July 1971.

[14] F. W. Stockwell, Jr., "Yield Line Analysis of Welded Beam Connections," Engineering Journal, AISC, January, 1974.

[15] G. P. Rentschler, W. F. Chen and G. C. Driscoll, "Tests of Beam-to-Column Web Moment Connections," Journal of the Structural Division, ASCE, Vol. 106, No. ST5, May, 1980.

[16] Tsai, K. C. and Popov, E. P., "Two Beam-to-Column Web Connections," Report No. UCB/EERC 86-05, Earthquake Engineering Research Center, University of California, Berkeley, April, 1986.

[17] J.E. Jubb and R.G. Redwood, "Design of Joints to Box Sections," Conference on Industrialized Building and the Structural Engineer, The Institution of Structural Engineers, U.K., 1966.

[18] R. M. Korol, M. El-Zanaty and F. J. Brady, "Unequal Width Connections of Square Hollow Sections in Vierendeel Trusses," Canadian Journal of Civil Engineering, Vol. 4, No. 2, 1977.

[19] J. L. Dawe and G. Y. Grondin, "Semi-Rigid Connections Between a W Beam and HSS Connection," CIDECT Report No. 5Ak-84/8-E, March 1985.

[20] C. K. Liew, "A Study of Connections Between Hollow Structural Section Columns and W Shape Beams," Master's Thesis, University of New Brunswick, Canada, January, 1988.

[21] A. Picard and Y. M. Giroux, "Moment Connections Between Wide Flange Beams and Square Tubular Columns," Canadian Journal of Civil Engineering, Vol. 3, No. 3, 1976

[22] A. Picard and Y. M. Giroux, "Rigid Connections for Tubular Columns," Canadian Journal of Civil Engineering, Vol. 4 No. 4, 1977.

[23] J. Wardenier, "Hollow Section Joints," Delft University Press, Delft, Netherlands, 1982.

[24] D. Cute, S. Camo and J.L. Rumpf, "Welded Connections for Square and Rectangular Structural Steel Tubing," Research Report No. 292-10, Drexel Institute of Technology, Philadelphia, Pennsylvania, 1968.

[25] R.N. Croad, F.H. Mead and R. Shepherd, "The Cyclic Yield Response of a Steel Star Plate Cruciform Joint," Bulletin of the New Zealand National Society for Earthquake Engineering, Vol. 8, No. 4, 1975.

[26] N.W. Hanson and H.W. Conner, "Seismic Resistance of Reinforced Concrete Beam Column Joints," ASCE, Journal of the Structural Division, Vol. 93, No. ST5, October, 1967.

[27] Measurements Group, Inc., "Shunt Calibration of Strain Gauge Instrumentation", Technical Notes, TN-514, Measurements Group, Inc., Raleigh, N.C., 1988.

[28] K. C. Tsai and E. P. Popov, "Steel Beam-Column Joints in Seismic Moment Resisting Frames," Report No. UCB/EERC/88-19, Earthquake Engineering Research Center, University of California, Berkeley, 1988.

[29] M. D. Engelhardt, "Behavior of Long Links in Eccentrically Braced Frames," Doctoral Dissertation, U.C. Berkeley, 1989.

[30] American Society for Testing Materials, "Standard Methods for Tension Testing of Metallic Materials," ASTM Designation E8-79, Philadelphia, Pennsylvania, 1980.

[31] J.O. Halquist, "NIKE2D -- A Vectorized Implicit, Finite Deformation Finite Element Code for Analyzing the Static and Dynamic Response of 2-D Solids with Interactive Rezoning and Graphics," University of California, Lawrence Livermore National Laboratory, UCID-19677, Rev. 1, 1986.

[32] J.O. Hallquist and D.J. Benson, "A Comparison of an Implicit and Explicit Implementation of the Hughes-Liu Shell," University of California, Lawrence Livermore National Laboratory, UCRL-94607, 1986.

[33] T.J.R. Hughes and W.K. Liu, "Nonlinear Finite Element Analysis of Shells: Part I, Three-Dimensional Shells." Computational Methods in Applied Mechanics, Vol. 27, 1981.